Copyright Warning & Restrictions

The copyright law of the United States (Title 17, United States Code) governs the making of photocopies or other reproductions of copyrighted material.

Under certain conditions specified in the law, libraries and archives are authorized to furnish a photocopy or other reproduction. One of these specified conditions is that the photocopy or reproduction is not to be "used for any purpose other than private study, scholarship, or research." If a, user makes a request for, or later uses, a photocopy or reproduction for purposes in excess of "fair use" that user may be liable for copyright infringement,

This institution reserves the right to refuse to accept a copying order if, in its judgment, fulfillment of the order would involve violation of copyright law.

Please Note: The author retains the copyright while the New Jersey Institute of Technology reserves the right to distribute this thesis or dissertation

Printing note: If you do not wish to print this page, then select "Pages from: first page # to: last page #" on the print dialog screen

ABSTRACT

INVESTIGATION OF DYNAMIC FRICTION IN LUBRICATED SURFACES

by
Hanuman Rachoor

The research reported in this dissertation is concerned with the development of friction models for lubricated contacts. A few analytical models have been developed to investigate the friction under dynamic velocity conditions. In this study, two different tribological situations such as conformal and non-conformal contacts have been chosen. Friction modeling covers boundary, mixed and full fluid film friction regions. A new theory based on the elastic properties of the surface materials, and fluid film properties of the lubricant at the contact has been developed to determine the dynamic friction in boundary, mixed and full hydrodynamic lubrication regions. In the full fluid film lubrication region, friction has been determined from the lubrication principles based on the tribological situation, i.e., hydrodynamic lubrication theory for a short journal bearing and elastohydrodynamic lubrication theory for a line contact.

A conformal contact formed by a short journal bearing operating in the region where hydrodynamic lubrication theory is valid has been considered to develop a model. The model is simulated for uni-directional as well as bi-directional sinusoidal velocity oscillations for various frequencies. Simulation resulted in a phase lag in the friction and hysteresis in friction versus velocity (f *vs* U) curves. The results obtained for uni-directional velocity oscillations indicate qualitative agreement with experimental work on lubricated line contact by Hess and Soom (1990). Results for bi-directional oscillations also show phase lag in friction and similar hysteresis in f *vs* U curves. In addition to the hysteresis, results for the bi-directional velocity oscillations show a discontinuity in friction at velocity reversals. These results have been verified experimentally.

A special apparatus to measure the friction has been designed and built by using a sleeve bearing. Experiments have been conducted to measure friction under various velocity conditions, and the results have been used to determine the coefficients required to simulate the analytical model. The analytical model has been simulated for the above

coefficients and the results have been compared with the friction measurements. The comparison shows similar hysteresis in f *vs* U curves for uni-directional and bi-directional velocity oscillations. However, the friction behavior of the apparatus during bi-directional oscillations differs in the magnitude of the discontinuity (step function) at velocity reversals.

The above analytical friction model developed for the hydrodynamic short journal bearing has been extended to investigate the effect of resisting forces on the dynamic friction behavior at low speed. Resistance forces include sliding friction as well as the presliding friction Dahl effect. The Dahl effect is due to elastic deformation of the compliance in the system before the force reaches the breakaway magnitude when sliding initiates. In this study, stiffness of the asperities as well as elastic support have been considered. Simulation results of the model for uni-directional velocity oscillations are in qualitative agreement with earlier experimental work. Simulation of the model for bi-directional velocity oscillations shows that the discontinuity at velocity reversals has been replaced by a line with slope. This work indicates that the stiffness of the elastic compliance can play a significant role in replacing the discontinuity.

The above concepts of friction modeling has been extended for a non-conformal contact formed with a cylindrical surface sliding over a flat surface operating on elastohydrodynamic lubrication theory. In this model, elastohydrodynamic lubrication theory has been used to determine the friction in full fluid film region. Simulation results of this model for uni-directional as well as bi-directional sinusoidal velocity oscillations indicate a similar phase lag in the friction and hysteresis in f *vs* U curves as observed in the earlier models.

Results of the present investigation indicate that the instantaneous friction is not only a function of the instantaneous velocity, but it is also a function of previous velocity or velocity history. These models can be improved with the aid of more experimental work. Also, these models can be extended for stick-slip analysis and for friction compensation.

INVESTIGATION OF DYNAMIC FRICTION IN LUBRICATED SURFACES

by
Hanuman Rachoor

A Dissertation
Submitted to the Faculty of
New Jersey Institute of Technology
in Partial Fulfillment of the Requirements for the Degree of
Doctor of Philosophy

Department of Mechanical Engineering

January 1996

APPROVAL PAGE

INVESTIGATION OF DYNAMIC FRICTION IN LUBRICATED SURFACES

Hanuman Rachoor

Dr. Avraham Harnoy — Date
Professor of Mechanical Engineering, NJIT

Dr. Bernard Friedland — Date
Distinguished Professor of Electrical Engineering, NJIT

Dr. Rong Chen — Date
Professor of Mechanical Engineering, NJIT

Dr. Roman Dubrovsky — Date
Associate Professor of Mechanical Engineering, NJIT

Dr. Zhiming Ji — Date
Assistant Professor of Mechanical Engineering, NJIT

BIOGRAPHICAL SKETCH

Author: Hanuman Rachoor

Degree: Doctor of Philosophy

Date: January 1996

Undergraduate and Graduate Education:

- Doctor of Philosophy in Mechanical Engineering
  New Jersey Institute of Technology, Newark, NJ, USA, 1996

- Master of Science in Mechanical Engineering
  Indian Institute of Science, Bangalore, Karnataka, India, 1980

- Bachelor of Mechanical Engineering
  Osmania University, Hyderabad, Andhra Pradesh, India, 1978

Major: Mechanical Engineering

Presentations and Publications:

Journal Publications:

H. Rachoor., and A. Harnoy. 1995. "Modeling of Dynamic Friction in Lubricated Line Contact for Precise Motion Control," *STLE Tribology Transaction*. 39(2):(to appear in 1996, manuscript # 94241). Presented at *50th STLE Annual meeting* at Chicago, IL, May 1995.

A. Harnoy, B. Friedland and H. Rachoor. 1994. "Modeling and Simulation of Elastic and Friction Forces in Lubricated Bearings for Precise Motion Control." *Wear*. 72: 155-165.

A. Harnoy., and H. Rachoor. 1993. "Angular Compliant Hydrodynamic Bearing Performance Under Dynamic Loads." *Transactions of American Society for Mechanical Engineers, Journal of Tribology*. 115(3): 342-347.

Conference Publications:

A. Harnoy, Bernard Friedland., Richard Semenock, Hanuman Rachoor, and Atif Aly. 1994. "Apparatus for Empirical Determination of Dynamic Friction." *Proceedings of American Control Conf., Baltimore, Maryland, June.* 3(2): 546-550.

Other Publications (Participated):

A. Harnoy., and B. Friedland. 1993. "Dynamic Friction Model of Lubricated Surfaces for Precise Motion Control." STLE *Tribology Transactions.* 37, 3: 608-614. Presented at *STLE/ASME Tribology Conference*, New Orleans, LA. : 24 - 27.

A. Harnoy 1995. " Model-Based Investigation of Friction During Start-Up of Hydrodynamic Journal Bearings." *Transactions of American Society for Mechanical Engineers, Journal of Tribology.* 117(4): 667-673.

A. Harnoy., and Michael. Khonsari. 1995 " Hydro Roll: A Novel Bearing Design with Improved Thermal Characteristics." *STLE Tribology Transaction.* 39(2): (to appear in 1996, manuscript # 94009).

This dissertation is dedicated to
my father, Krishnaiah Rachoor,
who brought me up to this stage, and I lost him on October 10, 1994

ACKNOWLEDGMENT

I would like to express my appreciation and sincere gratitude to my research advisor, Dr. Avraham Harnoy, for his valuable patient guidance, counsel, moral support, and friendship throughout this research. I am very grateful to Dr. Bernard Friedland for his suggestions to improve the dissertation. I thank Dr. Rong Chen, Dr. Roman Dubrovsky and Dr. Zhiming Ji for their active service on my committee.

I am very grateful to Mr. Atif Ali, Mr. Jayesh Amin and Mr. Richard Semenock for their help in setting up the apparatus, and conducting tests.

My thanks are due to the National Science Foundation for supporting the research, under Grant MSS 9215636. I also express my special thanks to the Graduate Student Association, New Jersey Institute of Technology, for sponsoring me to present my research work at the 50th Annual Meeting of the Society of Tribologists and Lubrication Engineers held at Chicago. I am also thankful to the Mechanical Engineering Department, New Jersey Institute of Technology for providing me support during my doctoral program.

Finally, I extend my thanks to all the members of my family for their love, support, patience, forgiveness, and inspiration provided to me at the moments of frustration, difficulties, and despair. Particularly, I thank my wife Jayalakshmi for her constant encouragement, support, and patience all these years of my life. Special thanks to my children Purnima, Swathi and Sai Simha for their co-operation. I also extend my thanks to my parents for their support. Finally, I ask the forgiveness of my father who passed away for not being with him during his last moments.

TABLE OF CONTENTS

TABLE OF CONTENTS
(Continued)

Chapter **Page**

TABLE OF CONTENTS
(Continued)

LIST OF TABLES

LIST OF FIGURES

LIST OF FIGURES
(Continued)

LIST OF FIGURES
(Continued)

NOMENCLATURE

a semiwidth of Hertzian zone
C radial clearance in the journal bearing
e eccentricity
e_b eccentricity at the transition from boundary to hydrodynamic region
e_{tr} eccentricity at the transition from mixed to hydrodynamic region
E equivalent modulus of elasticity
F external force
F_f friction force
f friction coefficient
f_m Coulomb's friction coefficient
h film thickness
h_m minimum film thickness
h_o central film thickness in the Hertzian zone of elastohydrodynamic line contact
h_{tr} film thickness at the transition from mixed to fully developed fluid film lubrication (hydrodynamic/elastohydrodynamic region)
h_b film thickness at the transition from boundary to elastohydrodynamic region
I_{eq} equivalent moment of inertia of the sleeve system
J_{11}, J_{12}, J_{22} integrals defined in Equations (2.23-2.25)
k torsional stiffness of the bearing support
$K(\delta)$ stiffness of contact between asperities
k_o constant coefficient of asperities' stiffness
K_n stiffness of surface asperities in the elastohydrodynamic line contacts
L length of the sleeve
m mass of journal or roller
M_j resistance torque between the journal and the sleeve
M_s reaction torque between the structure and the sleeve
O, O_1 sleeve and journal centers respectively (Figure 2.1 and 3.1)
p pressure in the contact (hydrodynamic/elastohydrodynamic)
R radius of cylinder or roller or journal
t time
U surface velocity of sliding surface (cylinder/roller/shaft)
U_b steady sliding velocity of sliding surface at transition from boundary to full film lubrication region (hydrodynamic or elastohydrodynamic region)
U_{tr} steady sliding velocity of sliding surface at transition from mixed to full film lubrication region (hydrodynamic or elastohydrodynamic region)
V radial component of the journal surface velocity (squeeze action against the y direction Figure 2.1)
W bearing load capacity, W_x, W_y components (Figure 2.1 and Figure 3.1)
W_e elastic reaction force at a contact between surfaces of journal and sleeve

W_h hydrodynamic oil film force in the journal bearing

w load capacity of the elastohydrodynamic line contact

w_e contact force between the asperities of elastohydrodynamic line contact

w_s steady elastohydrodynamic load in the elastohydrodynamic line contact

w_d unsteady elastohydrodynamic load in the elastohydrodynamic line contact

α dimensionless frequency ratio or frequency of velocity oscillations

ε eccentricity, e/C, ε_{tr} are ε_b are the magnitudes at steady velocities U_{tr} and U_b

ξ pressure viscosity coefficient

δ deformation of surface asperities at the contact surface

Δ a factor defined in Equations 2.4, 5.10

ν Poisson's ratio

η, η_o viscosity of lubricant, and viscosity at zero absolute pressure in elastohydrodynamic line contact

ϕ rolling to sliding ratio

κ_n dimensionless stiffness of surface asperities in elastohydrodynamic line contact

$\kappa(\varepsilon)$, $\kappa_n(\varepsilon)$ normal stiffness at the contact between the asperities in hydrodynamic contact

κ_o constant coefficient of asperities' stiffness

κ_t equivalent torsional stiffness due to the elastic shear of the surface asperities

τ dimensionless time, $\omega_{tr}t$

φ attitude angle (Figure 2.1 and Figure 3.1)

θ angular coordinate (Figure 2.1 and Figure 3.1)

θ_j, θ_s rotation angle of the journal and sleeve respectively

θ_j' initial condition used for θ_j when the presliding mode is restored

ω_o amplitude of velocity oscillations of the journal

ω_b steady angular velocity of journal at transition between boundary and mixed lubrication

ω_s angular velocity of the sleeve

ω_j angular velocity of the journal; ω_{tr} the transition value

μ viscosity of the lubricant in hydrodynamic contact of journal bearing

Ω frequency of journal oscillations rad/sec

Notations

$\bar{()}$ dimensionless

$()_{tr}$ magnitude at the transition between mixed and boundary lubrication, at steady speed.

$()_b$ magnitude at the transition from mixed to boundary lubrication, at steady speed

$\dot{()}$, $\ddot{()}$ first and second derivatives with respect to time.

PREFACE

Friction is present in all systems incorporating parts with relative motion. In many mechanical systems, friction is highly desirable as it enhances the performance, such as in clutches, brakes etc. But, in certain electro-mechanical systems such as in robots and tracking devices, friction is highly undesirable because it curtails the precision in motion. Presence of friction in such precise motion systems can cause limit cycles (known as "stick-slip" phenomenon) leading to instability in the system, or hang-off from the desired location. Therefore, friction is an impediment in closed-loop control systems requiring precise motion.

Friction can be reduced by use of passive techniques (such as air bearings, magnetic bearings, and improved lubrication). But, these passive techniques are expensive, cumbersome, and sometimes are not practical. Therefore, active techniques such as friction cancellation are desired to overcome the effects of friction. Model-based friction compensation is one of the important active methods. Therefore, in order to apply active techniques of friction cancellation, analytical models are required.

The present research work is a part of the major NSF (National Science Foundation) sponsored project undertaken by a team led by Dr. Bernard Friedland, Distinguished Professor of Electrical Engineering, and Dr. Avraham Harnoy, Professor of Mechanical Engineering. In the present research, analytical friction models for two different tribological situations are presented. Simulation results of the model are compared with experiments. The following paragraph describes the contribution made by the author for this project.

The author has developed computer programs to simulate the dynamic friction models of Harnoy and Friedland (1993) and Harnoy et. al (1994) as discussed in chapters 2 and 4. The author has participated in developing and building a friction measurement apparatus. The author compared experimental and theoretical dynamic friction which allowed to draw important conclusions about the dynamic friction as discussed in chapter 3. Also, the author has participated in analytical derivation of the friction model for a non-conformal contact H. Rachoor and A. Harnoy (1995). Author developed computer programs to simulate this model as discussed in chapter 5. The dissertation is organized as follows:

Chapter 1: A brief introduction on research in friction including scientific and historic background.

Chapter 2: Development of an analytical model for a conformal contact formed by a hydrodynamic journal bearing based on hydrodynamic lubrication theory.

Chapter 3: Development of the friction measurement apparatus, and experimental verification of the analytical model of the journal bearing model.

Chapter 4: Extension of the journal bearing model to analyze the resisting forces such as presliding friction (Dahl effect).

Chapter 5: Extension of the concept developed in the Chapter 2 to a non-conformal contact (elastohydrodynamic line contact) based on elastohydrodynamic lubrication theory.

Chapter 6: Conclusion of the present research work including recommendations for further research.

CHAPTER 1
FRICTION: A PHYSICAL PHENOMENA

Friction is an important physical phenomenon and is experienced by everyone. Friction is the principle of operation in many mechanical systems. But in most mechanical systems involving control applications, presence of friction is an impediment as it adversely affects the accuracy, precise motion, and stability. Particularly, friction study is very important in closed-loop control systems.

1.1 Background

Owing to significant adverse effects of friction on control systems, many scientists are focusing their attention to offer some solutions for the problems associated with the friction and its compensation. The monograph of Armstrong-Hélouvry (1991) indicates that Leonardo Da Vinci is the first researcher who studied the friction phenomenon in 1452. In his work, Da Vinci described friction as a force independent of the contact area, opposite to the motion and proportional to the surface force. Amontos rediscovered the friction phenomenon in 1699, and later Coulomb (1785) developed a friction model (Figure 1.1a). All these investigations describe friction for non-zero velocity conditions known as kinetic friction. Friction near zero velocity was first studied by Morin (1833), and is known as static friction. In 1866, Reynold described viscous friction which is present in a lubricated contact. Combination of kinetic, static, and viscous friction models constitutes the basic steady friction model (Figure 1.1b). Finally, in 1902, Stibeck had given a better explanation for the static and kinetic friction at low velocities (Figure 1.1c).

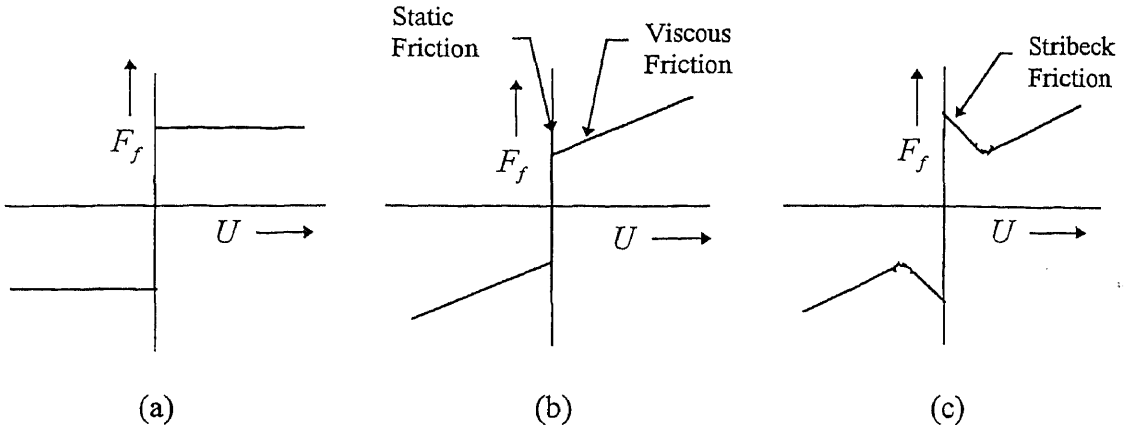

Figure 1.1 Friction models (friction force, F_f versus velocity, U curves) (a) Coulomb friction model, (b) static + viscous friction model and (c) static + viscous + Stribeck friction model.

During the 20th century, a systematic study of friction and wear evolved into the field called tribology. The traditional goals of tribology are to perceive friction phenomenon in respect of surface topography, and to develop better lubricants for effective friction minimization.

After World War II, a theoretical approach to understand the friction phenomenon in control systems begun. Theoretical models based on mathematics, physics, and experiments have been developed to analyze friction behavior.

1.2 Friction Modeling

Most of the moving components of mechanical systems are lubricated with liquid or solid lubricants. The main purpose of lubrication is to minimize the friction and reduce the wear of the mating parts. Lubricants provide a barrier between the sliding surfaces, so

that sliding friction is replaced by viscous friction of a lower magnitude. The fluid barrier in the load bearing interface is maintained by forcing the lubricant under pressure. There are two techniques to perform this lubrication process, known as hydrostatic and hydrodynamic lubrication. Hydrostatic lubrication is complex, and not applicable to many transmission devices. Hydrodynamic lubrication is simple, but it starts working only after some minimum velocity. At or below this velocity, there is no fluid film, but there is solid-to-solid contact.

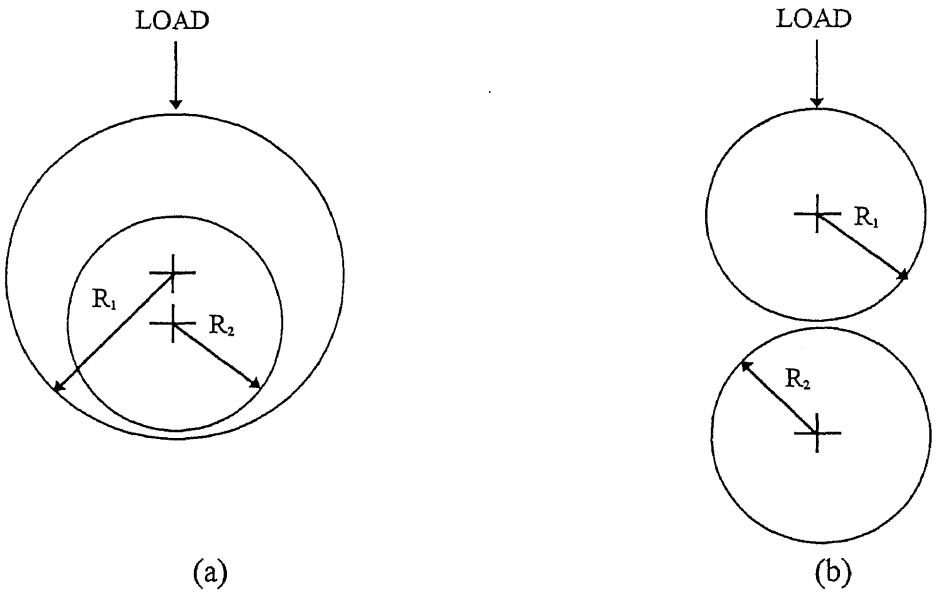

Figure 1.2 Topography of surface contacts. (a) Conformal contact and (b) Non-conformal contact.

Even though the hydrodynamic lubrication is simple, its operation varies with the type of surface contact between the mating surfaces. According to the surface topography, there are two types of surface contacts formed between the mating parts, conformal and non-conformal contacts. In conformal contacts (Figure 1.2a), geometry of the mating

parts determines the apparent area of the contact, and these types of contacts are known as area contacts. Journal bearings and machine tool guideways are two examples of conformal contacts. In contrast, in non-conformal contacts (Figure 1.2b), the mating parts don't have a matching surface profile, and these contacts are known as line or point contacts, depending on the surface profile and type of surface orientation. Roller bearings, gears, and cams are examples of non-conformal contacts. The present research deals with both types of contacts.

Prior research in the science of tribology led to better visualization of the hydrodynamic performance of full lubrication under steady velocity. Friction modeling involves establishing a relation between the system parameters, operating conditions, and friction. Particularly, the relation between friction versus velocity is considered as an important factor in modeling.

1.2.1 Friction as a Function of Velocity: Lubrication Regimes

Regimes of lubrication can be explained from the generalized Stribek (1902) curve as shown in Figure 1.3. There are four regimes of lubrication which are a function of operating velocity. The following is a brief discussion of the friction regimes. Armstrong-Hélouvry (1991) presented a detailed description of these regimes.

1.2.1.1 Static Friction: Friction at zero velocity is the first regime which is known as static friction. The static friction is due to the elastic deformation as well as plastic deformation of the fluid film and asperities at the contact junctions as a result of external

load. Dahl (1968, 76, 77) analyzed the static friction as spring-like behavior of the surface asperities at the contact.

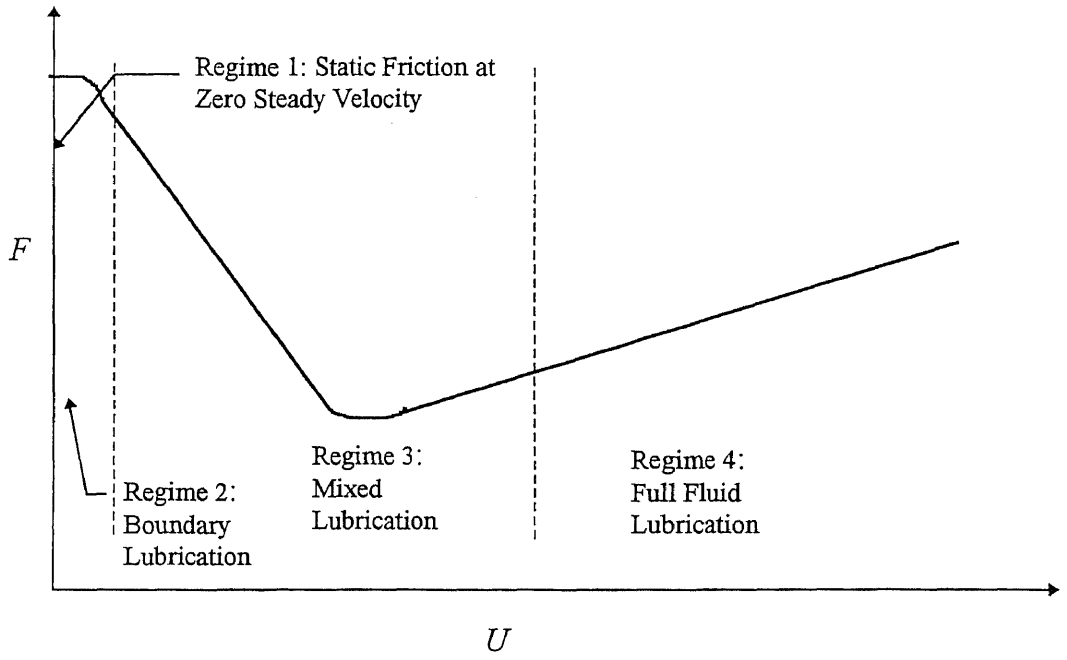

Figure 1.3 Stribeck curve, friction Force, F versus steady velocity, U curve and various lubrication regimes.

1.2.1.2 Boundary Lubrication: In this regime, the velocity of sliding surfaces is not adequate to generate a fluid film in the contact. Therefore, viscous lubrication does not play any role in this regime. An important aspect of this regime is shearing in the boundary lubricant due to the solid-to-solid contact. Based on the phenomenon of solid-to-solid contact and shearing of boundary lubricant, it is assumed that the friction is higher than the fluid lubrication.

1.2.1.3 Partial Fluid Lubrication: In this regime, sliding/rolling motion of the contact surfaces bring the lubricant into the load bearing region. Thickness of the film depends on the velocity of the sliding surfaces and viscosity of the lubricant. If the film thickness is

thinner than the height of the asperities, then solid-to-solid contact is formed, and the load is partially carried by asperities and partially by fluid film leading to partial fluid film lubrication. In contrast, if the fluid film is thicker than the asperities, then the two surfaces are separated completely by the fluid film, and the load is completely carried by the fluid film. Therefore, the partial fluid lubrication is one of the challenging friction regimes for a control engineer for controlling the purposes.

1.2.1.4 Full Fluid Lubrication: At sufficiently high operating velocities, the surface asperities are completely submerged by the thick fluid film, and the sliding/rolling surfaces are completely separated, and the load is completely supported by the fluid film. Hydrodynamic and elastohydrodynamic lubrication are two forms of full fluid lubrications. The former is for a conformal contact and the latter is for a non-conformal contact. In order to reach this regime, the fluid film thickness should reach a critical value of the film thickness, which depends upon the viscosity, load, and velocity. The magnitude of the velocity at the onset of full fluid lubrication corresponding to critical film thickness can be referred as critical or transition velocity for the given load and viscosity of the fluid film.

1.2.2 Friction as a Function of Steady Velocity

Stribeck friction is one of the most important friction models at steady velocity. To date there is no single theoretically investigated mathematical model available to explain the entire friction behavior. The shape of the friction-velocity curve ($f - U$) depends upon the degree of boundary lubrication. The research work of Bell and Burdekin, (1966, 969) and Hess and Soom (1990) indicates an $f - U$ curve as shown in Figure 1.4, which has been obtained for little or no lubrication condition. Fuller (1978) offers a very good

explanation of the boundary lubrication. Hess and Soom (1990) developed a model to simulate and analyze this kind of $f - U$ relationship. Bo and Pavelescu (1982) developed an exponential model to explain this kind of $f - U$ curve. Several researchers: Bo and Pavelescu (1982), Fuller (1984), Armstrong-Hélouvry (1988, 89, 91) worked to investigate the correct exponential index to fit these models.

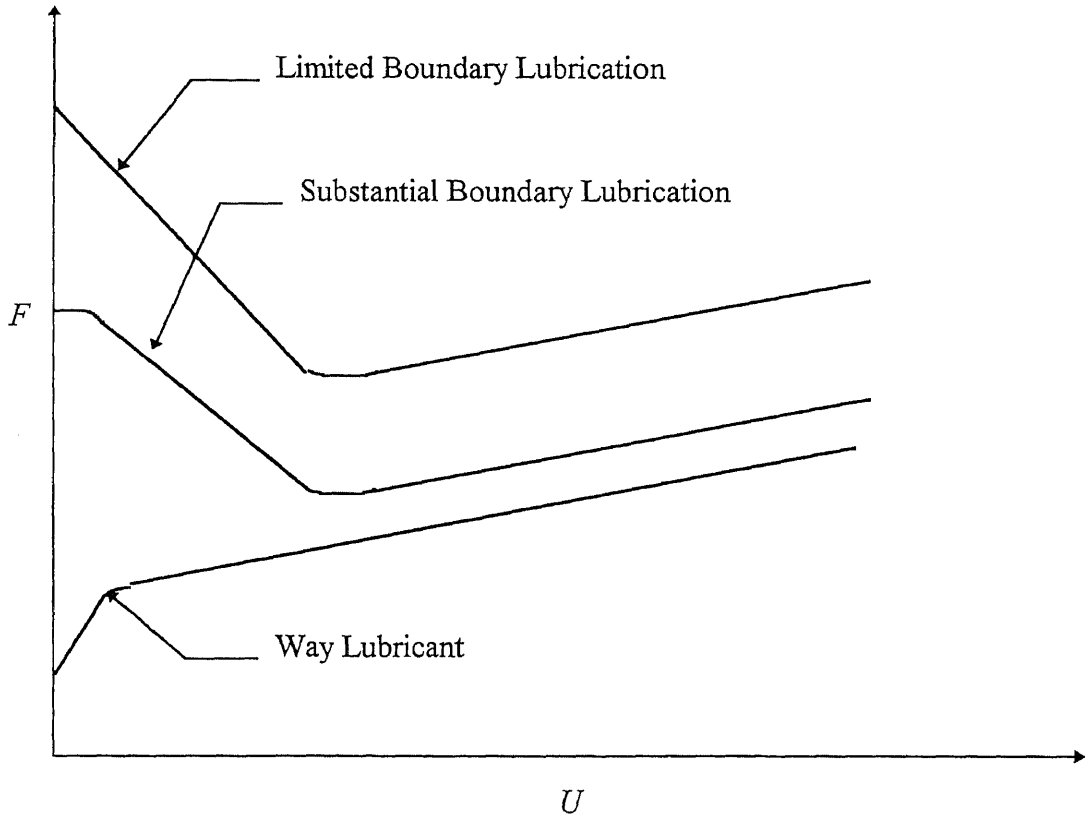

Figure 1.4 Friction force, F versus steady velocity, U.

1.2.3 Friction as a Function of Unsteady Velocity

The above paragraphs explain friction phenomenon under steady velocity conditions. Under dynamic velocity conditions, Hess and Soom (1990), Dupont and Dunlap (1993), Bell and Burdekin (1966, 1969) and Rabinowicz (1951) observed a phase lag in friction as indicated by hysteresis in friction versus velocity curves. At low frequency velocity oscillations, friction lag is present in partial fluid lubrication regime, where as at high frequency velocity oscillations, friction lag is present in partial fluid regime as well as in the full fluid lubrication regime. Armstrong-Hélouvry (1991) explains the friction lag as a pure delay in the onset of the destabilizing drop in friction.

Presence of the friction lag has been investigated experimentally by several researchers [Sampson et al. (1943), Rabinowicz (1958, 1965), Bell and Burdekin (1966, 1969), Walrath (1984), Rice and Ruina (1983) and Hess and Soom (1990)]. But there is no theoretical explanation for this phase lag based first principles. Hess and Soom (1990) observed hysteresis in friction for oscillating velocity conditions, for a lubricated line contact, and also measured friction lag for different load and lubricant combination. They observed that the lag was increasing with the contact load and lubricant viscosity. They also observed that the lag was independent of frequency of oscillations. Based on the experimental results, Hess and Soom (1990) offered an analytical with a correction to include the phase lag between friction and velocity oscillations. The friction models of Canudas et al (1993) also show hysteresis in friction-velocity curves. Dupont and Dunlop (1993) extended the work of Hess and Soom (1990) for a point contact at very low velocities, and their results show hysteresis in friction-velocity curves as observed by Hess

and Soom (1990). A detailed description of the research on friction is presented by Armstrong-Hélouvry (1991).

1.3 Presliding Friction (Dahl Effect)

At low velocities, many systems experience several types of resistance forces to their motion. Sliding friction and presliding elastic reaction are some of the resistance forces present in sliding contacts. The presliding elastic reaction is also known as Dahl effect. The Dahl effect is an elastic force present in the system due to compliance in the system, and this force reaches the break-away magnitude before the on-set of sliding. This is an important aspect for the systems working in closed-loop control, particularly, for precise motion control systems. The presliding friction is dominant when the operating velocity oscillates around zero or the motion of the system is not uni-directional. This Dahl effect is predominant when the system is in transition from rest to motion. The available friction models described by Armstrong-Hélouvry (1991) are based on steady $f - U$ curve, Stribeck (1902), and they do not address important phenomena such as friction function under dynamic velocity conditions, and elastic resistance forces due to the shear deformation of the surface asperities at the commencement of sliding. Dahl (1977) measured friction in bearings, and his model exhibited dynamic effects. Recently, Canudas de Wit et al. (1993) offered a couple of friction models. One of these models is modified version of Dahl model while the other model is improved version of Hess and Soom (1990) model. These models cover the important aspects of dynamic friction: hysteresis in friction under oscillating velocities, and presliding friction at zero velocity. These two models were reduced to Stribeck curve at constant velocity. Experiments were conducted

by Rabinowicz (1951) to measure the presliding elastic forces. He measured very small presliding deformation between two steel surfaces, and these measurements show that the presliding deformations are in the order of a few microns.

1.4 Present Investigation

According to the above discussion, the current friction models are empirical. These models are function of the steady Stribeck curve and the models have been developed by applying curve fitting techniques. However, closed-loop control systems often involve time-variable velocity oscillating at small amplitudes around zero velocity. In such cases, the steady friction models are inadequate for two important reasons. First, the friction is not a only a function of the instantaneous velocity, but also entails dynamic effects such as memory function of velocity history. Second, near zero velocity, there are significant elastic effects of surface asperities and supporting structure. Since the empirical models do not predict these dynamic effects, there is a need for the friction models to be developed from the first principles. Analytical models based on physical principles will predict the behavior of the dynamic system when compared to the empirical models developed from the steady models by curve fitting. Therefore, there is a need to develop analytical models based on physics of the system.

Present study is a part of a sponsored project focused on estimation and compensation of friction for precise motion control, and is investigated by a team comprising of faculty and students and of electrical and mechanical engineering departments at New Jersey Institute of Technology . The primary goal of the project is to estimate and compensate friction in closed-loop control systems. Friction can be

estimated in several ways, one important and useful method is model-based friction estimation. In this method, analytical models are developed to predict friction from the physical principles of friction processes.

The main objective of the present study is to develop analytical friction models from physical principles, and verify these models by appropriate experiments. As most of the systems operate in lubricated condition, the study is focused on developing friction models for lubricated surfaces. With this goal, analytical models to capture the friction behavior under dynamic velocity conditions have been developed from physics of the mechanism for two different tribological situations. Dynamic friction results obtained for these analytical models have been compared with the earlier experimental work as well as with friction measurements performed on a special apparatus developed for this comparison purpose.

The research discussed in this dissertation is an effort of the team including the author, and it is difficult to distinguish precisely the boundaries of each individuals' effort. In order to make the dissertation to be self contained, the contribution of the entire team is discussed. The contribution of the authors' work is as follows:

- The author has developed computer programs to simulate the dynamic friction models of Harnoy and Friedland (1993) and Harnoy et al. (1994) as discussed in chapters 2 and 4.
- The author has participated in developing and building a friction measurement apparatus.

- The author has compared experimental and theoretical dynamic friction which allowed to draw important conclusions about the dynamic friction as discussed in chapter 3.
- Also, the author has participated in analytical derivation of the friction model for a non-conformal contact H. Rachoor and A. Harnoy (1995). Author developed computer programs to simulate this model as discussed in chapter 5.

The following is the description of contribution of the individuals involved in the team including the author:

- Harnoy and Friedland have developed an analytical model for a short journal bearing operating on hydrodynamic lubrication theory [see Harnoy and Friedland (1993)]. The author has been actively involved in performing the simulations of the model. Subsequently, in this study, the model has been verified experimentally.
- The research team has developed an apparatus to measure friction in the lubricated surfaces. The author of this dissertation participated in the development of the experimental apparatus along with other graduate students, Aly Atif, Jayesh Amin and an undergraduate student, Richard Semenock. The analytical model of Harnoy and Friedland (1993) is verified conducting friction tests. The apparatus is described in this dissertation. Experimental results have been used for estimating the parameters required for simulating the analytical model, and comparing with simulation results of the analytical model for these data.
- A friction model to include the resistance forces is developed by extending the friction model of Harnoy and Friedland (1993). The objective of this study is to investigate the effect of different elastic resistance forces such as sliding friction,

presliding friction Dahl effect on friction behavior. In this model, attention is focused to evaluate the effect of elasticity of the surface asperities and the elasticity of the bearing support on friction behavior. The model can be simulated for different stiffness values of surface aperities as well as bearing support.

- Friction model for a non-conformal lubricated contact based on elastohydrodynamic lubrication theory is developed. A lubricated line contact formed by conformal surfaces such as roller bearings, gears is used in this investigation. The model uses all the techniques used by the earlier hydrodynamic model except the principle used in the full fluid film lubrication. In this model, elastohydrodynamic theory is used for modeling the friction in full fluid film lubrication region. The model is represented by a single fourth order non-linear differential equation and a friction equation.

CHAPTER 2

DYNAMIC FRICTION MODEL FOR A LUBRICATED CONFORMAL CONTACT

2.1 Introduction

In general, under steady conditions, the friction force between two sliding surfaces is a function of the relative velocity. But, under unsteady or dynamic conditions prevailing because of variations in velocity with time, the instantaneous friction is a function not only of the instantaneous velocity but also is a function of the velocity history. Dynamic conditions may be due to oscillatory motion or motion of constant acceleration.

The study is focused on developing an analytical model to investigate friction in the lubricated conformal contact formed a short journal bearing. The lubrication theory chosen for this bearing is hydrodynamic lubrication. The friction model is developed from the fundamental principles of physics based on lubrication theory and elastic properties of the metals in contact. Friction for steady and unsteady conditions can be simulated with aid of this model.

This study is extension of previous work, with the aim of investigating the physical mechanism for a phase-lag in friction shown in $f - U$ curves in lubricated surfaces. The development is based on first principles, and the model can predict the magnitude of the phase-lag between friction and velocity as well as hysteresis in friction. In addition, the model also predicts the conditions under which the steady curve, combined with a time lag, can be used as a model for dynamic friction. The result of the present investigation is dynamic model which can be expressed by a set of differential equations, relating the friction force to the time varying velocity of the sliding surfaces.

According to the classical hydrodynamic lubrication theory, film thickness is function of velocity. Full fluid film lubrication, in this case hydrodynamic lubrication commence only when the sliding velocity crosses a critical velocity. Above this critical velocity value, a lubrication film thicker than the size of the surface asperities is generated, and full fluid film lubrication is maintained. In the fully developed hydrodynamic lubrication regime, only viscous friction force is present and it increases with velocity since the shear rates and shear stresses are proportional to the sliding velocity.

According to the steady friction versus velocity ($f - U$) curve of Stribek (1902), for the velocities below the critical velocity, there is mixed lubrication (friction) region, where the thickness of the lubrication film is less than the maximum height of the surface asperities. Under the action of external load on two sliding surfaces, there is a contact between the surfaces, resulting in elastic as well as plastic deformation of the asperities at the contact. In the boundary lubrication region, load is completely carried by the asperities, and in the mixed region, the load is carried partly by fluid film and partly by the deformed asperities. The film thickness in the contact increases with velocity; therefore, as the velocity increases, a larger fraction of the external load is carried by the fluid film. The result is that in the mixed region, the friction decreases with increase in the velocity because the viscous friction is lower than the mechanical friction at the contact between the asperities.

The above discussion shows that the friction force is primarily dependent on the lubrication film thickness which in turn is an increasing function of the steady velocity. However for dynamic velocity, the relation between film thickness and velocity is not so simple. The following analysis attempts to capture the physical phenomena when the

lubrication film undergoes changes during owing to dynamic velocity. As a result of the damping in the system and the mass of the sliding body, there is a time delay to reach the film thickness that would be generated under steady velocity. The research reported in this chapter has been published already [see Harnoy and Friedland (1993)]. The author of this dissertation actively participated in the simulation of the model and computer programming. Since experimental verification of this theory is one of the objectives of the present study, the theory is presented in the following sections.

2.2 Theory for Model

In the present study, a short hydrodynamic journal bearing has been selected for friction modeling. The main reason is its wide use in machinery , steady in the fully developed hydrodynamic film region and it is well understood.

Consider a short journal bearing operating on hydrodynamic lubrication theory is under steady conditions as shown in Figure 2.1. Under steady condition, all the variables such as external load and operating speed are assumed to remain constant with time. During this steady condition, the journal center O_1 does not move relative to the bearing sleeve, and the friction between the journal and sleeve remains constant. This steady state situation prevail and continue to prevail after a transient interval having damping the initial motion of the journal center, if any. If there is any motion in the journal center O_1, there exists an unsteady or transient condition in the system. The motion of the journal center is due to the variations in the fluid film thickness and friction as a result of unsteady velocity conditions. This phenomenon explains the dynamic effects of unsteady friction.

In the development of the present model, relatively a new approach has been adopted by Harnoy (1993) to model friction in the steady state mixed friction region in which there is a contact between the surface asperities of the sliding surfaces. The asperities are assumed to deform under the constant force, and exert a reaction force.

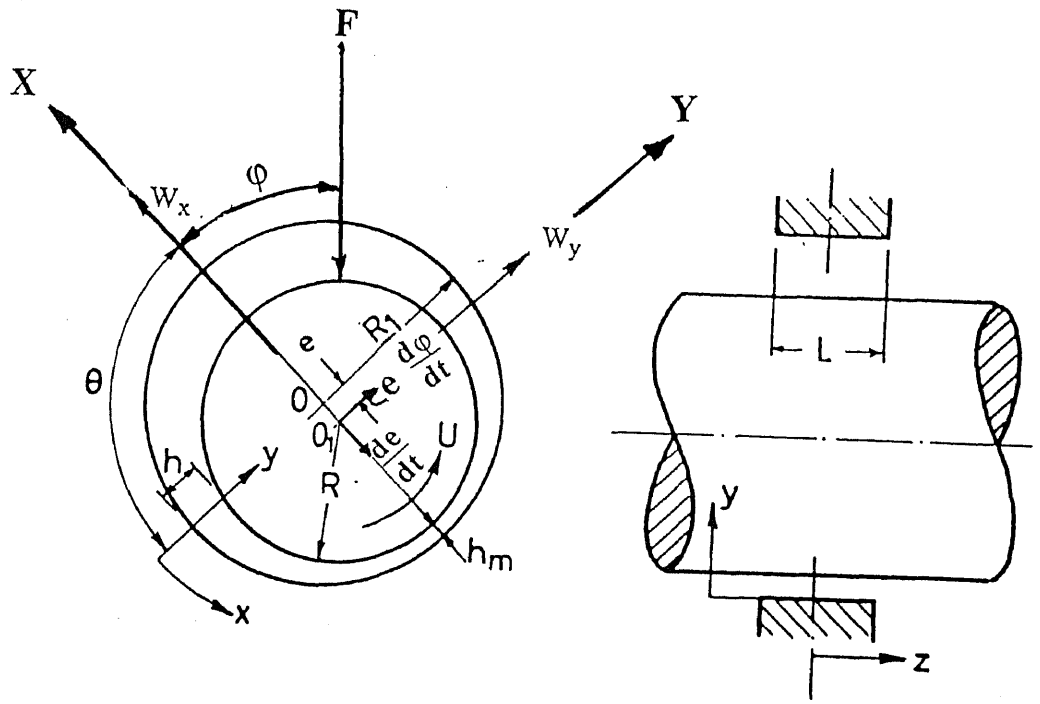

Figure 2.1 A schematic view of short journal bearing.

The theory is based on the minimum film thickness, h_m in the contact, see Figure 2.1. In the instant, when the minimum film thickness of lubrication, h_m goes below a certain small transition magnitude, h_{tr}, a part of the bearing load is carried by the reaction force exerted by the deformed surface asperities in the contact. The reaction force, between the asperities of the two surfaces, is assumed as an increasing function of the elastic part of the deformation, δ, it is like the displacement of a support by a non-linear spring.

The magnitude of the elastic deformation δ of the asperities is proportional to the difference in transition and actual minimum film thickness,

$$\delta = h_{tr} - h_m \tag{2.1}$$

The elastic reaction force, W_e exerted by the surface asperities can be obtained as,

$$W_e = K(\delta)\delta \tag{2.2}$$

where $K(\delta)$ is the equivalent stiffness of the surface asperities. The stiffness function $K(\delta)$ is a function of the shape of the asperities. The contact area between the surface asperities increases with the load and deformation δ. Hence, $K(\delta)$ must be an increasing function of δ.

According to theory of lubrication for a journal bearing, the deformation of asperities, δ, can be represented in terms of eccentricity, e, thereby relative eccentricity, $\varepsilon = e / C$ where C is the average radial clearance in the bearing (see Figure 2.1). With this observation, the reaction force, W_e can be expressed in terms of the relative eccentricity. Here onwards, the term "eccentricity" means "relative eccentricity". It is assumed that there exists a relative eccentricity of transition, ε_{tr}, from mixed to hydrodynamic lubrication. At the point that the eccentricity falls below this transition value, that is $\varepsilon < \varepsilon_{tr}$, contact and elastic reaction initiated. At the instant that the eccentricity reaches the transition value, that is $\varepsilon = \varepsilon_{tr}$, the minimum lubricant film thickness reaches to its transition value, $h_m = h_{tr}$. The magnitude of eccentricity at the transition, ε_{tr} can be calculated from the Stribeck curve at the transition from mixed to hydrodynamic lubrication for any given bearing geometry, lubricant viscosity, and the

velocity at the transition, U_{tr}. The deformation δ can be replaced by $C(\varepsilon - \varepsilon_{tr})$ and the equation for the elastic reaction is,

$$W_e = \kappa(\varepsilon) C(\varepsilon - \varepsilon_{tr}) \Delta \tag{2.3}$$

where $K(\delta) = \kappa(\varepsilon)$ and Δ is defined as

$$\Delta = \begin{cases} 1, & if\,(\varepsilon - \varepsilon_{tr}) > 0 \\ 0, & if\,(\varepsilon - \varepsilon_{tr}) < 0 \end{cases} \tag{2.4}$$

The total bearing load capacity $\vec{W}$ in the mixed region, can be obtained applying vector summation of the elastic reaction $\vec{W}_e$ and the hydrodynamic oil film force due to viscous friction, $\vec{W}_h$:

$$\vec{W} = \vec{W}_e + \vec{W}_h \tag{2.5}$$

The friction force F_f, in the bearing is in the tangential direction, and it is obtained by summing up of the mechanical and viscous friction forces in the contact. The mechanical part of the friction force is due to the deformation of the asperities at the contact, and it is assumed to follow the Coulomb's friction law. According to Coulomb's friction law, the friction force at the contact is proportional to the normal load. Further, it is also assumed that, in the mixed region, the density of surface asperities is sufficiently low, and their influence on the flow of the lubricant and hydrodynamic performance is insignificant.

With the above assumptions, Harnoy and Friedland (1993) derived an equation for the total friction force, F_f as,

$$F_f = f_m \kappa(\varepsilon) C(\varepsilon - \varepsilon_{tr}) \operatorname{sgn}(U) \Delta + \frac{L\mu R}{C} \frac{2\pi}{(1-\varepsilon^2)^{0.5}} U \tag{2.6}$$

where f_m is the Coulomb's friction coefficient, L, R are the length and radius of the bearing (Figure 2.1), U is the circumferential velocity at the surface of the rotating journal, μ is the lubricant viscosity, and sgn(U) is the sign of the velocity, U, which is defined as:

$$\text{sgn}(U) = \begin{cases} +1 & U \geq 0 \\ -1 & U < 0 \end{cases} \tag{2.7}$$

The hydrodynamic viscous friction force taken in the Equation 2.6 is represented by the short bearing formula Pinkus (1961), and Szeri (1980). The lubricant viscosity μ in Equation 2.6 is assumed as a constant in the development of the present model for both steady and dynamic conditions. Under dynamic conditions, ε and U vary with time, resulting in a time variable friction force, F_f. The time variable friction coefficient of the bearing $f(t)$ is calculated as a ratio of the friction force, F_f and external load F,

$$f(t) = \frac{F_f}{F} \tag{2.8}$$

2.3 Static Friction Model

A static friction model operating at a steady or constant velocity is developed for any given constant values of the system. The development of the model involves in determining the friction force. Following paragraphs explain friction modeling for any given constant journal speed.

The relative eccentricity ε of the journal bearing is determined from the load, F and the reaction force W_e. A set of equations relating the load, F on the journal bearing, and the relative eccentricity, ε have been derived for steady journal speed condition.

These equations are based on the hydrodynamic lubrication theory for a short journal bearing derived by Dubois and Ocvirk (1953).

$$F\cos\varphi = \kappa(\varepsilon)C(\varepsilon - \varepsilon_{tr})\,\mathrm{sgn}(U)\Delta + \frac{\varepsilon^2}{(1-\varepsilon^2)^2}\frac{\mu L^3}{C^2}U \tag{2.9}$$

$$F\sin\varphi = \frac{\pi\varepsilon^2}{(1-\varepsilon^2)^2}\frac{\mu L^3}{C^2}U \tag{2.10}$$

where φ is the attitude angle as shown in Figure 2.1. The direction of the elastic reaction force, W_e is along the symmetry line OO_1, (X direction) and is opposite to the direction of the load component, F_x. The load component in X direction $F_x(=F\cos\varphi)$ in Equation 2.9 is obtained by summing up the hydrodynamic reaction force component, F_h which is due to the fluid film pressure, and the elastic reaction force, W_e exerted by the asperities at the point corresponding to minimum film thickness. The load component in Y direction $F_y(=F\sin\varphi)$ in Equation 2.10 is equal to the hydrodynamic reaction force component, F_h only, which is due to the fluid film pressure, and there is no contact force in the Y direction. These two equations can be used to determine the magnitude of unknown variables, ε and φ.

In the mixed region, ($\varepsilon > \varepsilon_{tr}$), for any steady velocity, U, the magnitude of unknown variables, ε and φ can be computed by solving Equations 2.9 and 2.10 for any given values for C, L, F and $\kappa(\varepsilon)$. Thus the solution obtained for relative eccentricity, ε can be used to compute the friction force, F_f using Equation 2.6 there by the friction coefficient, $f(t)$ from Equation 2.7 for any given values of R and μ. This methodology

can be applied to plot the Stribeck Curve for the mixed and hydrodynamic lubrication regions.

For the purpose of simulation, the above equations have been transformed into dimensionless form by introducing the following dimensionless parameters:

$$\overline{F} = \frac{C^2}{\mu U_{tr} L^3} F, \qquad \overline{\kappa}(\varepsilon) = \frac{C^3}{\mu U_{tr} L^3} \kappa(\varepsilon) \qquad \text{and} \qquad \overline{U} = \frac{U}{U_{tr}} \tag{2.11}$$

The following are dimensionless form of Equations 2.9 and 2.10:

$$F\cos\varphi = \overline{\kappa}(\varepsilon)(\varepsilon - \varepsilon_{tr})\,\mathrm{sgn}(\overline{U})\Delta + 0.5 J_{12}\varepsilon\overline{U} \tag{2.12a}$$

$$F\sin\varphi = 0.5 J_{11}\varepsilon\overline{U} \tag{2.12b}$$

The integrals J_{11} and J_{12} used in the above equations are defined in the following section. The above dimensionless equations can be applied to derive or plot the $f - \overline{U}$ curve for any steady velocity in the mixed and hydrodynamic regions.

2.4 Dynamic Friction Model

Dynamic modeling involves computing the system parameters for dynamic or time variable velocity conditions. In this section, a dynamic friction model has been developed by incorporating the dynamic effects in the static model that has been developed in the previous section. In order to develop a dynamic friction model, the hydrodynamic short journal bearing theory is extended to include dynamic effects. In this study, the mixed and fully developed hydrodynamic fluid film regions have been considered to include the dynamic effects.

The friction model is developed by extending the assumptions of Dubois and Ocvirk (1953) valid for a short bearing under steady speed. According to these

assumptions, pressure gradients in the x (circumferential) direction are very small when compared with gradients in z (axial) direction, and they are neglected (Figure 2.1). The oil film forces are calculated only for the pressure distribution in the $0 < \theta < \pi$ region only, because the pressure in this region is above atmospheric. The traditional assumptions of Reynolds' classical hydrodynamic theory are extended. As mentioned earlier in the previous sections, the lubricant viscosity μ is assumed as a constant (at an equivalent average temperature). The effects of fluid inertia are neglected, but the journal mass is considered, since its magnitude is higher than the fluid mass.

The hydrodynamic pressure, P, for dynamic conditions is derived from the following Reynolds' equation for a thin incompressible fluid film Szeri (1980) (co-ordinates are shown in Figure 2.1):

$$\frac{1}{6\mu}\left[\frac{\partial}{\partial x}(h^3\frac{\partial p}{\partial x})+\frac{\partial}{\partial z}(h^3\frac{\partial p}{\partial z})\right]=U\frac{\partial h}{\partial x}+2V \qquad (2.13)$$

where V is the radial velocity of the journal surface causing squeeze film action in the direction opposite to the y direction. The right-hand side of Equation 2.13 can be stated by the boundary conditions of the fluid film. Under dynamic conditions, the journal center, O_1, does not remain constant but it is in motion. The surface velocity components, U and V, of the journal are obtained by adding the velocity vectors of the surface velocity relative to the journal center O_1 (velocity due to journal rotation) and velocity vector of O_1 relative to O. The radial and tangential components of the velocity of journal center are (de/dt and $d\varphi/dt$) respectively:

$$U=\omega_j R+\frac{de}{dt}\sin\theta-e\frac{d\varphi}{dt}\cos\theta \qquad (2.14)$$

$$V = \omega_j R\frac{\partial h}{\partial x} + \frac{de}{dt}\cos\theta + e\frac{d\varphi}{dt}\sin\theta \tag{2.15}$$

The last two terms on the right-hand side of Equation 2.15 for velocity component, V are negligible.

According to the assumptions of short bearing, the pressure gradient in the x direction can neglected relative to the gradient in the z direction (refer left-hand side terms of Equation 2.13). The Equations 2.14 and 2.15 for velocity components U and V are substituted into Equation 2.13, and integrated twice for pressure distribution, P, with the following axial boundary conditions:

$$P = 0 \text{ at } z = \pm L/2 \tag{2.16}$$

Following is the pressure distribution, P, obtained for an unsteady, short hydrodynamic journal bearing:

$$P = \frac{3}{4}\frac{\mu L^3}{C^2}(\omega_j \varepsilon \sin\theta - 2\varepsilon\frac{d\varphi}{dt}\sin\theta - 2\frac{d\varepsilon}{dt}\cos\theta)\frac{(L^2 - 4z^2)}{h^3} \tag{2.17}$$

where h is the film thickness in the contact of the hydrodynamic journal bearing (see Figure 2.1) and it can be expressed as a function of θ as:

$$h = C(1 + \cos\theta) \tag{2.18}$$

The force components, W_x and W_y of the hydrodynamic oil film as shown in Figure 2.1 are obtained by integrating the pressure in the converging clearance, $0 < \theta < \pi$,

$$W_x = -2R\int_0^{\pi}\int_0^{L/2} P\cos\theta \; d\theta \; dz \tag{2.19}$$

$$W_y = 2R\int_0^{\pi}\int_0^{L/2} P\sin\theta \; d\theta \; dz \tag{2.20}$$

The above load capacity Equations 2.19 and 2.20 have been converted into dimensionless form by substituting the pressure distribution, P, from Equation 2.17 and film thickness, h, from Equation 2.18 into Equations 2.19 and 2.20, and integrating. Following are the dimensionless form of Equations 2.19 and 2.20:

$$\overline{W}_x = -0.5J_{12}\varepsilon\overline{U} + J_{12}\varepsilon\dot{\varphi} + J_{22}\dot{\varepsilon} + \overline{\kappa}(\varepsilon)(\varepsilon - \varepsilon_{tr})\,\mathrm{sgn}(\overline{U})\Delta \tag{2.21}$$

$$\overline{W}_y = 0.5J_{11}\varepsilon\overline{U} - J_{11}\varepsilon\dot{\varphi} - J_{12}\dot{\varepsilon} \tag{2.22}$$

where the definition of $\mathrm{sgn}(\overline{U})$ is similar to the definition of $\mathrm{sgn}(U)$ as defined in Equation 2.7, the variable Δ is already defined in Equation 2.4, and the integrals J_{ij} :

$$J_{11} = \int_0^{\pi} \frac{\sin^2\theta}{(1+\varepsilon\cos\theta)^3} d\theta = \frac{\pi}{2(1-\varepsilon^2)^{3/2}} \tag{2.23}$$

$$J_{12} = \int_0^{\pi} \frac{\sin\theta\cos\theta}{(1+\varepsilon\cos\theta)^3} d\theta = \frac{-2\varepsilon}{(1-\varepsilon^2)^2} \tag{2.24}$$

$$J_{22} = \int_0^{\pi} \frac{\cos^2\theta}{(1+\varepsilon\cos\theta)^3} d\theta = \frac{\pi}{2}\frac{(1+2\varepsilon^2)}{(1-\varepsilon^2)^{5/2}} \tag{2.25}$$

According to Newton's second law of motion, the resultant force of the external load, F, and the of bearing force, W, accelerates the journal. The dimesionless form of

the equations of motion of the journal in the radial and tangential directions, X and Y as shown in Figure 2.1 have been obtained by substituting the acceleration terms as:

$$\overline{F}_x - \overline{W}_x = \overline{m}(\ddot{\varepsilon} - \varepsilon\dot{\varphi}^2) \tag{2.26}$$

$$\overline{F}_y - \overline{W}_y = \overline{m}(\varepsilon\ddot{\varphi} + 2\dot{\varepsilon}\dot{\varphi}) \tag{2.27}$$

where $\overline{m}$ is the dimensionless form of the mass, m, which is defined as:

$$\overline{m} = \frac{C^3 U_{tr}}{\mu L^3 R^2} m \tag{2.28}$$

The motion of the journal or the locus of the journal center, O_1 can be described by the time variable parameters in polar coordinates, ε and φ as shown in Figure 2.1. Now, substituting the components of the external load, F_x and F_y (Equations 2.12a-2.12b), and the components of the bearing load capacity, W_x and W_y (Equations 2.21-2.22), as shown in Figure 2.1, into and Equation 2.27 and Equation 2.28, results in the following set of differential equations, for ε and φ:

$$\overline{F}\cos\varphi = \overline{\kappa}(\varepsilon)(\varepsilon - \varepsilon_{tr})\,\mathrm{sgn}(\overline{U})\Delta - 0.5J_{12}\varepsilon\overline{U} + J_{12}\varepsilon\dot{\varphi} + J_{22}\dot{\varepsilon} + \overline{m}(\ddot{\varepsilon} - \dot{\varepsilon}\dot{\varphi}^2) \tag{2.29}$$

$$\overline{F}\sin\varphi = 0.5J_{11}\varepsilon\overline{U} - J_{11}\varepsilon\dot{\varphi} - J_{12}\dot{\varepsilon} - \overline{m}(\varepsilon\ddot{\varphi} + 2\dot{\varepsilon}\dot{\varphi}) \tag{2.30}$$

Solution of the above set of differential equations yields the time variable ε, which is used to compute friction force, F_f, by substituting it in Equation 2.6.

Applying the dimesionless variables defined in Equation 2.11, friction force, F_f, expressed by Equation 2.6, and friction coefficient, $f(t)$ expressed in Equation 2.7 can be converted into the following dimensionless forms respectively:

$$\overline{F}_f = f_m \overline{\kappa}(\varepsilon)(\varepsilon - \varepsilon_{tr})\,\mathrm{sgn}(\overline{U})\Delta + \frac{CR}{L^2}\frac{2\pi}{(1-\varepsilon^2)^{0.5}}\overline{U} \tag{2.31}$$

$$f(\tau) = \bar{f}(t) = \frac{\overline{F}_f}{\overline{F}} \tag{2.32}$$

Equations 2.29-2.32 represent the dynamic friction model for the conformal contact formed by the short hydrodynamic journal bearing. These equations can be used to determine the dynamic friction, $f(\tau)$, here after referred as f, for any dynamic shaft velocity, $U(t)$.

2.5 Simulation of Friction Model

To analyze the performance of the friction model developed in the preceding sections, the model is simulated for two different oscillating velocities, uni-directional and bi-directional oscillations. In order to perform successful simulation, the following five dimensionless constants of the bearing performance are necessary. Load on the bearing, geometry of the shaft, viscosity of the lubricant, and density of the shaft are the determining factors for these dimensionless constants. The five dimensionless constants listed in the following Table-1 have been selected for the simulation, which are calculated from the steady Stribeck curve, and other relevant information of the bearings and lubricants.

Table 2.1 List of dimensionless constants used in the simulation.

$\varepsilon_{tr} = 0.96$	$\varepsilon_b = 0.99$	$f_m = 0.2$	$RC/L^2 = 0.01$	$\overline{m} = 100$

It is very important to note that while repeating the simulation, the dimensionless load, $\overline{F}$ is not an independent constant, and it can be deduced from Equation 2.12 for any given value ε_{tr} while, the dimensionless velocitry, $\overline{U} = 1$. In the example simulations, the equation for dimensionless load (from Equation 2.12) becomes as:

$$\overline{F} = \sqrt{(-0.5J_{12tr}\varepsilon_{tr})^2 + (0.5J_{11tr}\varepsilon_{tr})^2} = 153.8 \tag{2.33}$$

where the J_{11tr} and J_{12tr} are the magnitudes of J_{11} and J_{12} evaluated at $\varepsilon = \varepsilon_{tr}$.

Now, the function representing the stiffness of the asperities in the contact $\overline{\kappa}(\varepsilon)$ is increasing function of ε, and it is assumed as a linear function of ε according to the following relation,

$$\overline{\kappa}(\varepsilon) = \overline{\kappa}_o \frac{\varepsilon - \varepsilon_{tr}}{\varepsilon_b - \varepsilon_{tr}} \tag{2.34}$$

where $\overline{\kappa}_o$ is a dimensionless spring constant equivalent to the stiffness of the asperities and it is determined from the following relation:

$$\overline{\kappa}_o = \frac{\overline{F}}{(\varepsilon_b - \varepsilon_{tr})} \tag{2.35}$$

where ε_b is the eccentricity at the border between boundary and mixed lubrication, [see friction versus velocity curve in Stribeck (1902)], and it can be calculated from the journal velocity, U_b , at this border line.

2.5.1 Simulation for Uni-directional Velocity Oscillations

Analysis of the friction model expressed by Equations 2.29-2.32 can be performed by verifying its results with earlier results of similar work. In this study, the simulation results of the present model have been compared with the empirical results of Hess and Soom(1990). Hess and Soom conducted tests for dynamic velocity oscillations having a uni-directional saw tooth wave form, oscillating between 0.01 and 1.0 m/s. Their study was focused on non-stick conditions.

To secure accuracy and continuity in the solution, the model is simulated for a uni-directional sinusoidal periodical velocity. The dimensionless dynamic velocity , $\overline{U}(\tau)$ (here after referred as $\overline{U}$) oscillates between 0.1 and 2.1, according to the following relation:

$$\overline{U}(\tau) = 1.1 + \sin(\alpha\tau) \qquad \text{or} \qquad \overline{U}(\tau) = 1.1 + \sin(\Omega t) \tag{2.36}$$

where α is the dimensionless form of the frequency of velocity fluctuations, which is defined as:

$$\alpha = \frac{\Omega}{\omega_{tr}} \tag{2.37}$$

where Ω is the frequency of the velocity oscillations, and ω_{tr} is the critical angular speed of journal at the transition point.

Friction simulation have been carried by numerically integrating Equations 2.29 and 2.30. Fortran language has been used for numerical integration (see Appendix). Later, special tools have been chosen for simulation. In the simulation, operating velocity has been chosen to oscillate according the Equation 2.36. The transition parameters for the simulation are determined from the operating conditions of bearings. The model has been simulated for the conditions listed in Table 1 and Equations 2.33-2.36. The solution of these equations (Equations 2.29 and 2.30) for the periodic velocity defined in Equation 2.36, yielded the periodic $\varepsilon(t)$. In the simulation, the initial values for ε, and φ have been selected arbitrarily, and Equations 2.29-2.30 have been integrated over several cycles until a periodic steady state solution is reached. Periodic steady state solution is that solution in which the values of periodic ε, and φ repeat for each cycle. Thus the solution obtained for ε is substituted in Equations 2.31-2.32 to determine the periodic friction coefficient, f. The results are presented in the form of $f - \overline{U}$.

Simulations have been carried for different frequency of velocity oscillations, α, different dimensionless journal mass, $\overline{m}$, and different dimensionless load $\overline{F}$. Dynamic $f - \overline{U}$ curves are shown in Figures 2.2- 2.4. At low frequency of velocity oscillations, (low α or Ω), the $f - \overline{U}$ plot reduces to the well known Stribeck curve, while at high frequency the dynamic effects are more pronounced (see Figure 2.2). The simulation results presented in the Figures 2.2-2.4 show that the differential equations representing

the friction model predict the existence of a phase shift between the velocity, U and the friction coefficient, f. It can be seen from the plot of f versus $\overline{U}$, the phase shift is manifested as a hysteresis phenomenon as observed by Hess and Soom (1990).

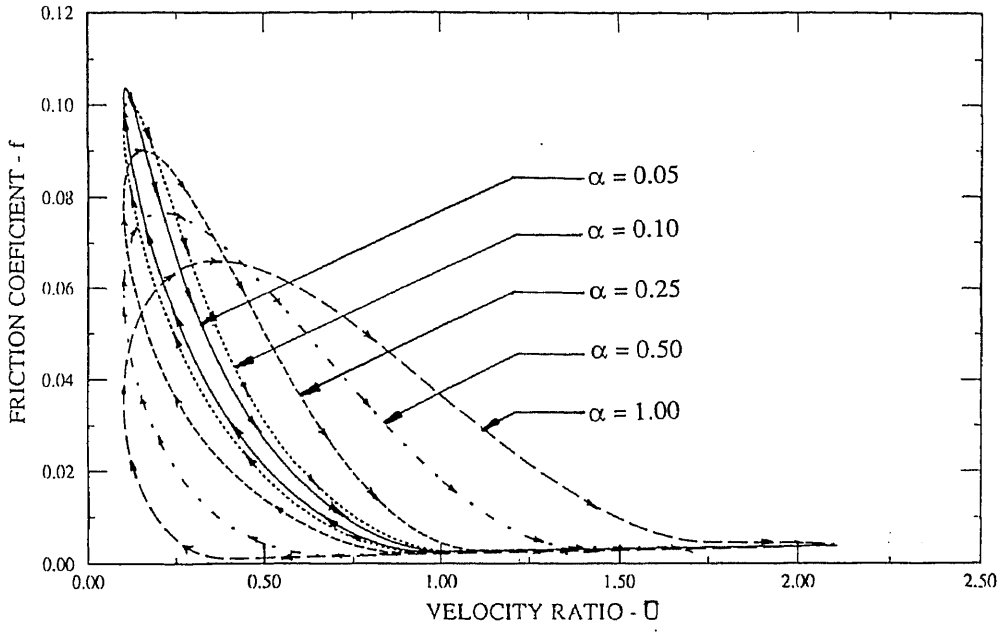

Figure 2.2 Friction coefficient, f *Vs* velocity ratio (journal velocity), $\overline{U}$ with $\overline{U} = 1.1 + \sin \alpha\tau$, and $\overline{m} = 100$ for various frequency ratio, α.

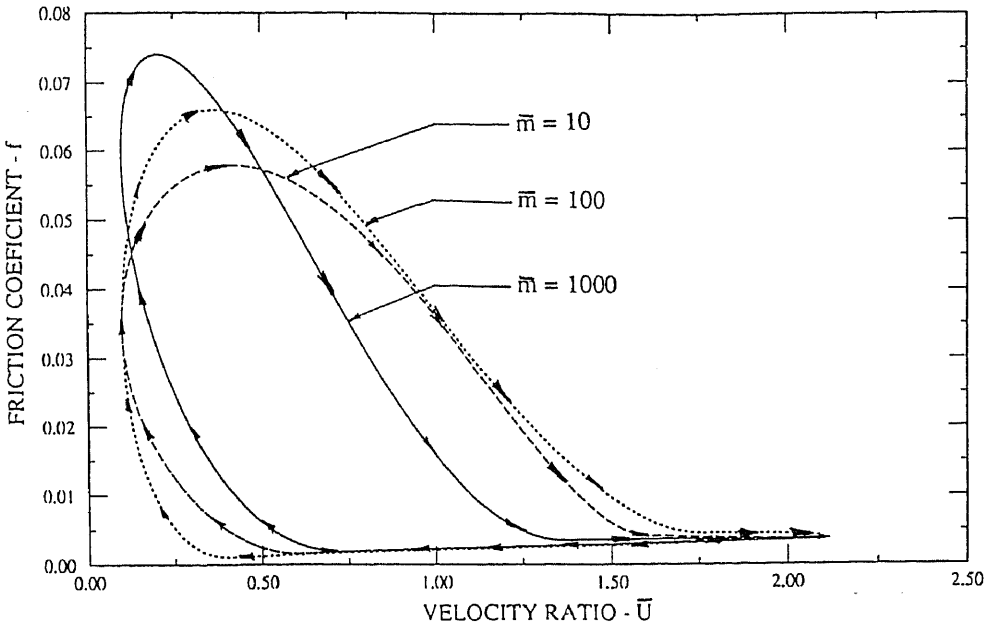

Figure 2.3 Friction coefficient, f *Vs* velocity ratio (journal velocity), $\overline{U}$ with $\overline{U} = 1.1 + \sin \alpha\tau$, and frequency ratio $\alpha = 1.0$ for various dimensionless mass $\overline{m}$.

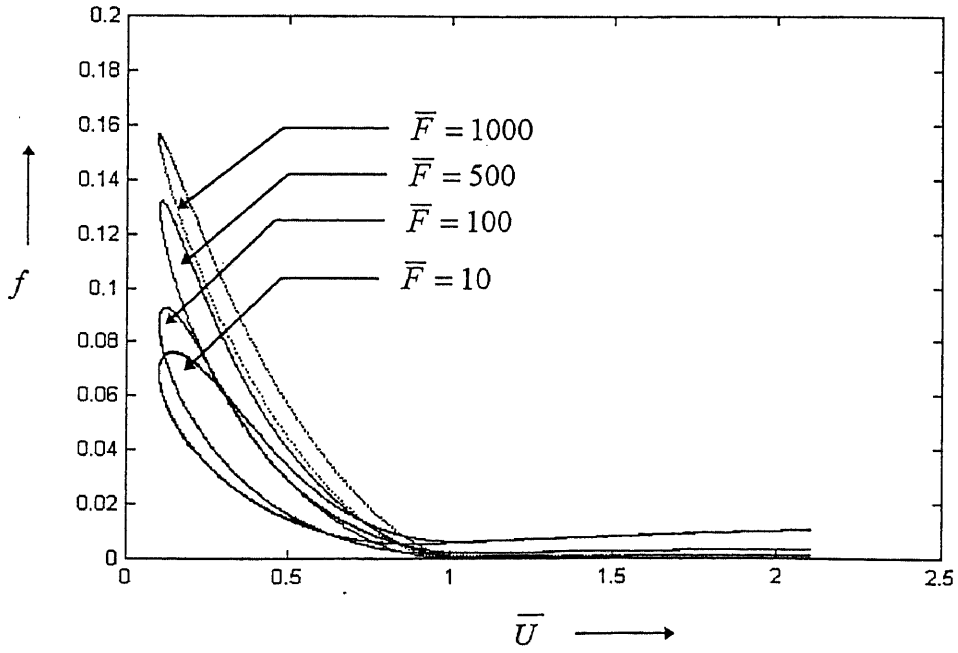

Figure 2.4 Friction coefficient, f *Vs* journal velocity, $\overline{U}$ with $\overline{U} = 1.1 + \sin \alpha\tau$, and frequency ratio $\alpha = 0.1$ for various dimensionless load, $\overline{F}$ with $\overline{m} = 100$.

2.5.2 Simulation for Bi-directional Velocity Oscillations

In most of the precise motion systems, the operating velocity oscillates in two directions passing through the zero velocity. Therefore, the model has been simulated for bi-directional velocity oscillations. This kind of velocity oscillations are very common in control systems. In this case, the dimensionless periodic velocity, $\overline{U}(\tau)$ oscillates sinusoidally between -2.0 and 2.0 according to the following relation.

$$\overline{U}(\tau) = 2\sin(\alpha\tau) \qquad \text{or} \qquad \overline{U}(\tau) = 2\sin(\Omega t) \tag{2.38}$$

The simulation results for the velocity oscillations expressed in Equation 2.38 have been presented as $f - \overline{U}$ curves for different frequencies as shown in Figure 2.5, which shows that the friction at zero velocity is less than the maximum friction as represented by Coulomb friction, and this maximum friction decreases with increase in frequency of oscillations. These curves show a discontinuity at zero velocity which increases with decrease in frequency ratio α. It is assumed that during bi-directional velocity oscillations, the viscosity in the contact varies as a result of heat dissipated at the contact due to high friction during velocity reversals. Based on this assumption, for any given load, the viscosity of the fluid film in the contact during bi-directional velocity oscillations is can be less than the viscosity of the fluid film in the contact during uni-directional velocity oscillations. As a result, it can be seen that the transition velocity during bi-directional velocity oscillations is different when compared to the transition velocity during uni-directional oscillations. This observation is very important when the model is verified with friction measurements.

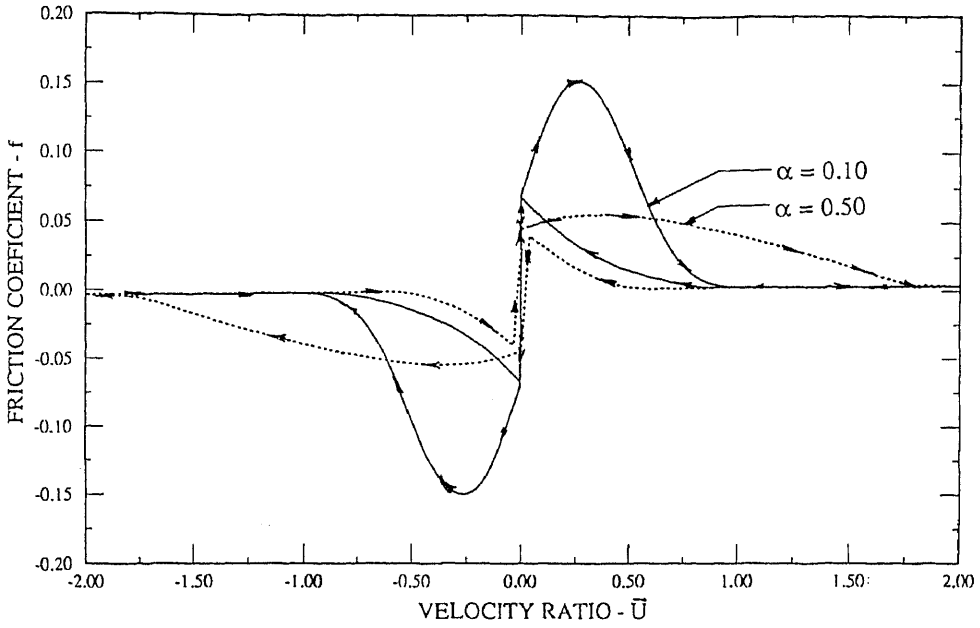

Figure 2.5 Friction coefficient, f *Vs* velocity ratio (journal velocity), $\overline{U}$ with $\overline{U} = 2\sin\alpha\tau$, and dimensionless mass $\overline{m} = 100$ for various frequency ratio α.

2.6 Summary

In this chapter, an analytical model have been developed for a lubricated conformal contact formed by a short journal bearing. The model is based on the physics of the system and the hydrodynamic lubrication theory of short journal bearing. The model is simulated for uni-directional and bi-directional velocity oscillations oscillating sinusoidally. Simulation results show that the model can successfully capture the friction behavior under any dynamic velocity conditions. According the simulation results, the dynamic friction under oscillating velocity shows an hysteresis effect in friction as exhibited by $f - \overline{U}$ curves, in agreement with the earlier experiments and empirical friction models. At relatively low frequency, the dynamic curves can be approximated by Stribeck curve. However, at high frequencies of velocity oscillations, this approximation is not valid. The

instantaneous friction is higher (compared with the steady friction) when the friction force is rapidly decreasing, due to increasing velocity, and lower when the friction is rapidly increasing, due to decreasing velocity. In other words, there is a "memory effect" in the sense that instantaneous friction is affected by the most recent friction. It is interesting that near the maximum velocity, the friction values at increasing and decreasing velocity almost coincide, because the rate of change of friction at this region is very low.

At low oscillating frequencies, there is an agreement with the conclusions of Hess and Soom (1990) concerning the trend of increasing time lag with the lubricant viscosity and external load. The curves of the present study show increasing phase-lag angle with the frequency, but one must keep in mind that at higher frequency, the complete cycle time is shorter. This compensation explains the interesting observation of Hess and Soom (1990) of a time lag independent of the oscillation frequency. This conclusion can be considered as an approximation, which is valid at relatively low frequencies and low mass. In addition, the study indicates that there is a significant effect of the mass of the sliding body and external load on dynamic friction. According to the results, in this model, the phase lag in friction is a function of the frequency of velocity oscillations, mass and load. The external force is not necessarily proportional to the mass of the journal, and should be considered as a separate parameter.

Simulation of the model for bi-directional sinusoidal velocity oscillations shows a discontinuity in $f - \overline{U}$ curve at zero velocity. The discontinuity is highly undesirable from the point of view of control theory , because the systems with discontinuity are very difficult to control. The discontinuity can be eliminated by introducing the Dahl effect.

The Dahl effect, Dahl (1977) can be defined as an elastic deformation of the surface asperities as well as bearing support due to the reaction forces which is proportional to the friction force. The effect is expected to be significant at zero velocity. In addition to the Dahl effect, it is also expected that the visco-elastic properties of the lubricant play an important role at dynamic condition. The visco-elastic oil film force equation Harnoy (1976) includes terms that are proportional to the rate of change of velocity and film thickness. Also, the maximum friction, as well as friction at the zero velocity are decreasing with the frequency ratio α. The discontinuity resulted in bi-directional velocity oscillations is one of the limitations for this model to use in precise motion. However, there is no significant limitation for this model when operated under uni-directional velocity oscillations.

The theory developed in this chapter has been verified experimentally by using a specially designed friction measuring apparatus. Design, development, and testing of the friction measurement apparatus as well as comparison of friction measurements with theoretical results have been discussed in Chapter 3.

To investigate the discontinuity in friction at zero velocity, during bi-directional velocity oscillations, the model is extended to study and analyze the effect of resistance forces such as elastic and friction forces present in the bearing system on friction behavior (Chapter 4).

The concepts introduced in developing this friction model are extended to develop friction model for a non-conformal line contact formed by roller sliding over a flat surface

(Chapter 5). The concepts of the current model can be used to develop analytical dynamic friction models for other non-conformal contacts such as point contacts.

CHAPTER 3

MEASUREMENT OF DYNAMIC FRICTION IN JOURNAL BEARINGS

3.1 Introduction

The analytical model developed in the previous chapter is based on the physics of the lubricated conformal contact to investigate friction in a hydrodynamic journal bearing under dynamic velocity conditions. The simulation results of the model is in agreement with the experimental work of Hess and Soom (1990), Polycarpou and Soom (1992) on dynamic friction in a line contact, which is a different tribological situation. Hess and Soom (1990), Polycarpou and Soom (1992) considered a line contact between a rotating disk and the flat face of a cylinder under a constant load for oscillating velocities. Even though, the comparison shows a qualitative agreement in the friction behavior, the results suggest a need for more experimental work in dynamic friction. Further, the model developed in Chapter 2 will be valid and useful for on-line friction estimation and compensation only if it is verified with the appropriate experimental work.

With the aim of verification of the analytical model, immediate objective of this study has been extended to conduct friction tests on lubricated sleeve bearings. The goal is to measure friction for different oscillating velocity conditions including uni-directional as well as bi-directional oscillations for various frequencies. A special apparatus has been designed and developed for measuring the dynamic friction in short journal bearings. This apparatus can be used to test each of the parameters affecting dynamic friction so that the role of each can be assessed separately and effectively. Long term objectives of this apparatus are to use the apparatus for further refinement and verification of theoretical models, and to obtain insight into areas which require further investigation including

friction compensation methods. The apparatus can be utilized for estimating the effect of friction on the parameters such as displacement, velocity by using the observers of closed-loop control theories. Stick-slip friction in the journal bearings can be investigated by modifying this model.

3.2 Experimental Apparatus

Commercially available friction testing machines for sleeve bearings are suitable only for experiments at constant shaft speed. One example of such machines is a testing machine in which a pendulum is attached to the bearing and its swing angle determines the friction coefficient. These machines are very well suitable for testing the bearing under steady velocity conditions. However, under dynamic conditions, these testing machines have errors caused by inertial forces. Moreover, in many cases it is impossible to separate the bearing friction from other friction in the system. Further, most of these types of machines do not have on-line recording for time-variable friction. To overcome all these problems, a special apparatus has been designed and developed by the research team including the author, in which the average friction of four equally loaded sleeve bearings can be isolated from any other forms of friction present in the system. In addition, the errors caused by inertial forces can be reduced to a negligible magnitude.

The sectional view of the friction measurement apparatus for sleeve bearings is shown in Figure 3.1. Figure 3.2 is a photograph of the friction apparatus. The design concept of this apparatus is to apply internal load, action and reaction, between the housing of each two of four equal sleeve bearings. In the system, two of the bearings are

prestressed toward the other two by means of a thin elastic ring. The total friction torque of the four equally loaded sleeve bearings can be measured by load cells. These load cells measure the friction torque while preventing the rotation of the external bearing housing. Thus, the friction torque of the four bearings is isolated from other sources of friction, such as friction in the ball bearings supporting the shaft. The magnitude of the normal load on the two test-bearings together can be obtained by measuring the deformation of the calibrated elastic ring. Load on the bearing can be applied by tightening the nut to prestress the ring. The load-cell readings are stored in a computer-assisted data acquisition system. Any desired controllable time-variable motion of the shaft can be generated with a reasonable accuracy with a computer controlled DC servo motor.

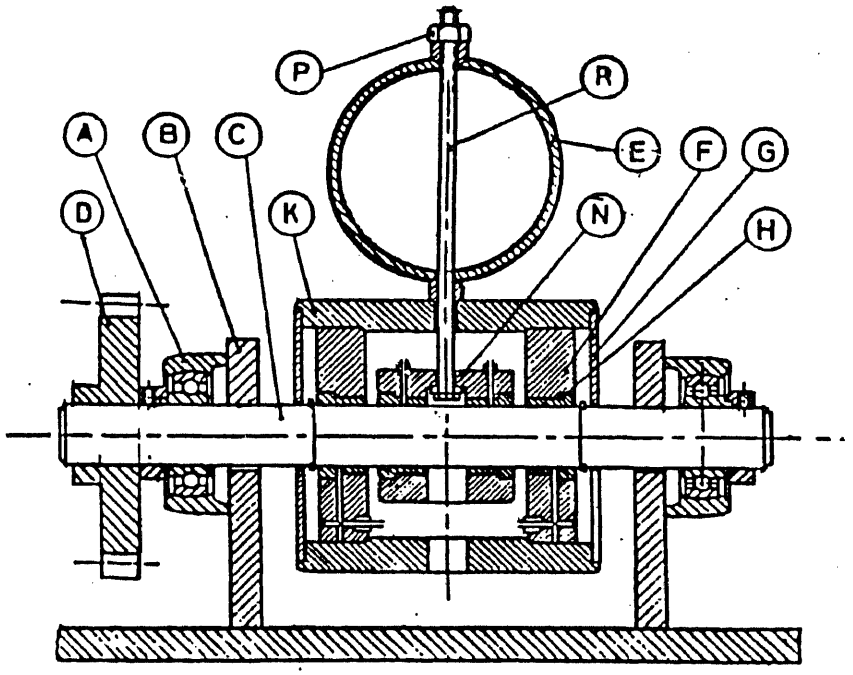

Figure 3.1 Cross-sectional view of friction measurement apparatus.

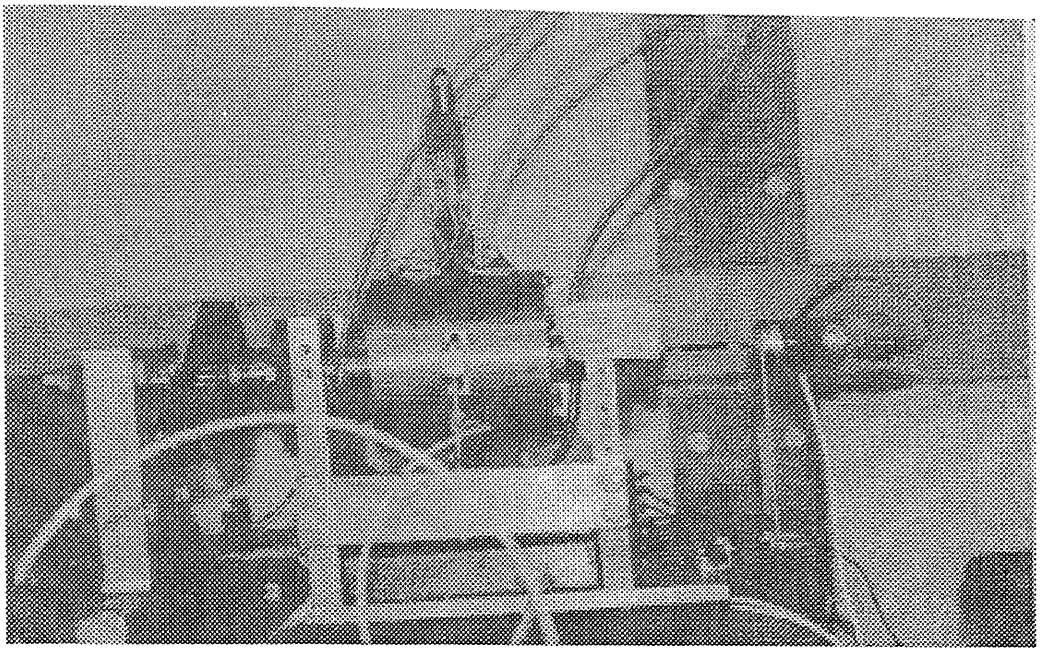

Figure 3.2 A photograph of friction measurement apparatus.

3.2.1 Experimental Layout

The layout of the friction measurement system comprises a mechanical test apparatus, a personal computer, a data acquisition unit, a control interface board, a load cell, a digital strain indicator, signal amplifiers and DC power supplies as shown in Figure 3.3.

The friction measurement apparatus shown in Figure 3.1, contains a main support frame, shaft-bearing assembly, bearing loading assembly, DC servo-motor, tachometer (calibrated DC generator), strain gage mounting block and lubrication system with reservoir.

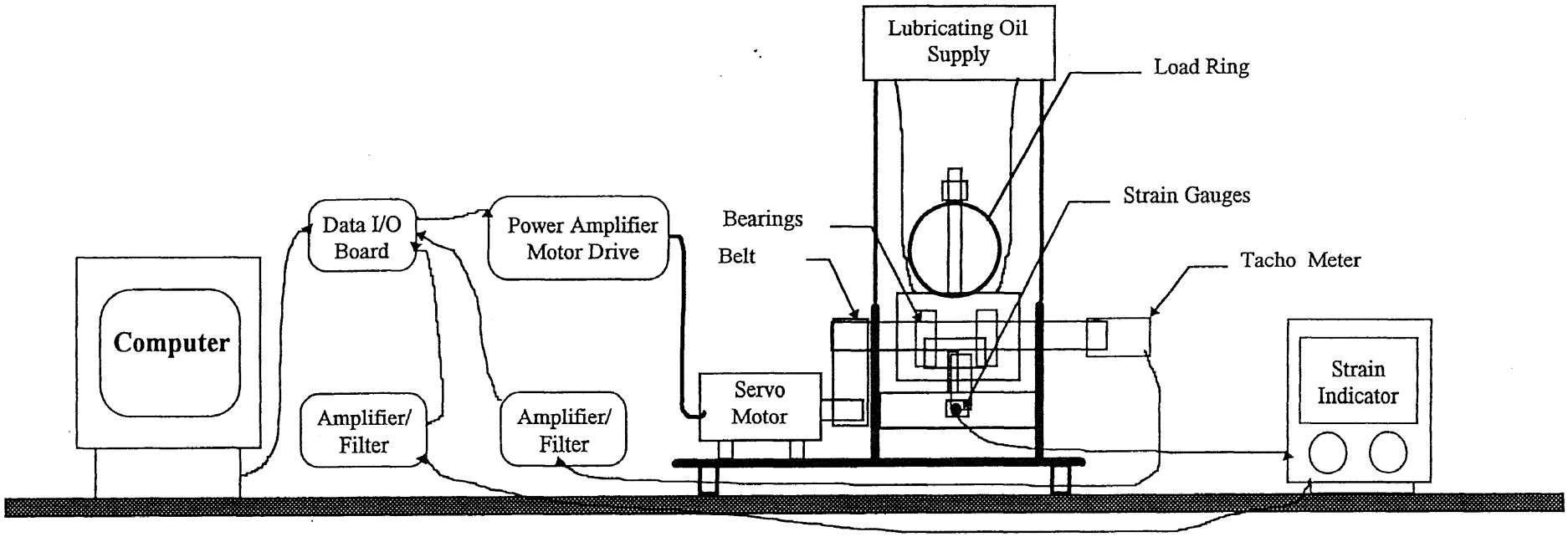

Figure 3.3 Experimental set-up for measuring friction in hydrodynamic journal bearings.

3.2.2 Design Features and Operation Principle of Apparatus

Design features of the mechanical test apparatus are explained with the aid of Figure 3.1. The test shaft (*C*) is supported by two ball bearings (*A*) attached to the main support frame (*B*). There are four brass sleeve test-bearings (*H*). Data related to the dimension of the test bearings used in the apparatus are given in Table 3.1.

Table 3.1 Dimensional data of test bearing

Diameter of the bearing ($D = 2R$)	$D = 25.4 \times 10^{-3}$ m
Length of the bearing	$L = 19 \times 10^{-3}$ m
Radial clearance in the bearing	$C = 0.001 \times 2R$
Mass of the journal	$m = 1.250$ kg

The adjustable load can be applied by tightening the nut (*P*) on bolt (*R*) which applies internal force between the inner and outer housings (*N*) and (*K*) and causing the two inner bearings and the two outer bearings to be loaded equally in opposite directions. Thus the load can be applied equally on each of the bearings. The apparatus uses a computer controlled DC motor, in which the computer generates voltage signals to drive the servo-motor which causes the shaft in the sleeve to rotate at specified velocity conditions. The transmission consists of a DC servo-motor connected through a timing belt and two pulleys (*D*). A lubricating oil reservoir as shown in Figure 3.3 is mounted above the mechanical apparatus in order to supply oil by gravity into the four bearings through four segments of flexible tubing. Oil expelled out from the bearings accumulate in the external bearing housing and drains through a hole into a collecting vessel through an outlet tube.

The friction torque of the four bearings is measured by a load cell having a full bridge strain gage. The strain gage consists four strain-gages mounted on a specially designed device which supports the external housing and prevents its rotation. The output signals of friction torque and test-shaft tachometer are filtered, amplified, and transferred to the computer for further processing such as data conversion, storage and analysis.

3.3 Experimental Investigations

The apparatus described in the above sections has been used to measure the dynamic friction between the shaft and four sleeve bearings for different sinusoidal excitations. The sinusoidal excitation voltage applied to the servo-motor has been generated by the computer system which causes the shaft to oscillate periodically in the specified frequency. Friction measurements have been conducted for uni-directional and bi-directional oscillations with various frequency ratios for two different loads. The frequency determines the rate of change in the magnitude of friction which is shown to be an important parameter of dynamic friction. Results are presented in the form of friction versus velocity curves.

Experiments have been conducted for two different constant loads of 308 N and 386 N, as measured at the elastic ring, for two kinds of velocity oscillations. Each bearing, in this case, is loaded by a normal force of 154 N, 193 N respectively. The lubricant used is a commercial multi-grade engine oil *SAE 10 W-40*. Viscosity of multi-grade oils is less sensitive to variation of temperature, but one must keep in mind that the viscosity of the oil film in the bearing is not constant, but varies with temperature

variations caused by dissipation of friction energy during the test. This certainly affects the repeatability of the tests, but after several cycles, a steady state has been reached in which repeatability has improved.

The results obtained from the friction measurements have been used to determine the dimensionless data required for simulating the analytical model of Harnoy and Friedland (1993) discussed in Chapter 2. Equations 2.29-2.32 of the short journal bearing model have been solved to simulate the dynamic friction. From the experimental Stribeck curve for the load $F = 308$ N, velocity at the transition $U_{tr} = 0.125$ m / s ($\omega_{tr} = 9.8$ rad / sec), and $f_{tr} = 0.0015$ have been obtained. Using these results and Equations 2.31-2.33, eccentricity at the transition, ε_{tr}, viscosity of the oil, μ have been determined. The viscosity of the oil was found to be $\mu = 0.0127$ N.s.m^{-2}. For load, $F = 386$ N, the transition velocity has been found as $U_{tr} = 0.145$ m / s ($\omega_{tr} = 11.47$ rad / sec), and all other data remain same. Following are the dimensionless data obtained from the friction measurements which has been used in simulating the theoretical model:

Table 3.2 List dimensionless constants.

$\varepsilon_{tr} = 0.71$	$\varepsilon_b = 0.995$	$f_m = 0.1$
$\overline{m} = 8.5x10^{-6}$	$\overline{F} = 2.5984$	$\overline{\kappa}_o = 9.1173$

3.3.1 Friction Measurements for Uni-directional Sinusoidal Oscillations

Friction measurements in the sleeve bearings for uni-directional velocity oscillations are shown in Figures 3.4-3.12 for various frequencies and for various loads. These curves

shows very good qualitative as well as quantitative agreement between experimental and analytical solutions. It is interesting to note that hysteresis effect in mixed region is in very good agreement. At low frequency of velocity oscillations, analytical solution shows a repetitive linear relation in fully developed region with out any hysteresis when compared to the experiments. At high frequency, both analytical and experimental solutions display almost same hysteresis. Plots at higher load of 386 N also displays similar hysteresis phenomena. The analytical model has been simulated for the following dimensionless periodic velocity oscillations.

$$\overline{U} = 1.85 + 1.75\sin(\alpha t) \tag{3.1}$$

where α is the frequency of shaft oscillations, $\overline{U}(=U/U_{tr})$, is dimensionless velocity of the shaft, and U_{tr}.

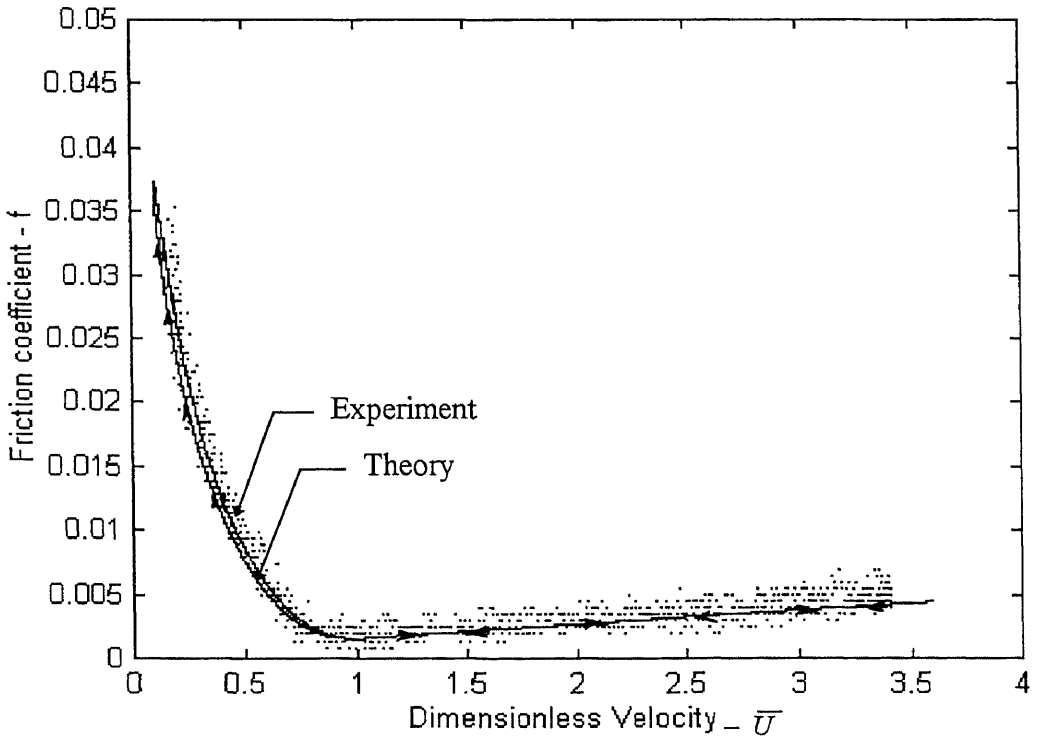

Figure 3.4 Friction coefficient f *Vs* dimensionless velocity $\overline{U} = 1.85 + 1.75\sin(\alpha\tau)$ at frequency $\omega = 0.05$ rad / sec, $(\alpha = 0.006)$ for the load $F = 308$ N.

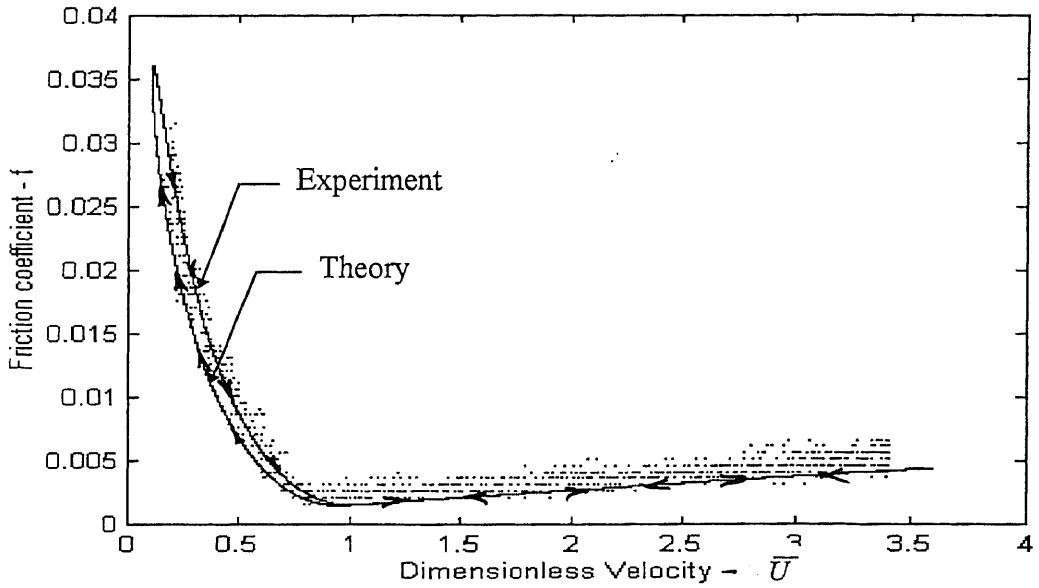

Figure 3.5 Friction coefficient f *Vs* dimensionless velocity $\overline{U} = 1.85 + 1.75\sin(\alpha\tau)$ at the frequency $\omega = 0.1$ rad / sec, $(\alpha = 0.012)$ for the load $F = 308$ N.

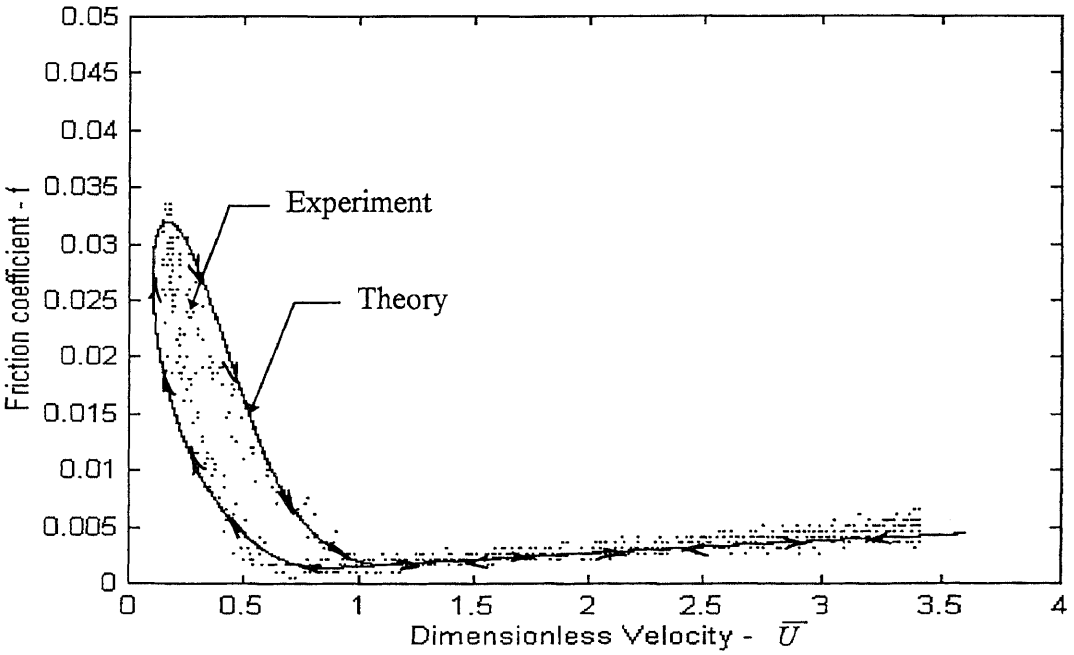

Figure 3.6 Friction coefficient f *Vs* dimensionless velocity $\overline{U} = 1.85 + 1.75\sin(\alpha\tau)$ at frequency $\omega = 0.5$ rad / sec, $(\alpha = 0.06)$ for the load $F = 308$ N.

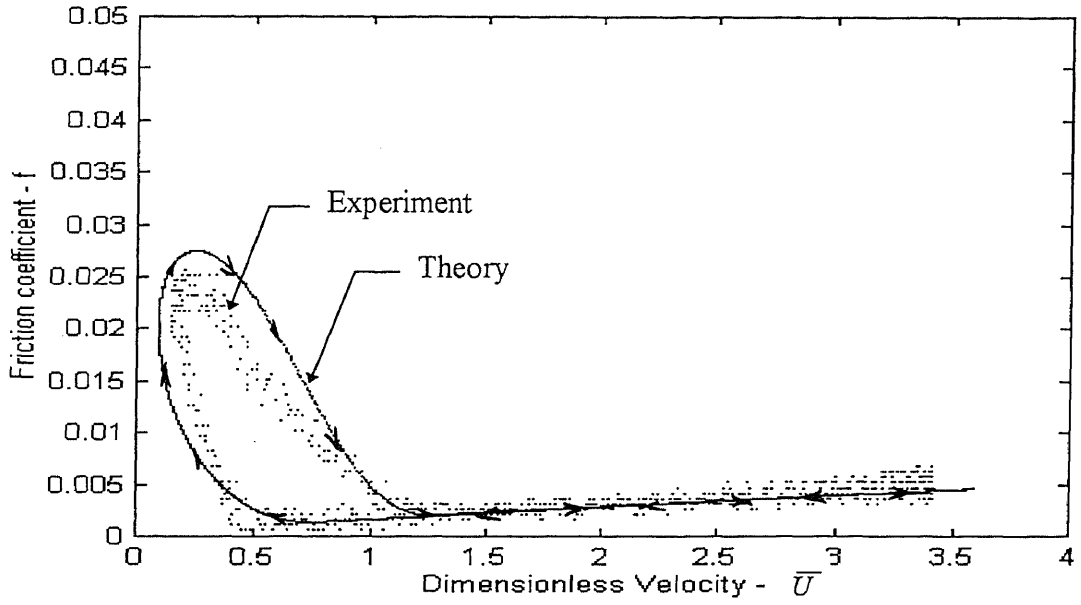

Figure 3.7 Friction coefficient f *Vs* dimensionless velocity $\overline{U} = 1.85 + 1.75\sin(\alpha\tau)$ at frequency $\omega = 1.0$ rad / sec, $(\alpha = 0.12)$ for the load $F = 308$ N.

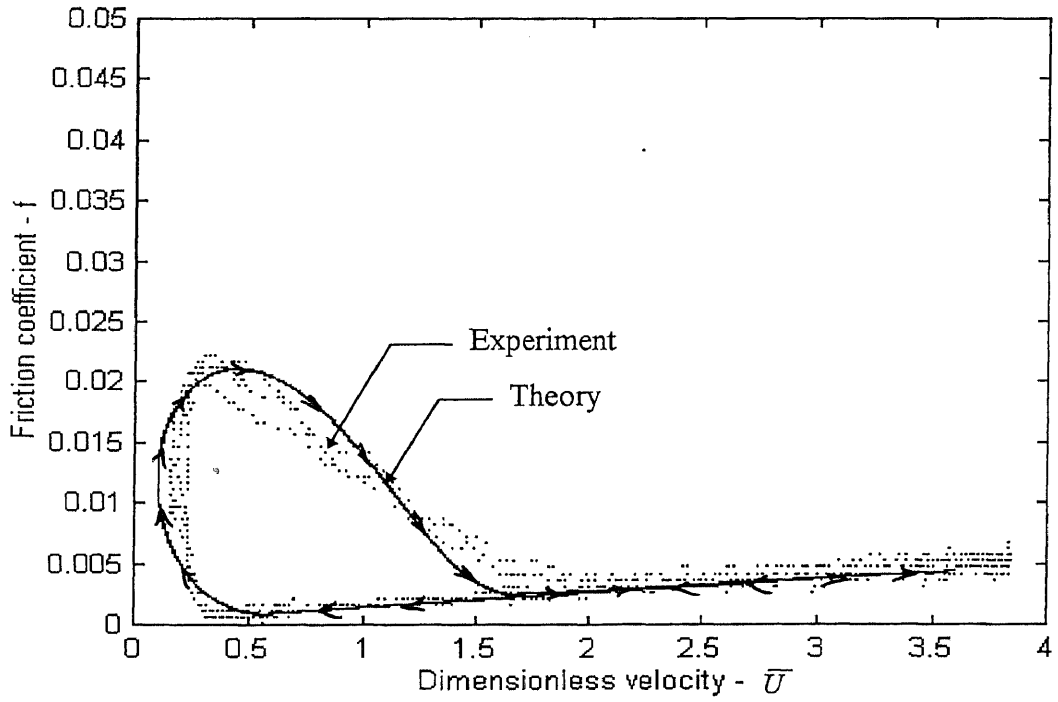

Figure 3.8 Friction coefficient f *Vs* dimensionless velocity $\overline{U} = 1.85 + 1.75\sin(\alpha\tau)$ at frequency $\omega = 2.0$ rad / sec, $(\alpha = 0.24)$ for the load $F = 308$ N.

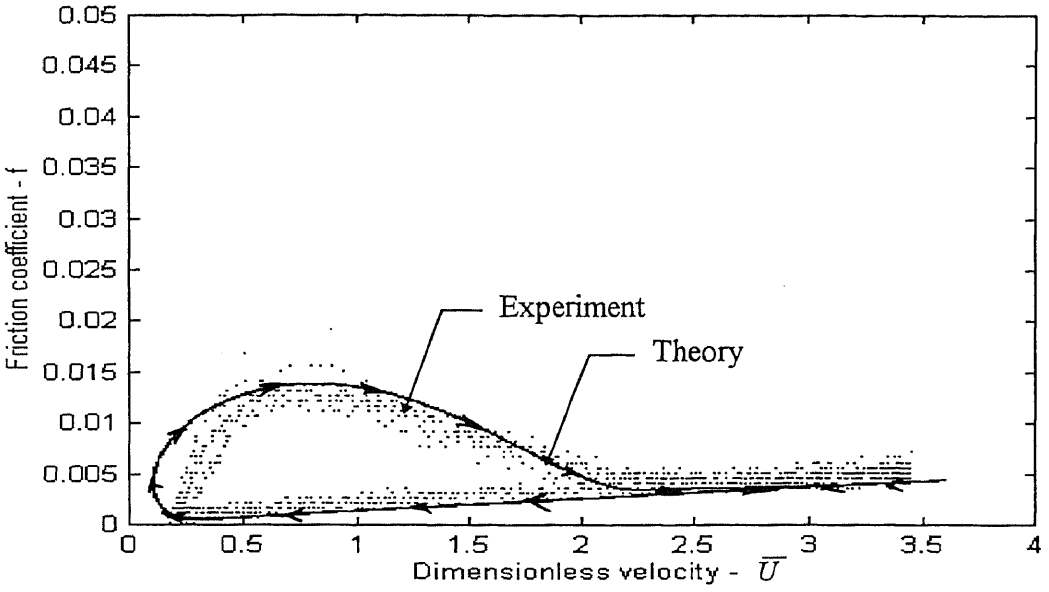

Figure 3.9 Friction coefficient f *Vs* dimensionless velocity $\overline{U} = 1.85 + 1.75\sin(\alpha\tau)$ at frequency $\omega = 4.0$ rad / sec, $(\alpha = 0.48)$ for the load $F = 308$ N.

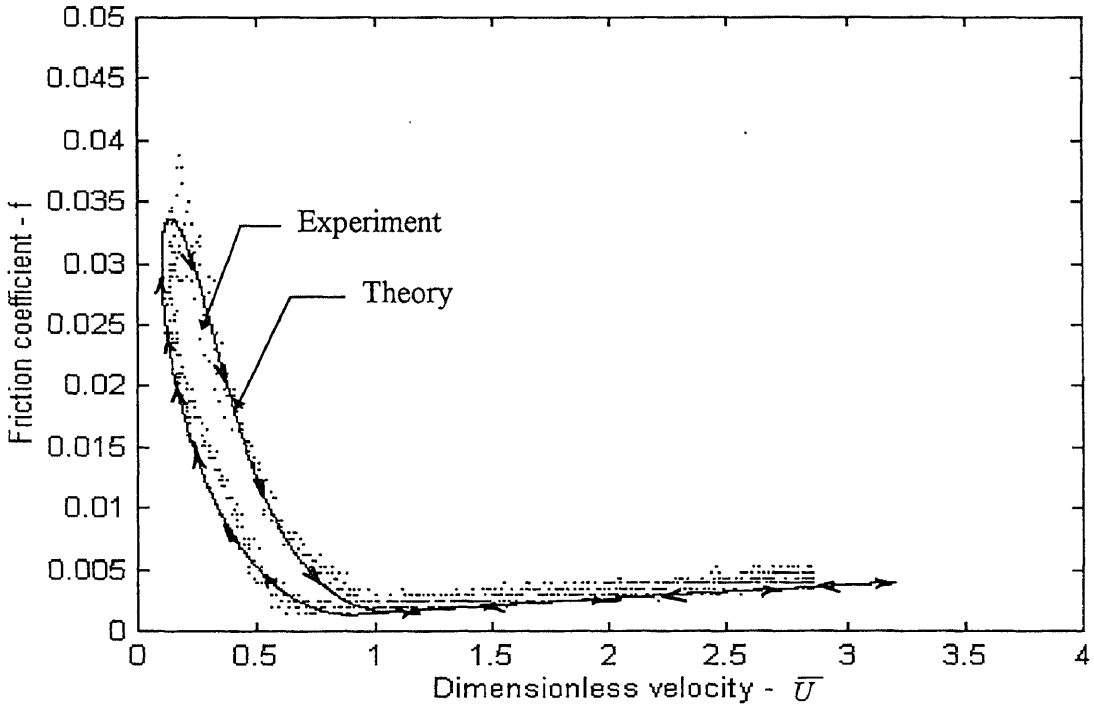

Figure 3.10 Friction coefficient f *Vs* dimensionless velocity $\overline{U} = 1.85 + 1.75\sin(\alpha\tau)$ at frequency $\omega = 0.5$ rad / sec, $(\alpha = 0.044)$ for the load $F = 386$ N.

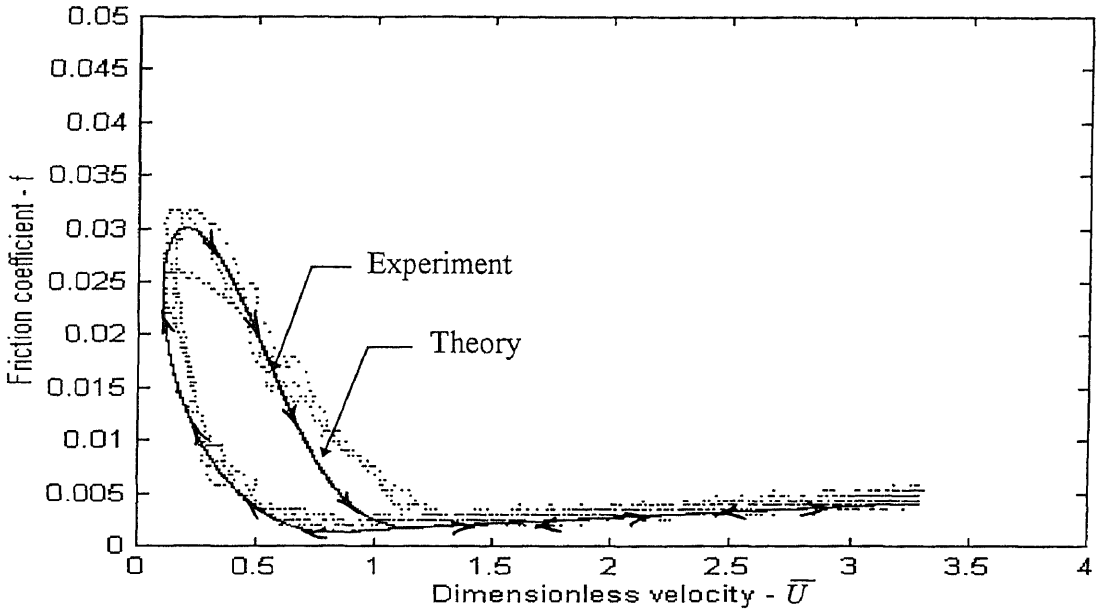

Figure 3.11 Friction coefficient f *Vs* dimensionless velocity $\overline{U} = 1.65 + 1.55\sin(\alpha\tau)$ at the frequency $\omega = 1.0$ rad / sec, $(\alpha = 0.0877)$ for the load $F = 386$ N.

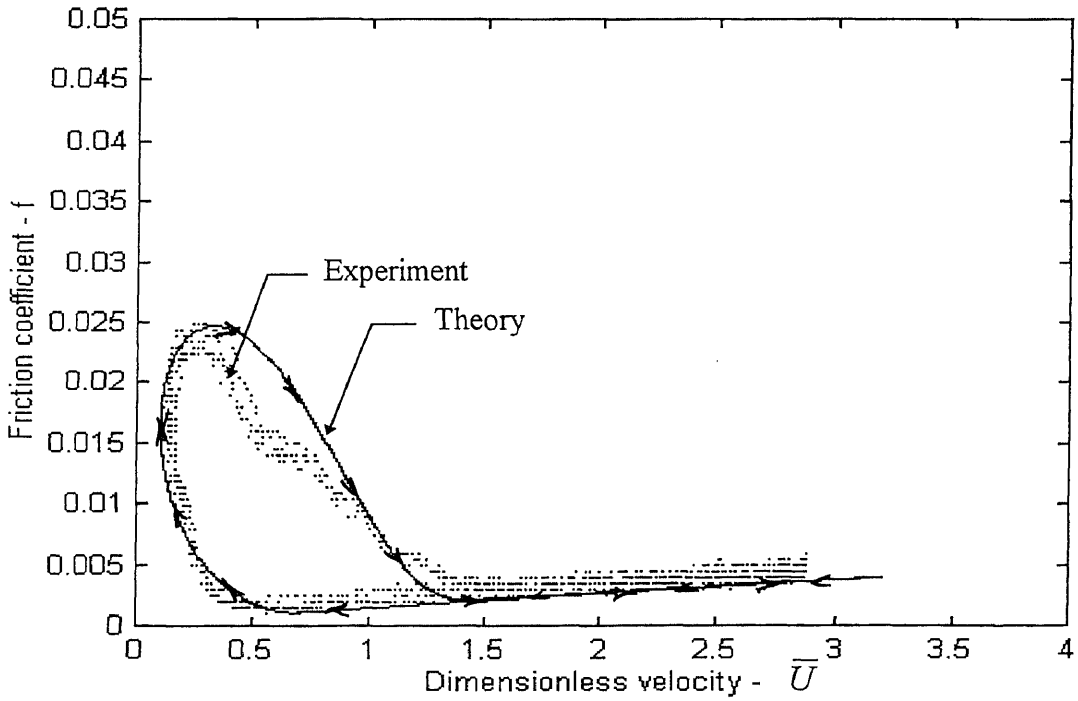

Figure 3.12 Friction coefficient f *Vs* dimensionless velocity $\overline{U} = 1.65 + 1.55\sin(\alpha\tau)$ at frequency $\omega = 2.0$ rad / sec, $(\alpha = 0.175)$ for the load $F = 386$ N.

3.3.2 Friction Measurements for Bi-directional Sinusoidal Oscillations

Friction measurements have been conducted for bi-directional velocity oscillations also, and the results are shown in Figures 3.13-3.20. These curves show very good qualitative and quantitative agreement between experimental and analytical solutions in mixed as well as full lubrication regions. But, at zero velocity, the magnitude of discontinuity differs. The friction observed in the experiments at zero velocity is higher than that obtained in analytical model. It is interesting to note that the magnitude of discontinuity at zero velocity both in the experimental as well as analytical solution reduces with increase in the frequency of velocity oscillations. The model has been simulated for the following dimensionless periodic velocity oscillations.

$$\overline{U} = 3.0\sin(\alpha t) \tag{3.2}$$

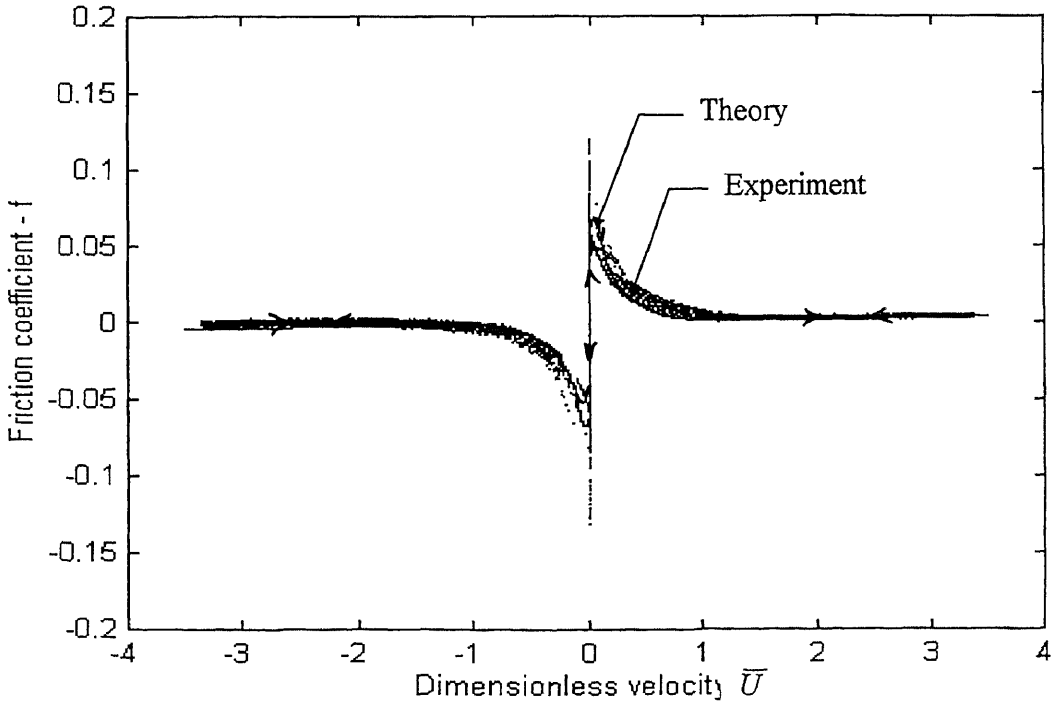

Figure 3.13 Friction coefficient f *Vs* dimensionless velocity $\overline{U} = 3.5\sin(\alpha\tau)$ at frequency $\omega = 0.01$ rad / sec, ($\alpha = 0.00125$) for the load $F = 308$ N.

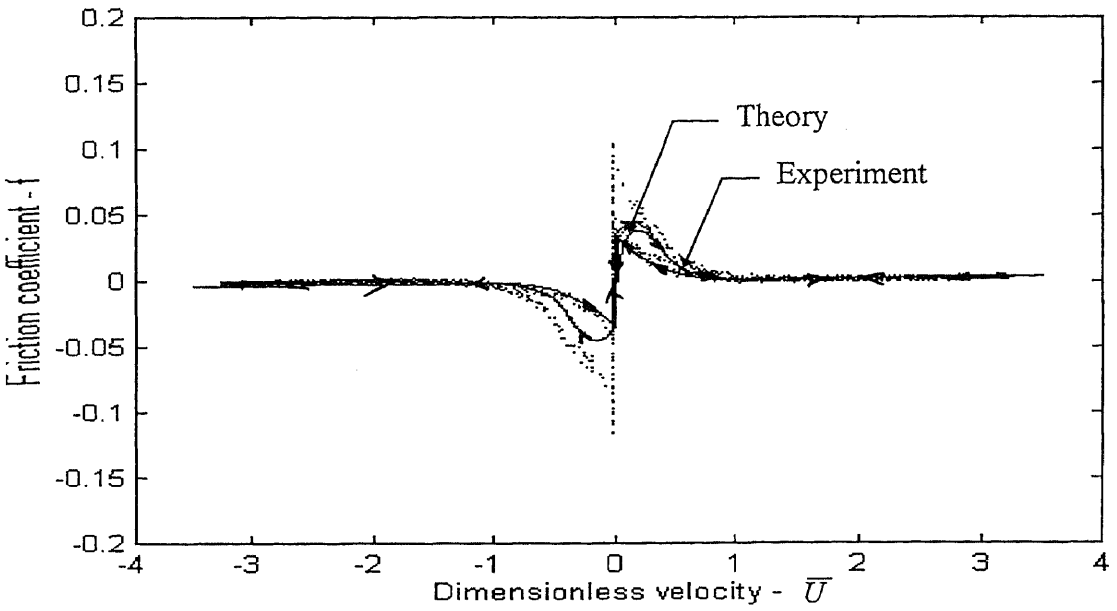

gure 3.14 Friction coefficient f *Vs* dimensionless velocity $\overline{U} = 3.5\sin(\alpha\tau)$ at frequency $= 0.1$ rad / sec, $(\alpha = 0.01)$ for the load $F = 308$ N.

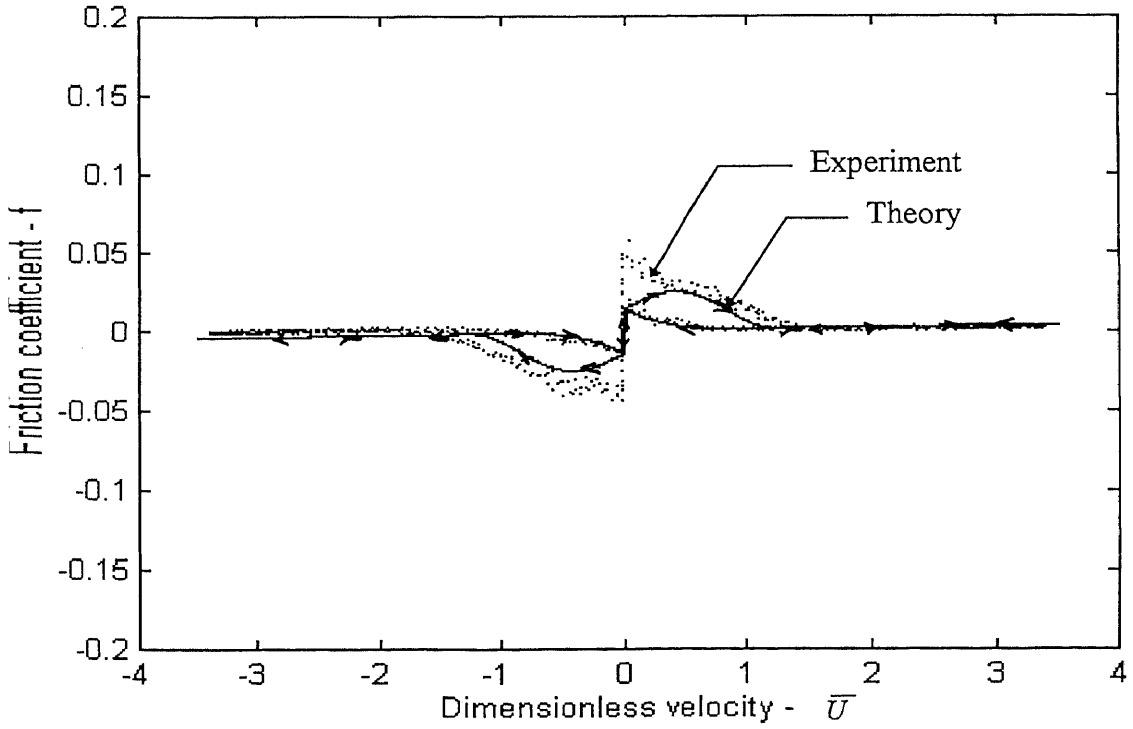

Figure 3.15 Friction coefficient f *Vs* dimensionless velocity $\overline{U} = 3.5\sin(\alpha\tau)$ at frequency $\omega = 0.5$ rad / sec, $(\alpha = 0.05)$ for the load $F = 308$ N.

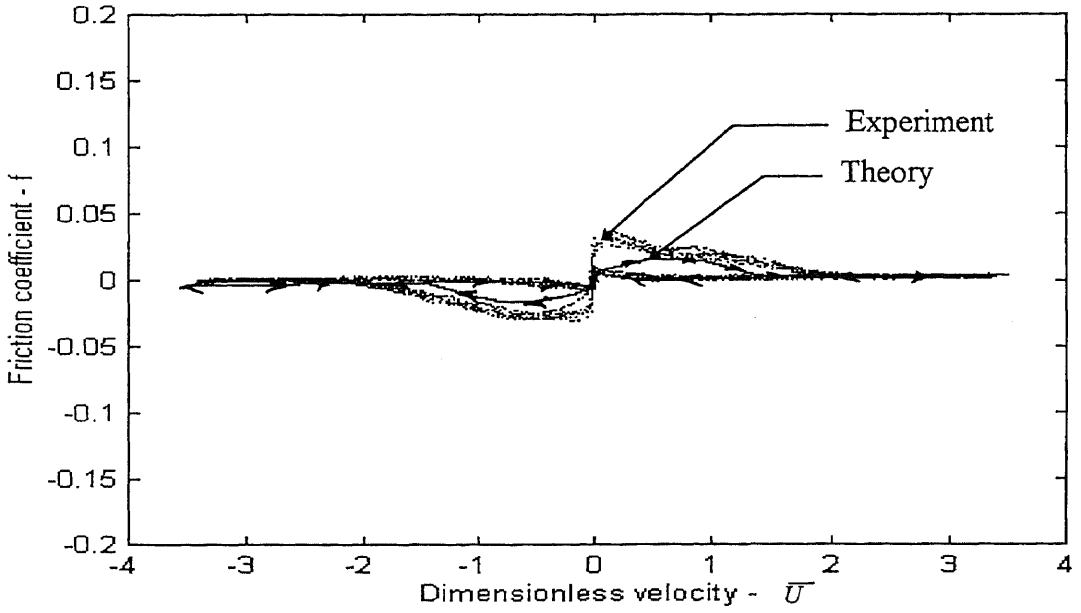

Figure 3.16 Friction coefficient f *Vs* dimensionless velocity $\overline{U} = 3.5\sin(\alpha\tau)$ at frequency $\omega = 1.0$ rad / sec, $(\alpha = 0.1)$ for the load $F = 308$ N.

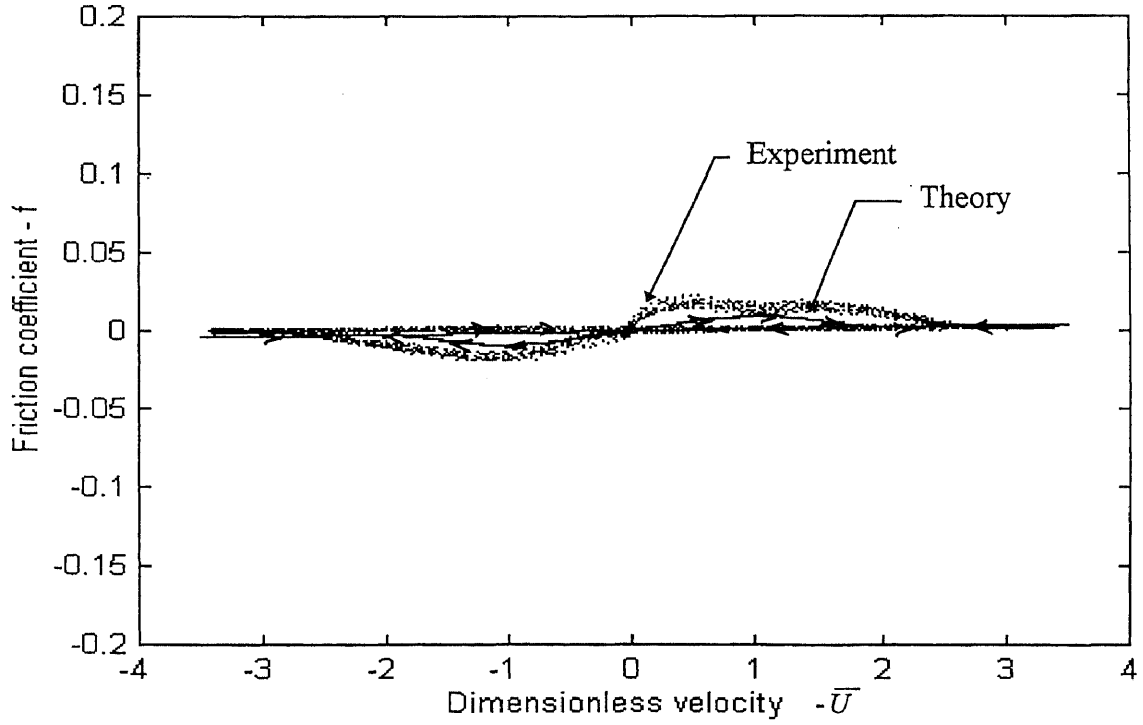

Figure 3.17 Friction coefficient f *Vs* dimensionless velocity $\overline{U} = 3.5\sin(\alpha\tau)$ at frequency $\omega = 2.0$ rad / sec, $(\alpha = 0.2)$ for the load $F = 308$ N.

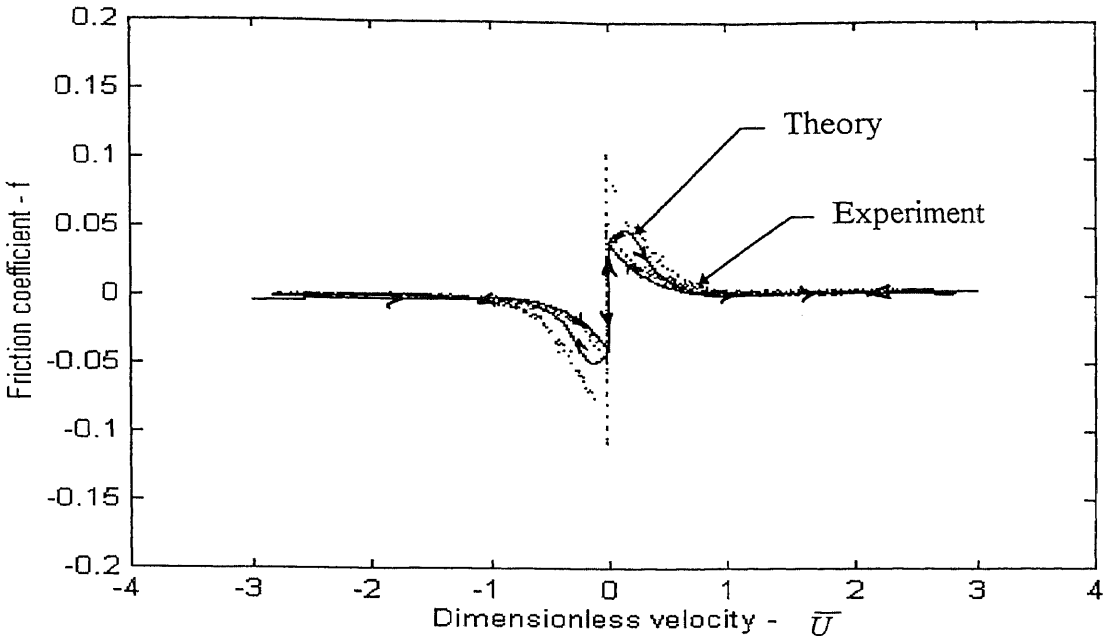

Figure 3.18 Friction coefficient f *Vs* dimensionless velocity $\overline{U} = 3.0\sin(\alpha\tau)$ at frequency $\omega = 0.1$ rad / sec, $(\alpha = 0.0087)$ for the load $F = 386\,\mathrm{N}$.

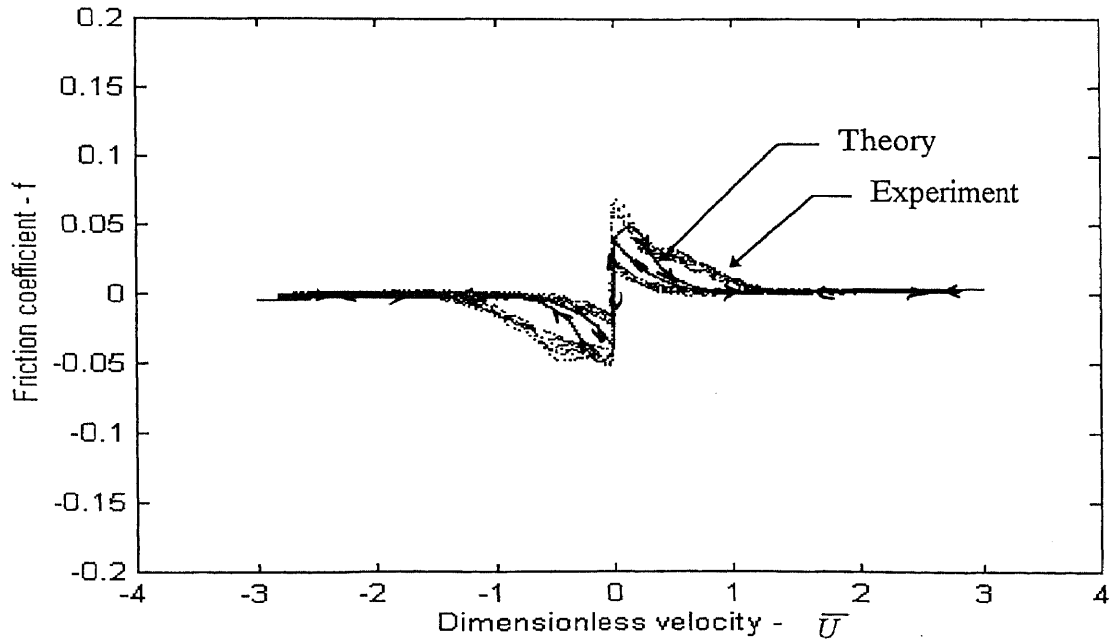

Figure 3.19 Friction coefficient f *Vs* dimensionless velocity $\overline{U} = 3.0\sin(\alpha\tau)$ at frequency $\omega = 0.5$ rad / sec, $(\alpha = 0.044)$ for the load $F = 386\,\mathrm{N}$.

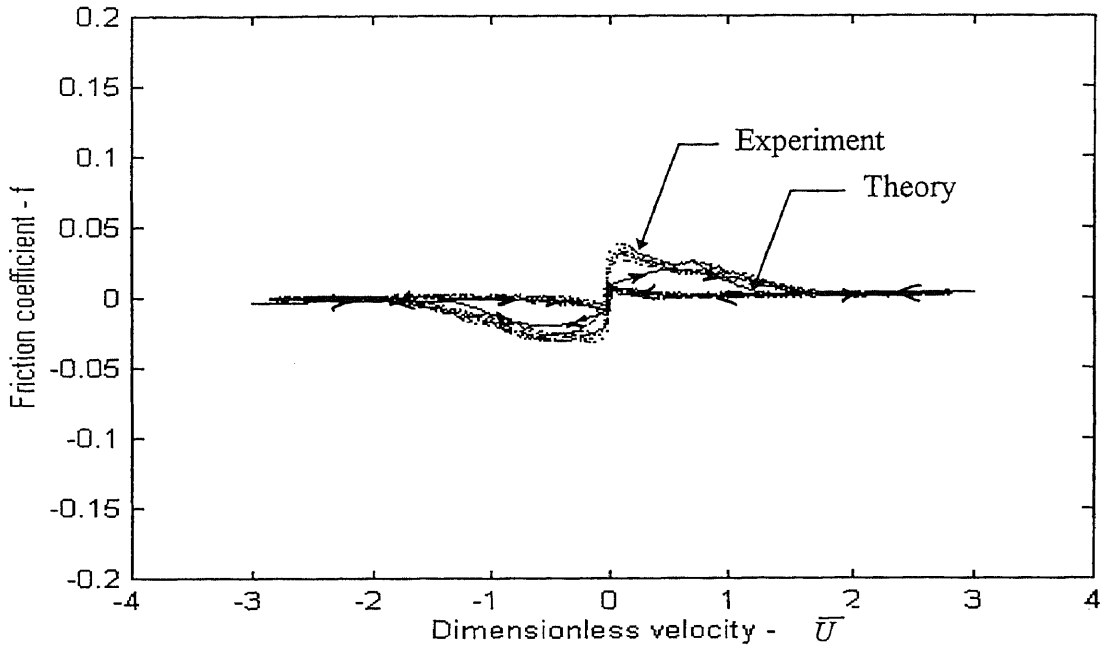

Figure 3.20 Friction coefficient f *Vs* dimensionless velocity $\overline{U} = 3.0\sin(\alpha\tau)$ at frequency $\omega = 1.0$ rad / sec, ($\alpha = 0.087$) for the load $F = 386\,\mathrm{N}$.

Following are the important observations drawn from the experimental results and the analytical solutions shown in Figures 3.4-3.20:

- The hysteresis phenomenon, in which the friction for increasing velocity is not the same as the friction for decreasing velocity.
- There is a discontinuity in friction at zero velocity when the operating velocity of the system oscillate in two directions. The magnitude of the Dahl effect is not significant, to show an inclination during this transition. It is also observed that during bi-directional velocity oscillations, friction at the starting point and stopping point at zero velocity is different in friction measurements, when compared to the friction at the starting point and stopping point at zero velocity of analytical solution. This phenomenon can be seen in clearly in Figure 3.21

which is the enlarged view of Figure 3.14. In Figure 3.21, this difference in starting point and stopping point at zero velocity are clearly distinguished. This phenomena may be due to the existence of dry friction at zero velocity. This phenomenon can be seen in clearly in Figure 3.21 which is the enlarged view of Figure 3.14.

- At low frequencies, experimental as well as analytical solution results in high friction at zero velocity, because velocity is too low to generate the fluid film thickness that is sufficient to take the load; therefore, there is a contact between the surfaces for long time.
- At higher frequencies, there is a clear reduction in the magnitude of the. The reason for the reduction in discontinuity is that there is no time for the fluid film to be squeezed at low velocities which has been developed at high velocities; therefore the contact between the asperities is for short time.

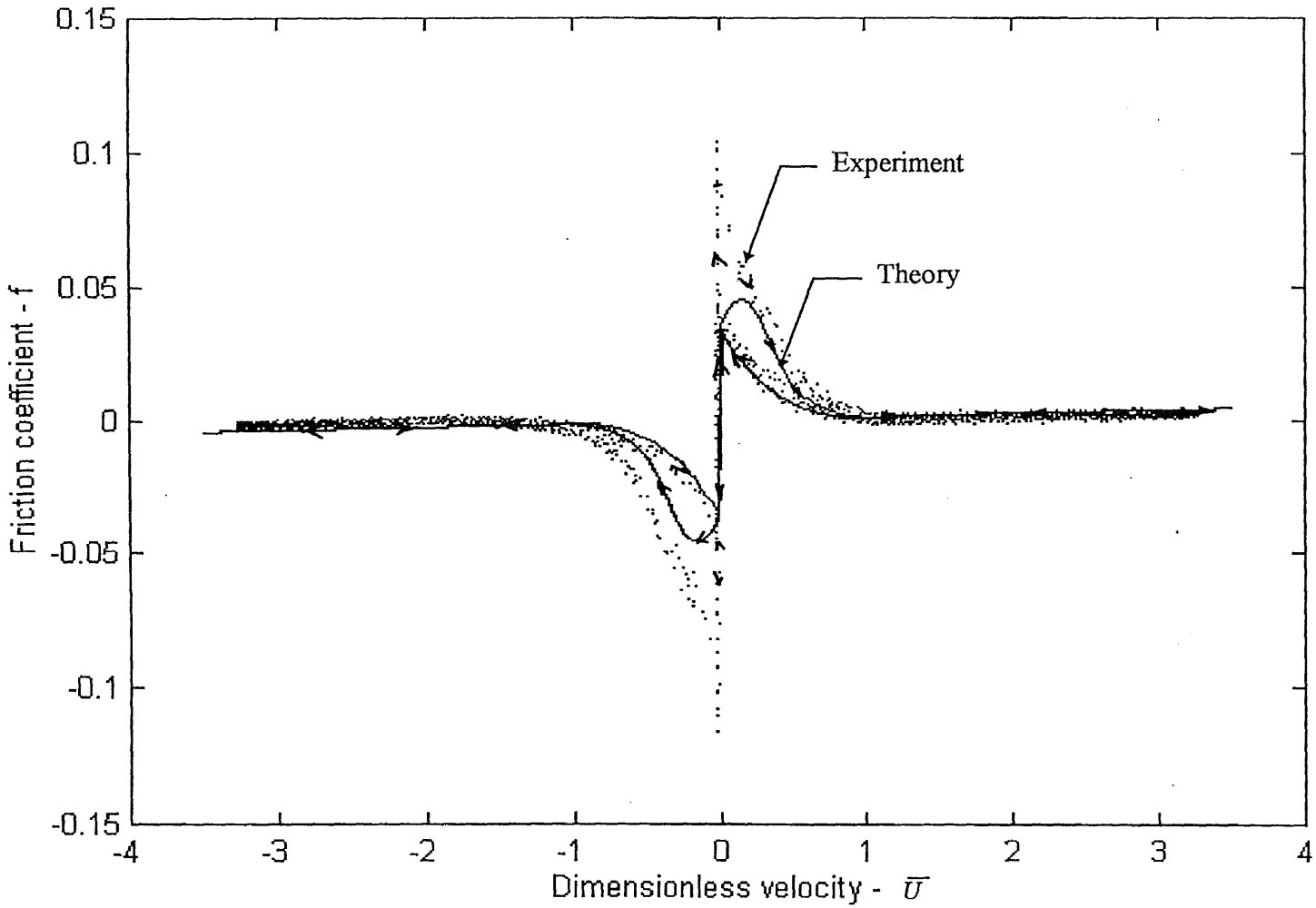

Figure 3.21 Friction coefficient f *Vs* dimensionless velocity $\overline{U} = 3.5\sin(\alpha\tau)$ at frequency $\omega = 0.1$ rad / sec, $(\alpha = 0.01)$ for the load $F = 308$ N. This is an enlarged view of Figure 3.14.

3.4 Error Analysis

The load-cell made of an aluminum frame supports the bearing housing, prevent its rotation and measure the torque on the housing M_h by calibrated strain gages bonded to it. The friction torque, M_j, between the bearings and journal is equal to M_h only when housing is completely static. However, the load-cell support has a certain elastic deformation, resulting in a small rotation of housing, θ_h. The equation of motion of the housing is,

$$M_j = M_h + I_h \ddot{\theta}_h \tag{3.3}$$

where I_h is the moment of inertia of the housing around it's axis. The last term in Equation 3.3, $I_h \ddot{\theta}_h$, is the magnitude of the measurement error caused by inertial effects. If the rotational stiffness of the housing is $k_h = M_h / \theta_h$, the following relation should be observed,

$$\left| I_h \ddot{\theta}_h \right| = \left| K_h \theta_h \right| \tag{3.4}$$

The maximum of $\ddot{\theta}_{h(t)} = \left| \Omega^2 \theta_h \right|$, where Ω is the frequency of oscillations of the housing as well as shaft. Following is the resulting condition for negligible error obtained from Equation 3.4:

$$\Omega^2 = \frac{k_h}{I_h} \tag{3.5}$$

The numerical values of the above design parameters for the friction measurement apparatus are listed in the following Table 3.3.

Table 3.3 Design parameters of the apparatus

Spring constant (Rotational stiffness of the Housing)	$k_h = 102$ Nm
Moment of inertia of the housing	$I_h = 10^{-2}$ kgm^2

In conducting the friction measurements for oscillating velocities, the frequency of oscillations should be restricted to $\Omega << 100$ rad / sec, or less than 16 Hertz. All the test have been conducted at very small frequencies, therefore, the Equation 3.3 is valid.

3.5 Summary

Investigation indicated in this chapter deals with the experimental analysis of dynamic friction in journal bearings operated on hydrodynamic lubrication theory. A special apparatus for measuring friction in sleeve bearings has been designed, developed and built by the team. The apparatus can be used to measure friction in the journal bearing for any shaft velocity.

Experiments have been conducted on this flexible system to measure dynamic friction in journal bearing for uni-directional and bi-directional velocity oscillations. These results have been used to determine data required for simulating the analytical model of Harnoy and Friedland (1993). With these data, the analytical model is simulated and the results are compared. Comparison of theoretical and experimental results for uni-directional velocity oscillations indicate very good qualitative and quantitative agreement. Both experimental and theoretical curves show similar hysteresis in friction, and similar friction behavior with frequency changes. In the case of the bi-directional velocity oscillations, the comparison shows agreement between experimental and analytical results

in respect of hysteresis in friction, but there is a significant difference in friction behavior at zero velocity. At zero velocity, experimental results show higher maximum friction when compared to the analytical results. In addition, at zero velocity, the staring point and stopping points are different in experimental results as compared to the theoretical results. This effect may be due to the presence of dry friction in the system at zero velocity. The trend of reduction in the maximum friction with increase in frequency is in qualitative agreement between experimental and analytical results. At higher frequency, in analytical model, the discontinuity is completely eliminated, but in experimental measurements discontinuity is not eliminated.

The apparatus can be further used to improve the existing analytical model. Also, the apparatus can be used to study the effect of stiffness of the asperities, stiffness of the bearing support on dynamic friction. The concept can be extended for developing the apparatus for other tribological situations, non-conformal contacts based elastohydrodynamic lubrication theory such as line contacts or point contacts.

CHAPTER 4

MODELING AND ANALYSIS OF RESISTANCE FORCES IN LUBRICATED CONFORMAL CONTACTS

4.1 Introduction

Current precise motion control systems such as positioning mechanisms, robots, demand higher accuracy and precision. In order to achieve very high precision and accuracy, friction in the system should be minimized or eliminated. Particularly, at low velocities, friction effects are significant. Among all the available techniques, friction compensation is the only active method to minimize the effects of friction. For applying model based friction estimation and cancellation techniques, a theoretical friction model is essential. The model to be developed should characterize dynamic friction in the system under dynamic velocity conditions, focusing on low velocity regions. The friction model developed in Chapter 2, and the friction measurements presented in Chapter 3 for a short journal bearing exhibit a discontinuity in friction at zero velocity when the operating velocity oscillates in two directions. This type of behavior is highly undesirable from the control point of view, as it effects the controllability, stability and performance of the system. To avoid such phenomena, the discontinuity must be eliminated which can be achieved by incorporating the effect of resistance forces on friction in the model. Most of the resistance forces in the system are due to elastic deformation of the supporting structure and surface asperities at the contact. In fact, the control community is interested in all the resistance forces, sliding friction as well as presliding elastic reaction. The objective of the present study is to develop a dynamic model for these resistance forces at slow, time-variable velocity. The model, with proper coefficients, can be expected to

predict the resistance torque between a bearing and rotating shaft at any instant of time. In fact, the model shows that the friction is a memory function of the velocity history. With the known coefficients, the model can be applied for on-line compensation which can be achieved by producing an additional, equivalent control torque to counteract the resistance in the bearings Friedland and Park (1992).

Research shows that the available friction models are based on empirical functions of friction versus steady velocity curve Stribeck (1902). However, closed loop control systems often operate under dynamic velocity, oscillating at small amplitudes around the zero velocity. In such cases, the steady friction model are inadequate for two reasons: First, the actual friction is not only a function of the instantaneous velocity, but also it entails some dynamic effects, such as memory function of velocity history. Second, near zero velocity, the elastic effects of shear deformation of the surface asperities as well as deformation of the supporting structure of the bearing are significant. Consider a case where a shaft is mounted inside a bearing, in such a case, most of the times the resistance force to the rotation of the shaft is sliding friction. However, at very low speed of the shaft, during the change in direction of velocity, there is a presliding torque in the system which is a result of an elastic compliance. The energy losses due to sliding friction are dissipated in the form of heat in the bearing, while the elastic displacement generates a recoverable potential energy.

The development of earlier friction models of Hess and Soom (1990), Dahl (1977), Canudas de Wit et al (1993) was purely based on equations that fit the observed friction characteristics. In contrast, the development of present model is based on first principles derived by the analysis of the physical phenomena of lubricated surfaces and the dynamics

of the system. A preliminary dynamic friction model have already been developed as a part of the current project by the research team including the author. The results of this preliminary model have been presented by Harnoy and Friedland (1993), but, the model doesn't include elastic effects. In the present work, an improved model have been developed which includes the presliding elastic forces. The model is so important as it takes care of the resistance forces which have a significant effect on control systems, particularly, for the systems operating with the velocity oscillating around zero. The present model is an extension of the earlier model for a short bearing developed in Chapter 2, and it covers the regions of hydrodynamic, mixed and boundary lubrication as well as elastic presliding. The present model can offer a better insight into the dynamic friction behavior of lubricated surfaces. The model is described by a set of differential equations, and can be used for simulation for any time varying velocity, including transition between positive and negative velocities.

The proposed model reveals that there is an interesting relation between the various friction regions, in the sense that the friction in one region is affected by a memory function of the velocity within another region. In fact, the model proposed herein suggests that, in certain cases, the previous models can be considered as approximations to the model presented here.

Consider a simple case of a sleeve bearing, where the sleeve is supported by an elastic structure and it has a small angular compliance when subjected to the bearing friction torque. This study investigates the role of the sleeve angular compliance, which is included in the dynamic model.

A set of differential equations relating instantaneous friction to the dynamic state of the system have been developed and simulated. The simulation results have been presented in the form of friction versus velocity curves which show a hysteresis effect, in agreement with earlier dynamic friction experiments on lubricated surfaces. These results also indicate the elastic deformation eliminates the discontinuity at zero velocity as predicted by the classical Coulomb friction model (In fact, in reality, a discontinuity never occurs because, there is always some elastic compliance in the bearing system). In addition, it is shown that, in a journal bearing, the elastic compliance influences the friction over the complete velocity range, including the sliding region, and not merely the behavior near zero velocity.

Closed loop motion control entails small oscillations at low velocity with frequent changes in sign. In certain cases where the velocities are very small, it is possible to have vibration without sliding, and the dynamics of the motion is governed by the moment of inertia of the bearing system and its elastic compliance. Presliding conditions are similar to the dynamics of a gear having torsional oscillations and meshed by elastic flexible teeth to an internal gear supported by a torsional spring. At higher velocity, sliding initiates between the journal and sleeve as the torque between shaft and sleeve exceeds the static friction torque.

In the classical hydrodynamic lubrication theory of journal bearings, the sleeve is considered to be rigid. Neglecting the sleeve compliance in a bearing operating at steady journal speed has been justified. However, this study shows, that the elastic displacement of the angular compliance of the sleeve is significant under dynamic velocity conditions.

4.2 Presliding Motion of Shaft and Sleeve

Consider a shaft accelerating from zero speed inside the sleeve of a short journal bearing as shown in Figure 4.1. Initially, there is a contact between the journal and sleeve, and owing to the elasticity in the system there is an angular compliance, namely, the sleeve has a small rotary motion before the initiation of sliding, and the journal rolls inside the sleeve like internal friction pulleys.

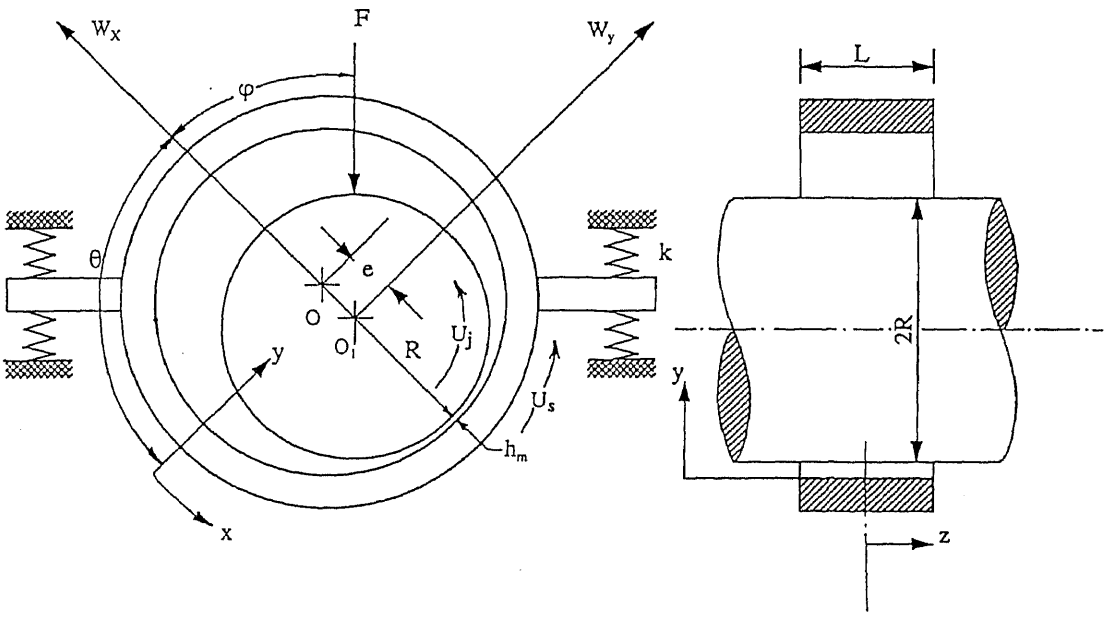

Figure 4.1 Short journal bearing with angular compliance.

The friction resistance torque, M_j between the journal and sleeve increases radually. Sliding process is initiated whenever the friction torque, M_j exceeds the agnitude of the Coulomb friction torque in the contact between the journal and sleeve:

$$M_j > f_m R W_e \tag{4.1}$$

where W_e is the normal reaction force resulting from a direct contact between the journal and the sleeve surfaces, R is the journal radius and f_m is the coulomb friction coefficient at this contact.

The elastic structure of every real bearing support must allow for a small angular sleeve compliance. In Figure 4.1, the elastic support of the sleeve is represented by springs. The motion of the sleeve causes a reaction torque, M_s, of the structure on the sleeve in the direction opposite to the rotation of the sleeve, according to the equation of a torsional spring is,

$$M_s = k\theta_s \tag{4.2}$$

where k is the torsional stiffness of the bearing support and, θ_s is the angular rotation of the sleeve.

An additional contribution to the compliance of the system is the elastic shear deformation of the surface asperities in the contact area between the sleeve and journal. The elastic component of the shear deformation of the surface asperities creates a second torsional spring between the sleeve and the journal. Before initiation of the sliding, the journal rotates the sleeve as a result of an internal resistance torque M_j, which is proportional to the difference between the rotation angle of the journal θ_j and that of the sleeve, θ_s according to the equation,

$$M_j = k_t(\theta_j - \theta_s) \tag{4.3}$$

where k_t is the equivalent torsional stiffness due to elastic shear of the surface asperities of the journal and sleeve at the contact area.

The resultant of M_j and M_s accelerates the sleeve according to the following equation:

$$k_t(\theta_j - \theta_s) - k\theta_s = I_{eq}\ddot{\theta}_s \tag{4.4}$$

where I_{eq} is the equivalent moment of inertia of the sleeve system. In real bearings with an elastic support, the sleeve can turn together with the bearing housing. In such cases I_{eq} refers to all the rotating parts together (see Figure 4.1). For the presliding mode, Equation 4.4 is the governing differential equation of motion, and it can be numerically integrated for any given dynamic journal speed, $\dot{\theta}_j$. One example of the dynamic journal speed, $\dot{\theta}_j$, is a periodic bi-directional journal oscillations:

$$\dot{\theta}_j = \omega_o \sin \Omega t \tag{4.5}$$

where the amplitude ω_o is the maximum angular velocity of the journal, and Ω is the frequency of velocity oscillations. The differential equations expressed by Equations 4.4-4.5 can be integrated together to determine the time variable rotation angles θ_j and θ_s. Subsequently, M_j and M_s can be obtained from Equations 4.2 and 4.3 respectively as functions of time or journal velocity.

4.2.1 Returning from Sliding to Presliding Mode

It is very important to observe the criterion for transition between the sliding and presliding modes at each step of integration of Equation 4.4. To assure this, at each step of integration, the journal torque, M_j for the sliding mode and presliding mode must be computed and compared. The mode having the minimum journal torque, M_j is selected.

Whenever there is a return from sliding to presliding mode, then the sliding rotation angle, θ_j is no longer appropriate for Equation 4.4, since the journal has already rotated to a large angle during sliding. Therefore, Equation 4.4 requires a new reference for the measurement of initial journal angle, θ'_j, at the instant whenever the presliding mode is restored. This initial journal angle, θ'_j is almost the same as the sleeve angle, θ_s, except that there is a small shift between the journal and sleeve, owing to elastic shear deformation of the asperities. The equation for the initial θ'_j at the return to the presliding mode thus is,

$$\theta'_j = \theta_s + \frac{f_m W_e R}{k_t} \tag{4.6}$$

Once the presliding mode is restored, θ_j in Equation 4.4 is measured by the same reference as the sleeve, having initial value θ'_j. The variable θ_j, for integrating Equation 4.4, during the presliding, is obtained from the initial θ'_j in Equation 4.6 and shaft velocity according to the equation:

$$\theta_j = \theta'_j + \int_0^t \theta_j dt \tag{4.6}$$

where θ'_j is the time varying periodic speed defined in Equation 4.5.

The initial value θ'_j must be computed at each step of the sliding mode. It is used to calculate the hypothetical next presliding torque, M_j, for testing the possible return to presliding mode.

4.3 Dynamic Friction at the Sliding Mode

At the initiation of sliding, the journal velocity is too small to generate a lubrication film of sufficient thickness so that the rubbing surfaces are completely separated; therefore, there is a contact between the surface asperities. The friction in the contact can be either boundary or mixed lubrication region.

The mixed lubrication region occurs when minimum film thickness of lubrication, h_m, (see Figure 4.1) falls below a certain small critical value, h_{tr}. The magnitude of h_{tr} is the minimum film thickness at the transition between mixed and hydrodynamic lubrication regions at steady journal speed, which can be determined from the constant journal speed, ω_{tr} corresponding to the transition point. The journal speed ω_{tr} can be obtained from the Stribeck curve (1902). In the mixed region, there is a contact between the surface asperities, and they are deformed under the action of applied load which results in generating a reaction force, W_e. The reaction force, W_e, between the asperities of the two surfaces is an increasing function of the elastic deformation δ, of the asperities, which behaves like a spring in the direction normal to the contact area. However, this spring-like behavior is not linear. The development of theory and equations for the elastic reaction force, W_e, already have been developed in Chapter 2. The elastic reaction force, W_e, is defined in Equation 2.3, and all the related terms are defined in Equations 2.1-2.4. Following is the equation (Equation 2.3) for reaction force, W_e, taken from Chapter 2.

$$W_e = \kappa(\varepsilon)C(\varepsilon - \varepsilon_{tr})\Delta \tag{4.8}$$

The magnitude of the variable Δ is either 0 or 1 which had been already defined in Equation. 2.4. In the hydrodynamic lubrication region, there is no contact between the

two surfaces, therefore there is no reaction force, i.e. $W_e = 0$, and this region is represented as $\Delta = 0$. But, in the mixed or boundary lubrication region, there will be a reaction force, $W_e > 0$ in the contact, and this region is represented by $\Delta = 1$. In the mixed region, the bearing load capacity $\vec{W}$ is obtained by adding the vectors of the contact reaction force, $\vec{W}_e$, and the hydrodynamic fluid film force, $\vec{W}_h$ as defined in Equation 2.5, as:

$$\vec{W} = \vec{W}_e + \vec{W}_h \tag{4.9}$$

The bearing friction force, F_f, in the tangential direction is the sum of contact and viscous friction forces. The contact friction force is assumed to follow Coulomb's law, and hence, it is proportional to the normal contact load, W_e, while the hydrodynamic, viscous friction torque follows the short bearing equation as given in Pinkus (1961, 12) and Szeri (1980, 64). It is also assumed that the density of the asperities in the mixed region is sufficiently low so that it does not have any significant effect on the hydrodynamic performance. With the above assumptions, the total friction torque, ($M_j = F_f R$) between the journal and sleeve can be expressed as:

$$M_j = f_m \kappa(\varepsilon) CR(\varepsilon - \varepsilon_{tr}) \operatorname{sgn}(\dot{\theta}_j)\Delta + \frac{L\mu R^3}{C}\frac{2\pi}{(1-\varepsilon^2)^{0.5}}(\dot{\theta}_j - \dot{\theta}_s) \tag{4.10}$$

where f_m is the Coulomb friction coefficient, L and R are the length and radius of the bearing (Figure 4.1), C is the average radial clearance, and μ is the viscosity of the lubricant. The term $\operatorname{sgn}(\dot{\theta}_j)$ represents the direction of motion of the journal which is defined as,

$$\mathrm{sgn}(\dot{\theta}_j) = \begin{cases} +1 & \dot{\theta}_j \geq 0 \\ -1 & \dot{\theta}_j < 0 \end{cases} \tag{4.11}$$

Under dynamic conditions, friction torque, M_j on the journal is function of dynamic variables ε, θ_j and θ_s. For any known journal speed and bearing data, these dynamic variables, ε and θ_s are required to determine the friction torque, M_j, from Equation 4.10. Following sections show the detailed description for determining these two dynamic variables ε and θ_s based on the equation of motion and the theory of hydrodynamic lubrication.

The friction coefficient of the bearing, $f(t)$ is determined from the resistance torque M_j, and the applied torque proportional to the load,$(M = FR)$ according to the following equation:

$$f(t) = \frac{M_j}{M} \tag{4.12}$$

4.3.1. Calculation of θ_s During the Sliding Mode

A differential equation for the torque between the journal and the sleeve similar to Equation 4.4 have been derived for sliding conditions, as following. The torque includes the contact and viscous components.

$$f_m \kappa(\varepsilon) CR(\varepsilon - \varepsilon_{tr}) \,\mathrm{sgn}(\theta_j)\Delta + \frac{L\mu R^3}{C} \frac{2\pi}{(1-\varepsilon^2)^{0.5}} (\dot{\theta}_j - \dot{\theta}_s) = I_{eq} \ddot{\theta}_s \tag{4.13}$$

4.3.2. Hydrodynamic Force

As this model is an extension of the friction model developed for a short hydrodynamic journal bearing in Chapter 2, the hydrodynamic force developed in Equations 2.13-2.20 is valid for the present analysis with a minor modification in pressure distribution. In this model, derivation of the pressure distribution is similar to the Equation 2.17, but it includes an extra term to account the angular rotation of the sleeve in addition to the angular rotation of the shaft as described in the following equation:

$$P = \frac{3}{4}\frac{\mu L^3}{C^2}\left\{(\omega_j + \omega_s)\varepsilon\sin\theta - 2\varepsilon\frac{d\varphi}{dt}\sin\theta - 2\frac{d\varepsilon}{dt}\cos\theta\right\}\frac{(L^2 - 4z^2)}{h^3} \tag{4.14}$$

Following are the equations for the fluid film force components of the bearing obtained by substituting the pressure distribution, P in Equation 4.14, and integrating with boundary conditions given in Equations 2.16.

$$W_x = \frac{\mu RL^3}{C^2}\left\{-0.5J_{12}\varepsilon(\dot{\theta}_j + \dot{\theta}_s) + J_{12}\varepsilon\dot{\varphi} + J_{22}\dot{\varepsilon}\right\} + \overline{\kappa}(\varepsilon)(\varepsilon - \varepsilon_{tr})\,\mathrm{sgn}(\dot{\theta}_j)\Delta \tag{4.15}$$

$$W_y = \frac{\mu RL^3}{C^2}\left\{0.5J_{11}\varepsilon(\dot{\theta}_j + \dot{\theta}_s) - J_{11}\varepsilon\dot{\varphi} - J_{12}\dot{\varepsilon}\right\} \tag{4.16}$$

where $\dot{\theta}_s$ is the rate of angular rotation of the sleeve, which is determined from the dynamic equation of the bearing, Equation 4.4 or Equation 4.13, depending upon the presliding or sliding mode.

The integrals J_{ij} occurring in Equations 4.15 and 4.16 have been defined already in Equations 2.23-2.25.

According to the Newton's law of motion, the resultant force of the external load, $\boldsymbol{F}$, and fluid film force, $\boldsymbol{W}$, accelerate the journal center with an acceleration, $\boldsymbol{a}$, as per the equation:

$$\boldsymbol{F} + \boldsymbol{W} = m\boldsymbol{a} \tag{4.17}$$

where $\boldsymbol{m}$ is the journal mass. Substituting the acceleration terms, in polar coordinates, in the radial and tangential directions (directions opposing to W_x, and W_y in Figure 4.1) and the load components F_x and F_y in the same directions, Equation 4.17 yields:

$$F_x - W_x - W_e = mC(\ddot{\varepsilon} - \varepsilon\dot{\varphi}^2) \tag{4.18}$$

$$F_y - W_y = mC(\varepsilon\ddot{\varphi} + 2\dot{\varepsilon}\dot{\varphi}) \tag{4.19}$$

where F_x and F_y the load components can be obtained from the external load as (see Figure 4.1),

$$F_x = F\cos\varphi \tag{4.20a}$$

$$F_y = F\sin\varphi \tag{4.20b}$$

Substituting the appropriate definitions into Equations 4.18-4.19, obtained the following differential equations:

$$F\cos\varphi = \frac{\mu RL^3}{C^2}\left\{-0.5J_{12}\varepsilon(\dot{\theta}_j + \dot{\theta}_s) + J_{12}\varepsilon\dot{\varphi} + J_{22}\dot{\varepsilon}\right\} + mC(\ddot{\varepsilon} - e\dot{\varphi}^2) + \overline{\kappa}(\varepsilon)(\varepsilon - \varepsilon_{tr})\,\mathrm{sgn}(\dot{\theta}_j)\Delta \tag{4.21}$$

$$F_y\sin\varphi = \frac{\mu RL^3}{C^2}\left\{0.5J_{11}\varepsilon((\dot{\theta}_j + \dot{\theta}_s)_s) - J_{11}\varepsilon\dot{\varphi} - J_{12}\dot{\varepsilon}\right\} + mC(\varepsilon\ddot{\varphi} + 2\dot{\varepsilon}\dot{\varphi}) \tag{4.22}$$

These equations together with Equations 4.10 and 4.13 constitute the dynamic friction model being sought for the sliding mode. Equations 4.21 and 4.22 together with Equations 4.3 and 4.4 describe the presliding mode.

4.4 Dynamic Friction Simulation for Periodic Journal Speed

The model developed in the previous sections need to be analyzed for its friction behavior, by simulating it for known bearing data. To simulate the model for friction, the variable ε must be determined by integrating Equations 4.21 and 4.22 numerically together with the equation for angular rotation, θ_s, (Equation 4.4 for the presliding mode or in combination with Equation 4.13 for the sliding mode). Once ε, and θ_s are determined, friction torque between the journal and the sleeve, M_j is computed using Equation 4.3 for presliding, Equation 4.10 for sliding conditions. Finally, the friction coefficient, $f(t)$ is determined from Equation 4.12. The simulation of the model requires the following twelve constants listed as in Table 4:

Table 4.1 Data required for simulation

ε_{tr}	ε_b	f_m
R (m)	L (m)	C (m)
I_{eq} (kgm^2)	μ (Nsm^{-2})	F (N)
m (kg)	k_t (Nm)	k (N)

The magnitude of the angular velocity of the journal, ω_{tr}, at the transition between mixed and hydrodynamic friction can be calculated from the external load (Equations 4.15 and 4.16) at constant journal velocity and when the relative eccentricity, $\varepsilon = \varepsilon_{tr}$.

For the convenience of simulation, Dimensional analysis have been performed on Equations 4.4, 4.13, 4.21 and 4.22, which suggests that the data can be reduced from twelve to seven independent dimensionless parameters. In addition to the three dimensionless constants ε_{tr}, ε_b, and f_m, the simulation of the model depends on the following four dimensionless parameters, which are defined as:

$$\bar{k}_t = \frac{1}{I_{eq}\omega^2_{tr}} k_t \qquad \bar{k} = \frac{1}{I_{eq}\omega^2_{tr}} k \qquad \bar{\mu} = \frac{LR^3}{CI_{eq}\omega^2_{tr}} \mu \qquad \bar{m} = \frac{C^3\omega_{tr}}{\mu L^3 R} m \quad (4.23)$$

Either in the above set of equations and or in Table 4.1, the external force term, F does not appear, since it has already been considered in the calculation of ω_{tr}. The angular velocity at the transition point, ω_{tr} has been obtained from Equations 4.21 and 4.22 for steady conditions: when all time derivatives are zero, except $\dot{\theta}_j$, and for $\varepsilon = \varepsilon_{tr}$.

The function $\kappa(\varepsilon)$ related to the stiffness of the surface asperities which have been used in Equations 4.8, 4.10, 4.13, 4.15 and 4.21 is assumed to vary linearly with the asperity deformation, $\delta = C(\varepsilon - \varepsilon_{tr})$ according to the relation defined in Equations 2.34 and 2.35 as discussed in Chapter 2. Terms relating to the definition of $\kappa(\varepsilon)$ have been discussed in 2.5.

Data required for simulation as expressed by seven dimensionless variables is listed in Table 4.2 as below:

Table 4.2 Dimensionless bearing data.

	$\varepsilon_{tr} = 0.96$	$\varepsilon_b = 0.99$	$f_m = 0.1$
$\bar{\kappa}_t = 1000$	$\bar{k} = 500$	$\bar{\mu} = 0.1$	$\bar{m} = 100$

4.4.1 Simulation for Bi-directional Velocity Oscillations

The first part of simulation have been performed for bi-directional journal speed oscillations. The journal oscillates sinusoidally and passes through zero velocity according to the Equation 4.5. Following is the dimensionless form of journal velocity, $\overline{U} = U_j / U_{tr}$

Equation 4.5.

$$\overline{U} = 2\sin(\alpha\tau) \tag{4.24}$$

where τ is the dimensionless time, α is the dimensionless frequency of journal oscillations which is defined as,

$$\alpha = \frac{\Omega}{\omega_{tr}} \tag{4.25}$$

Simulation results for the data given in Table 4.2, have been presented as $f - \overline{U}$ (friction coefficient, $f(t)$ versus dimensionless velocity of journal, $\overline{U}$), plots as shown in Figure 4.2. These plots indicate hysteresis in friction. It is interesting to note that these results are similar to the dynamic friction measurements of Ting (1993) on an piston ring of an engine. Figure 4.2 shows the simulation results for various frequency values of journal oscillations, α. These plots show that at low frequency of oscillations, the presliding curve is steeper, and the maximum sliding friction increases. The most important result is that at high oscillating frequency, the overall sliding friction of a journal bearing has been reduced significantly.

The presliding mode near zero velocity, in Figure 4.2, is followed by the sliding mode at higher velocity. The friction coefficient in the presliding mode is inclined, nearly a linear function (more precisely, it is parabolic) located between two turning points,

instead of a discontinuity as predicted by the classical Coulomb model. However, at high values of stiffness, $\bar{k}_t$ and stiffness, $\bar{k}$, the presliding characteristics become steeper.

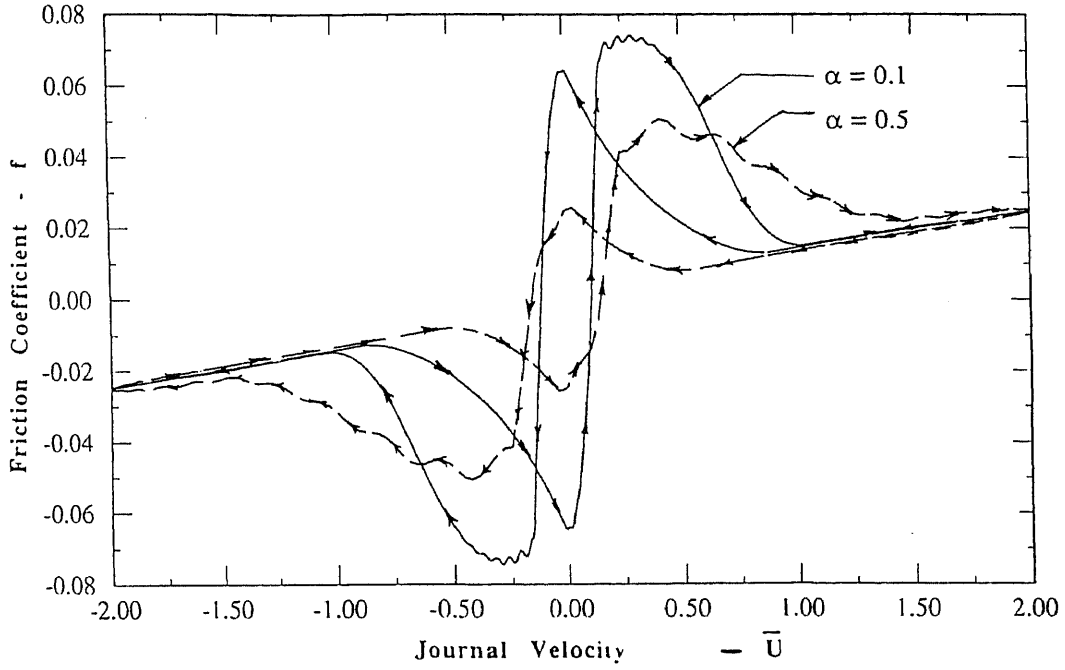

Figure 4.2 Friction coefficient, f *Vs* journal velocity, $\bar{U}$ with $\bar{U} = 2\sin\alpha\tau$, for various frequencies journal oscillations, α.

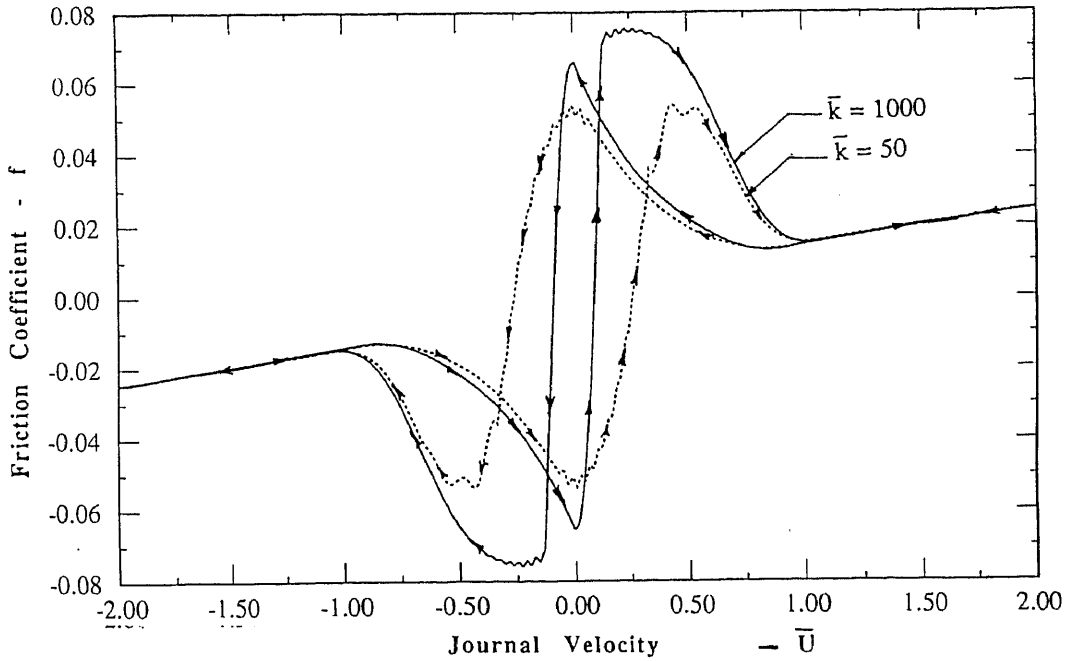

Figure 4.3 Friction coefficient, f *Vs* journal velocity, $\overline{U}$ with $\overline{U} = 2\sin(0.1\tau)$, for various bearing support stiffness, $\overline{k}$.

Dynamic friction simulations also have been performed for various values of torsional stiffness, $\overline{k}$, of the bearing support, and the results are shown in Figure 4.3. The most interesting result in this simulation is that the peak friction in a journal bearing is reduced by decreasing the stiffness $\overline{k}$. The result suggests that a journal bearing with a soft support has an advantage of reduced sliding friction, when compared to a rigid support. This is an interesting interrelation between the elastic presliding characteristic and the sliding friction. This phenomena demonstrates the merit of the proposed model, as in most of the previous empirical models, the system compliance affects only the presliding region. The effect can be explained as an initial compliant rotation of the sleeve Szeri (1980). The sleeve rotation results in presliding rolling between the journal and sleeve (like internal friction pulleys). During this rolling, the lubrication film pressure

builds up, and reduces the maximum friction at the initiation of sliding. This effect is unique to journal bearings, and it is not expected in other geometries such as plane sliding.

The dynamic friction curves in Figures. 4.2 and 4.3 exhibit fluctuations in the sliding friction near the peak friction. This phenomena can be explained as the torsional vibrations of the sleeve, which is a dynamic system of inertia in torsional springs.

Dynamic friction curves for various values of torsional stiffness due to the elastic shear deformation of the surface asperities, $\overline{k}_t$, are shown in Figure 4.4. The results indicate that there is a wider presliding region and a reduction in the maximum sliding friction with a softer stiffness of the asperities. The slope of the curve in the presliding mode is less steep for softer $\overline{k}_t$.

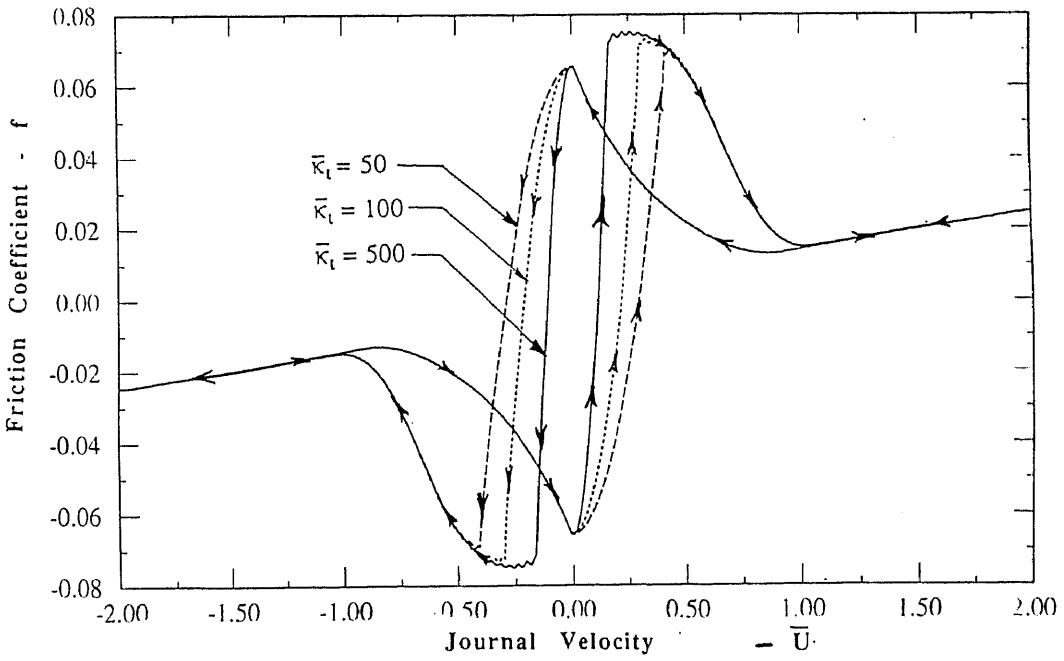

Figure 4.4 Friction coefficient, f *Vs* journal velocity, $\overline{U}$ with $\overline{U} = 2\sin(0.1\tau)$, for various shear stiffness of the asperities, $\overline{\kappa}_t$.

4.4.2 Simulation for Uni-directional Velocity Oscillations

To verify the performance of the current model, with earlier experimental work of Hess and Soom (1990), the model also have been simulated for uni-directional oscillations. Hess and Soom (1990), measured dynamic friction for velocity fluctuations between 0.01 and 1.0 m/s (to eliminate the presliding mode. For comparison purposes, the current model is simulated for the following sinusoidal velocity:

$$\overline{U} = 1.1 + \sin(\alpha\tau) \tag{4.26}$$

Simulation results of friction for the above journal oscillations are shown in Figure 4.5 for various values of torsional stiffness of the support, $\overline{k}$.

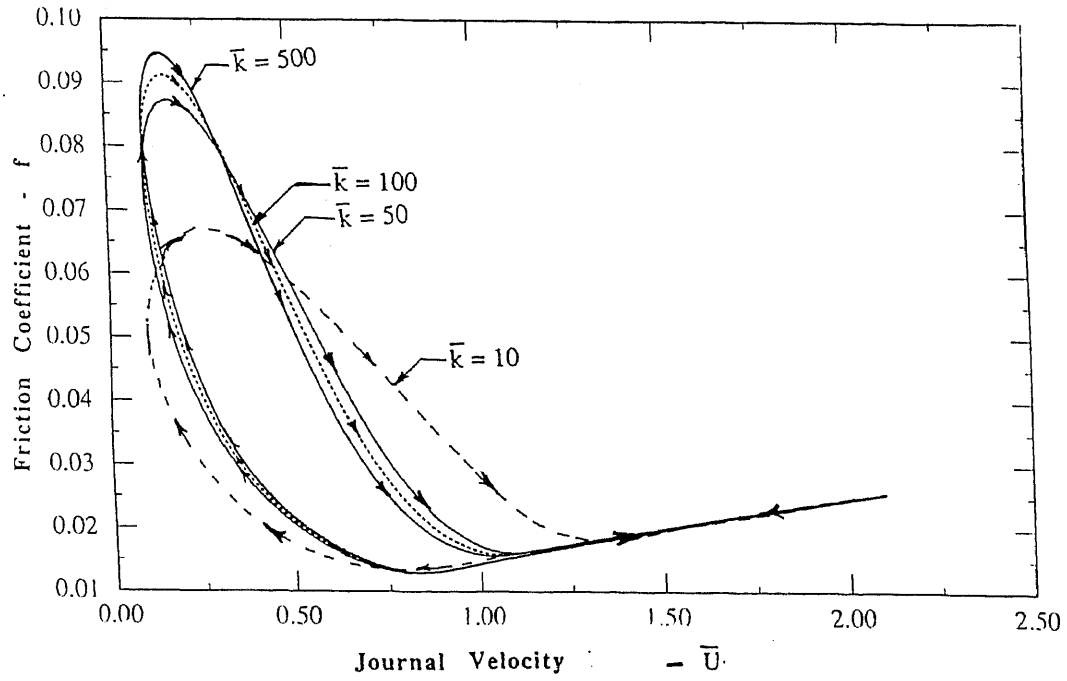

Figure 4.5 Friction coefficient, f *Vs* journal velocity, $\overline{U}$ with $\overline{U} = 1.1 + \sin(0.1\tau)$, for various values of bearing support stiffness of the asperities, $\overline{k}$.

Hess and Soom (1990) measured the dynamic friction between the two sliding surfaces having a line contact with lubrication. They measured friction between a rotating disc and a circular button, while the present model is for a short journal bearing. Moreover, they conducted experiments for velocity oscillations with a triangular profile, while this study is for sinusoidal. Irrespective of these variations, the simulation results show that there is a qualitative agreement in respect of hysteresis in friction versus velocity curves.

4.5 Summary

A model for dynamic friction, based on the physical phenomenon of hydrodynamic lubrication, and effect of resistance forces on friction behavior for a lubricated journal bearing has been developed and simulated. The model considers the compliance in the bearing system resulting from elasticity of surface asperities in the contact between the sleeve and journal (Dahl effect) as well as the elasticity of the bearing support, and the model can effectively simulate the transition from presliding to sliding modes and a return to presliding mode. The simulation of the model yields dynamic friction versus journal velocity ratio $f - \overline{U}$ curves. Simulation results of the model indicate replacement of the step function at zero velocities, when the journal undergoes bi-directional velocity oscillations. Also, the results for various frequencies of velocity oscillations, torsional stiffness of the support, indicate significant reduction in the maximum friction with increase in frequency or decrease in torsional stiffness of the support. The results also indicate that the width of the presliding region increases with decrease in the stiffness of the asperities. In fact, rigid asperities generate a steeper presliding region when compared

to the soft asperities, as depicted by the simulation results shown in $f - \overline{U}$ curves for different asperities' stiffness values.

Simulation of the model for dynamic friction shows a memory effect in $f - \overline{U}$ curves indicating that the instantaneous friction is a function of instantaneous velocity, and velocity history. At very low frequency of journal oscillations, the $f - \overline{U}$ curve reduces to the steady velocity Stribeck curve and the effects of the compliance of the system disappear.

An additional important conclusion, for a journal bearing, is that the model shows a relation between presliding and sliding modes. In this model, pre-sliding and sliding friction have been modeled separately. If the stiffness of the bearing support is reduced, it reduces presliding resistance, as well as the maximum sliding friction, as demonstrated by the results. This effect in a journal bearing has been explained earlier as initial rolling between the journal and sleeve. This conclusion can have important practical applications. The friction in a journal bearing can be reduced by a proper design, i.e., by employing a soft support to the sleeve. In particular, if the small oscillations involved in controlling the system are within the presliding range, the soft bearing supports can benefit in control of precise motion.

The model was developed for a conformal contact formed by a short journal bearing, assuming the viscosity of the lubricant to be constant. This model can be extended, for non-conformal contacts such as line or point contacts formed by cylindrical rolling elements, roller/ball bearings, operating on elastohydrodynamic lubrication theory where the elastic deformation of the surfaces and pressure-viscosity variation are

significant. In addition to variable viscosity, under these extreme pressures, the lubricant undergoes changes in its rheological properties and becomes visco-elastic. The performance of the current model can be verified with proper experiments considering all the above factors. The present model has been extended to investigate the friction during start-up of hydrodynamic journal bearings, and the work has been published Harnoy (1995). Author has actively involved in computer programming and simulation of the model.

CHAPTER 5

DYNAMIC FRICTION MODEL FOR A LUBRICATED NON-CONFORMAL CONTACT

5.1 Introduction

Earlier work on friction as well as previous chapters on friction modeling shows that friction has an adverse effect on the precision of motion of dynamic systems governed by automatic control. In particular, in closed-loop control systems, friction may induce undesirable tracking errors, limit cycles and stick-slip motion. The negative effect of the friction is more significant at low velocity, where there is a negative slope in the friction versus velocity curve. The precision of closed-loop control systems can be improved by compensating for the friction by applying an additional force or torque through a servo-motor in the opposite direction to the friction force. A suitable friction model is required to estimate the friction as a function of measured unsteady velocity so that the friction is compensated.

In friction modeling, there is a trade-off between the simplicity and the precision of the model. The accuracy of the friction model can be improved by increasing the complexity of the model. However, for a complex friction model, the computation time is too long for on-line compensation. A simplified friction model is practically more efficient than a complicated model. Therefore, in the present study, a relatively simple friction model has been developed derived by focusing on the most significant physical principles. The precision of the model can be improved when it includes parameters which are determined experimentally.

In Chapter 2, an analytical model for a conformal contact formed by a short journal bearing based on hydrodynamic lubrication theory has been developed. This model is applicable only for the mechanical systems which use the components that form conformal contacts such as journal bearings, guide ways etc. But, the model may not be applicable to the mechanical systems having non-conformal contacts such as point or line contacts, formed by roller bearings, cams and gears. Point contacts as well as line contacts are just idealization, in fact, the parts in the contact will deform to create an apparent area of contact and which increases with load. Therefore, this property of non-conformal contacts may affect the friction behavior. The objective of the present study is to develop a dynamic friction model for a non-conformal contact, by incorporating the theory similar to the that developed for conformal contact. A line contact based on elastohydrodynamic theory have been chosen for this investigation. This model can be applied to many practical systems as well to any specific systems such as roller bearings or gears.

Although there is a considerable difference in the approach, analytical and experimental models developed by Hess and Soom (1990), Canudas de Wit et. al. (1993), Harnoy and Friedland (1993), and Harnoy et. al. (1994), indicate similar type of phase lag manifested as hysteresis in friction under dynamic velocity conditions. Recent experiments of Harnoy et. al. (1994), indicate that earlier empirical models are suitable for low frequency oscillations, but are not in complete agreement with the measured friction at high frequency velocity oscillations where the measured friction is zero at zero velocity. The advantage of models by Harnoy and Friedland (1993) and Harnoy et. al. (1994) is that it can describe the above effect at high frequencies as well as low frequencies for any time-variable velocity oscillations.

The present study applies the techniques of the model Harnoy and Friedland (1993), and Harnoy et. al. (1994), to elastohydrodynamic line contact where the elastic deformation of the contact is considered as well as the variation of lubricant viscosity with the contact pressures. Particularly, the area of the contact as a result of deformation of the contact surfaces which is due to the load has been considered in computing the friction force. The present model can predict similar phase lag manifested as hysteresis in the friction-velocity curves. The model also shows that the friction-velocity curve reduces to the Stribeck curve at steady velocities.

5.2 Development of Friction Model

The present friction modeling is focused on non-conformal line contact based on elastohydrodynamic lubrication theory. The model uses the elastohydrodynamic lubrication theory developed by Grubin (1949), and Hamrock (1994). Consider a rectangular line contact obtained by two parallel cylinders loaded against each other as shown in Figure 5.1*a*. In this system, one cylinder can roll or slide over the other, and these cylinders also can have a combination of rolling and sliding motion which is common in the operation of gears. Under the applied load, the surfaces at the contact undergo significant amount of elastic deformation resulting an area which is a function of the load. The rectangular contact has a width of $2a$ as shown in Figure 5.1a is very well known as Hertzian width. The isothermal elastohydrodynamic theory includes the combined effects of elastic deformation and viscosity dependence on the pressure distribution. Grubin, (1949) introduced combinations of these effects on the fluid film pressure distribution. Hamrock (1994) recently reviewed elastohydrodynamic lubrication theory for rectangular

conjunctions which are formed due to deformation of line contacts. One important aspect of this work is that the fluid film thickness at the contact is almost uniform, and its width as well as corresponding pressure distribution are closer to that of Hertzian dry contact. In the present investigation, the central film thickness, h_o, of the Hertzian zone have been taken as a uniform film thickness along the Hertzian width. The minimum film thickness corresponding to the pressure spike is neglected and only the central film thickness is considered.

5.2.1 Steady Elastohydrodynamic Load

Consider a general case of elastohydrodynamic line contact as shown in Figure 5.1a, with two rollers of radii R_1, and R_2 having surface velocities U_1, and U_2 respectively. A simplified case of the line contact have been shown in Figure 5.1b for pure sliding ($\phi = 0$) condition, where the cylinder slides over a stationary plane with a velocity, U_r.

In the present study, elastohydrodynamic analysis assumes constant fluid temperature and an incompressible fluid with a variable viscosity-pressure relation. Neglecting leakage in the axial direction, Reynolds equation for steady conditions in the contact has been obtained as,

$$\frac{d}{dx}\left(\frac{h^3}{\eta}\frac{\partial p}{\partial x}\right) = 6\,U_r(1+\phi)\frac{dh}{dx} \tag{5.1}$$

where U_r ($U_r = U_1$) is surface velocity of the moving surface, ϕ is the rolling to sliding ratio [($\phi = U_2/U_1$ with $U_2 < U_1$) Harnoy (1976)], p is absolute pressure, η is fluid viscosity and h is film thickness at the contact. The fluid viscosity, η in the contact is not

constant, but is function of pressure which have been taken from Barus (1949), and it can be expressed as,

$$\eta = \eta_o e^{\xi p} \tag{5.2}$$

where η_o is viscosity at zero absolute pressure, and ξ is the pressure-viscosity coefficient.

The steady elastohydrodynamic fluid film load capacity, w_s, per unit length is obtained by solving Equation 5.1 and Equation 5.2. The solution includes elastic deformation of the surfaces in contact [see Hamrock (1994)]. The following dimensionless equation for fluid film load capacity, $\overline{W}_s$, has been obtained by rearranging the equation of Pan and Hamrock (1989) as:

$$\overline{W}_s = 635.91\,[0.5\overline{U}_r(1+\phi)]^{4.169}(\overline{E})^{2.831}(\overline{H})^{-6.024} \tag{5.3}$$

where $\overline{W}_s, \overline{U}_r, \overline{E}$, and $\overline{H}$ are dimensionless static load capacity per unit length, velocity, elastic modulus, and central film thickness, respectively, which are defined as follows:

$$\overline{W}_S = \frac{1}{ER_{eq}} w_S, \qquad \overline{U}_r = \frac{\eta_O}{ER_{eq}} U_r, \qquad \overline{E} = \xi E, \qquad \overline{H} = \frac{h_o}{R_{eq}} \tag{5.4}$$

where h_o is the central fluid film thickness, E is the equivalent elasticity modulus of the two surfaces in contact, R_{eq}, is an equivalent radius of the two cylinders which are determined from the following relations as:

$$2E^{-1} = (1-\nu_1^2)E_1^{-1} + (1-\nu_2^2)E_2^{-1} \tag{5.5}$$

$$R_{eq}^{-1} = R_1^{-1} + R_2^{-1} \tag{5.6}$$

ıere E_1 and E_2 are the modulii of elasticity, and ν_1 and ν_2 are Poisson's ratio and

and R_2 are radii of the two rollers respectively. The radius of curvature for a concave rface is negative, and it is infinity for a plane surface. In this case, according to Figure 1*b*, $R_1 = R$ and $R_2 = \infty$, therefore, $R_{eq} = R_1 = R$.

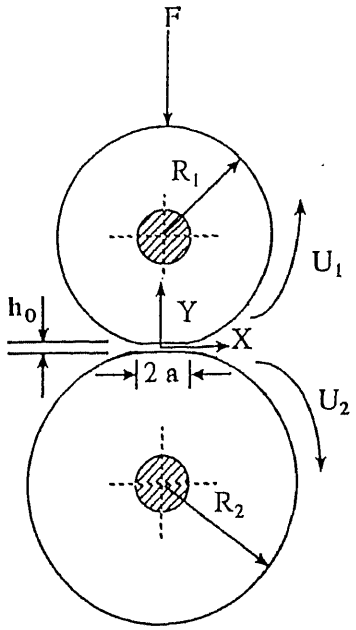

Figure 5.1a

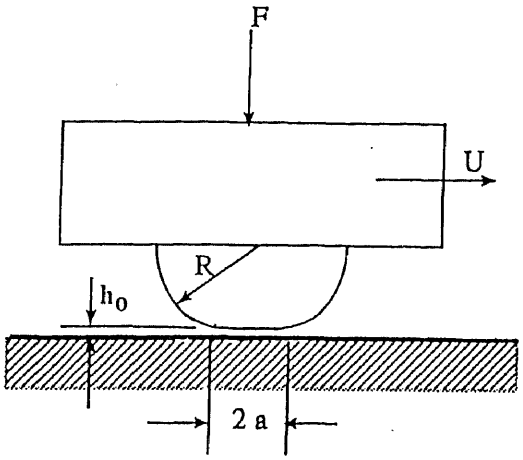

Figure 5.1b

Figure 5.1 Non-conformal contact (Elastohydrodynamic line contact) (a) between two cylinders (b) between a plane and translating roller ($\phi = 0$).

2.2 Contact Force w_e in Mixed Friction Region

he mixed friction region in the contact occurs at low velocity. According to the cperiments, the mixed region is shown as a negative slope in the steady friction versus elocity ($f - U$) curve. In the mixed region, the load is carried partly by the contact etween the asperities and partly by the elastohydrodynamic fluid film. As the sliding and olling velocity, $U_r(1+\phi)$, increases, a larger part of the load is carried by the fluid film nd the friction force decreases, because the viscous friction is less than the contact

friction. At higher velocities, the fluid film completely separates the surfaces. There is a transition velocity, U_{tr}, corresponding to the transition from mixed to elastohydrodynamic lubrication region. The transition velocity, U_{tr}, is equal to the steady sliding and rolling velocity, $U_r(1+\phi)$. The magnitude of the transition velocity, U_{tr}, can be obtained from the experimental Stribeck curve, while the fluid film thickness at the transition, h_{tr}, can be obtained from the elastohydrodynamic equation and U_{tr}.

Surface asperities at the contact undergo appreciable elastic as well as plastic deformation due to the contact force or load. These deformed asperities behave like non-linear springs and generate a reaction force at the contact in the direction normal to the surface. The stiffness of these asperities can be assumed as a function of the elastic deformation, δ of the asperities in the direction normal to the surface. The average elastic deformation of the asperities δ, can be expressed as the difference between the transition and the central film thickness,

$$\delta = h_{tr} - h_o \tag{5.7}$$

The reaction force, w_e, per unit length, between the asperities can be expressed as [Harnoy (1993, 1994)]:

$$w_e = K_n \delta \tag{5.8}$$

where K_n is the stiffness of the surface asperities per unit length in the direction normal to the surface. The contact area increases with the deformation δ of the surface. Therefore, the stiffness, K_n, is an increasing function of deformation, δ.

Substituting the definition of elastic deformation δ defined in Equation 5.7 in Equation 5.8, the elastic reaction force w_e can be expressed in the following form:

$$w_e = K_n(h_{tr} - h_o)\Delta \tag{5.9}$$

;re Δ is defined as:

$$\Delta = \begin{cases} 1, & if\,(h_{tr} - h_o) > 0 \\ 0, & if\,(h_{tr} - h_o) < 0 \end{cases} \tag{5.10}$$

The elastic reaction force, w_e, defined in Equation 5.9 reduces to zero as the film kness, h_o, increases above the transition film thickness h_{tr}. This phenomenon indicates : in the fully developed elastohydrodynamic lubrication region, $w_e = 0$ and there is no tact friction. However, in the mixed lubrication region, whenever h_o goes below the ısition film thickness h_{tr}, there is a contact between the surface asperities exerting a -zero contact force, w_e. The contact force, w_e defined in Equation 5.9 can be ısformed into the following dimensionless form:

$$\overline{W}_e = \kappa_n(\overline{H}_{tr} - \overline{H})\Delta \tag{5.11}$$

ere $\overline{W}_e$ and κ_n are the dimensionless reaction force and stiffness of the asperities ined as follows:

$$\overline{W}_e = \frac{1}{ER_{eq}} w_e \qquad \kappa_n = \frac{K_n}{E} \tag{5.12}$$

.3 Unsteady Elastohydrodynamic Load

s very well understood that from previous chapters that the friction behavior under ıamic or unsteady velocity conditions is different from the steady velocity conditions. erefore, it is necessary to introduce the dynamic conditions. Under dynamic velocity ıditions, there is an additional load capacity component, w_d, associated with time- iable fluid film thickness (squeeze film force). It is assumed that there exists an

quivalent viscosity, η_{eq}, of the lubricant, so that w_d can be derived from the principles of queeze film action. The equivalent viscosity, η_{eq}, is calculated from Equation 5.2, based n the average pressure $(F/2a)$. Also, the film thickness, h_o, in the contact is assumed to e constant, and is approximated to the central film thickness. The dynamic load mponent, w_d, per unit length is:

$$w_d = -\eta_{eq} \frac{(2a)^3}{h_o} \frac{dh_o}{dt} \tag{5.13}$$

here a is the semiwidth of the Hertzian zone which is assumed to be a function of nstant external force (load), F, per unit length, and can be determined from the llowing equation as:

$$a = (\frac{8}{\pi} \frac{FR_{eq}}{E})^{0.5} \tag{5.14}$$

Substituting lubricant viscosity, η from Equation 5.2, and dimensionless variables efined in Equation 5.4, the dimensionless dynamic load, $\overline{\ }_d$ is obtained as:

$$\overline{W}_d = -8\overline{\eta}_{eq}\overline{a}^3(\overline{H})^{-3}\dot{\overline{H}} \tag{5.15}$$

here $\dot{\overline{H}}$ is derivative with respect to dimensionless time, τ, and the dimensionless arameters defined as:

$$\overline{V}_d = \frac{1}{ER_{eq}} w_d, \qquad \overline{\eta} = \frac{U_{tr}}{ER_{eq}}\eta, \qquad \overline{a} = \frac{a}{R_{eq}} \qquad \tau = \frac{U_{tr}}{R_{eq}} t \tag{5.16}$$

The total fluid film force in the contact can be obtained by summing up the steady nd dynamic (squeeze film) load capacities w_s, and w_d. In fact, in the classical ydrodynamic theory, these two effects are superimposed. Since the steady pressure is

high enough, cavitation due to positive film thickness, $\overline{H}$ in line contacts (in Equation 5.15) is not expected.

The load of the capacity fluid film in the contact is obtained by assuming the density of asperities in the mixed region is sufficiently low so that it does not affect the flow of fluid significantly, and does not influence the hydrodynamic action Harnoy and Friedland (1993). Even though the fluid film forces, w_s, and w_d are very low in mixed region ($\Delta =$), they are not neglected. The load capacity, w, in the mixed region is a vector summation of elastic reaction, w_e, and elastohydrodynamic loads, w_s, and w_d. However, in the elastohydrodynamic region, $\Delta = 0$, there is no surface contact, therefore, there is no elastic reaction force. The dimensionless form of the load capacity, $\overline{W}$ on the contact per unit length is obtained by adding Equation 5.11, Equation 5.3 and Equation 5.15 as:

$$\overline{W} = \kappa_n(\overline{H}_{tr} - \overline{H})\Delta + 635.91\,[0.5\,\overline{U}_r(1+\phi)]^{4.169}(\overline{E})^{2.831}(\overline{H})^{-6.024} - 8\overline{\eta}_{eq}\overline{a}^3(\overline{H})^{-3}\dot{\overline{H}} \quad (5.17)$$

5.2.4 Dynamic Equation of System

The mass of the roller surface, m, which is supported by the fluid film undergoes a small motion in y direction normal to the surface as a result of acceleration of the fluid film in the contact. Therefore, the acceleration of the mass, m is equal to the acceleration of the fluid film thickness, $\ddot{h}_o$, which is determined by the difference of the load capacity, w, and the external force, F. According to the Newton's second law of motion (m, F and w are per unit length), the acceleration of the mass is given as:

$$w - F = m\ddot{h}_o \tag{5.18}$$

Substituting Equation 5.17 into Equation 5.18, the following dimensionless equation of motion is obtained:

$$\overline{F} = \kappa_n(\overline{H}_{tr} - \overline{H})\Delta + 635.91\,[0.5\,\overline{U}_r(1+\phi)]^{4.169}(\overline{E})^{2.831}(\overline{H})^{-6.024} - 8\overline{\eta}_{eq}\overline{a}^3(\overline{H})^{-3}\dot{\overline{H}} - \overline{m}\ddot{\overline{H}} \tag{5.19}$$

Dimensionless forms of $\overline{m}$ and $\overline{F}$ are defined as:

$$\overline{m} = \frac{U_{tr}^2}{ER_{eq}^{\ 2}}\,m, \qquad \overline{F} = \frac{1}{ER_{eq}}F \tag{5.20}$$

5.2.5 Friction Force at Contact

The friction force, F_f, at the contact, in the tangential direction of the contact surface, is a combination of contact and viscous friction forces. The mechanical contact part of the friction force is proportional to the normal reaction load, w_e, and is assumed to follow the well known Coulomb's law of friction. Adding viscous friction, based on equivalent viscosity, to the mechanical friction, the total friction, F_f, per unit length in the contact can be expressed as:

$$F_f = f_m K_n(h_{tr} - h_o)\Delta\ \mathrm{sgn}(U_r) + \frac{2a\eta_{eq}U_r(1-\phi)}{h_o} \tag{5.21}$$

where $\mathrm{sgn}(U_r)$ term is same as $\mathrm{sgn}(U)$ which have been defined already in Equation. 2.7, and f_m is mechanical friction coefficient accounted for by Coulomb's friction law at the contact, which can be determined from friction measurements. The mechanical friction

coefficient is equal to the maximum friction in the $f-U$ (Stribeck) curve at zero sliding velocity. The equivalent viscosity, η_{eq}, can be determined by integrating Equation 5.2 as:

$$\eta_{eq} = \frac{\eta_o}{2a}\int_{-a}^{a} e^{\xi p} dx \tag{5.22}$$

Precision of the model can be improved by solving Equation 5.21 for the equivalent viscosity, η_{eq}, by from the measured friction force F_f with the aid of steady friction experiments. The dimensionless form of Equation 5.21 is:

$$\overline{F}_f = f_m \kappa_n (\overline{H}_{tr} - \overline{H})\Delta \ \mathrm{sgn}(\overline{U}_r) + 2\overline{a}\frac{\eta_{eq}}{\eta_o}\frac{\overline{U}_r(1-\phi)}{\overline{H}} \tag{5.23}$$

where the friction force $\overline{F}_f$ can be defined as:

$$\overline{F}_f = \frac{1}{ER_{eq}} F_f \tag{5.24}$$

The coefficient of dynamic friction, $f(\tau)$, at the contact is defined as the ratio of the friction force, $\overline{F}_f$ and external force, $\overline{F}$.

$$f(\tau) = \frac{\overline{F}_f}{\overline{F}} \tag{5.25}$$

Equation 5.19 and Equation 5.23 represent the dynamic friction model for a non-conformal line contact. Equation 5.19 can be integrated numerically to solve for the dimensionless central film thickness, $\overline{H}$, which in turn is substituted into Equation 5.23 for friction force. The time variable friction coefficient, "$f(\tau)$" here after referred as "f" can be determined as a function of the sliding velocity.

5.3 Simulation of Model for Dynamic Friction

The model can be used to simulate dynamic friction for any dynamic velocity, provided that all the model coefficients such as η_{eq}, h_{tr} and the stiffness, κ_n, of the asperities, are known. In the following simulations, it is assumed that κ_n is an increasing linear function of the deformation of the asperities, $(h_{tr} - h)$, since the contact area between the asperities increases with the deformation. A linear relation for stiffness, κ_n, is:

$$\kappa_n = \kappa_o \frac{\overline{H}_{tr} - \overline{H}}{\overline{H}_{tr} - \overline{H}_b} \tag{5.26}$$

where the dimensionless central clearance, $\overline{H}_b$, corresponds to the film thickness h_b at the transition from the boundary to the elastohydrodynamic region, and κ_o is a constant dimensionless coefficient of stiffness of the asperities defined as:

$$\kappa_o = \frac{\overline{F}}{\overline{H}_{tr} - \overline{H}_b} \tag{5.27}$$

The model is simulated for two types of velocity oscillations with pure sliding mode, $\phi = 0$, and the mechanical friction factor, $f_m = 0.1$, as shown in Figure 5.1*b*. The data required for the simulation have been and derived for a typical line contact and is presented in the following Table 5.1 along with other data such as mechanical friction coefficient:

Table 5.1: Data required for simulation

$\overline{U}_{tr} = 1.5x10^{-10}$	$\overline{E} = 4200$	$\eta_{eq}/\eta_o = 2.7$
$\overline{H}_{tr} = 4.4x10^{-5}$	$\overline{H}_b = 5.2x10^{-6}$	$\overline{m} = 2.4x10^{-2}$

From the above dimensionless parameters, external force at transition, $\overline{F}$ and stiffness constant of the asperities, κ_o have been computed using Equation 5.19 and Equation 5.27 respectively as given in Table 5.2:

Table 5.2 Additional data required for simulation

$\overline{F} = 0.0223$	$\kappa_o = 575.37$

5.3.1 Uni-directional Oscillating Sliding Velocity

The first example selected for simulating the model for dynamic friction is an uni-directional oscillating velocity. Uni-directional velocity oscillations have been chosen to compare the performance of the current model with the experimental results of Hess and Soom (1990). This example is relatively simple since there is no transition at zero velocity. The dimensionless velocity chosen for the simulation oscillates between two 0.1 and 2.1, according to the following equation:

$$\overline{U} = 1.1 + \sin\alpha\,\tau \qquad \text{or} \qquad \overline{U} = 1.1 + \sin\omega t \tag{5.28}$$

where $\overline{U}$ is the velocity ratio ($\overline{U} = U_r/U_{tr}$), and α is the dimensionless frequency of velocity oscillations as defined in Equation 2.37 ($\alpha = \Omega/\omega_{tr}$).

The time-variable friction is simulated by performing numerical integration of Equation 5.19 to solve for the film thickness, $\overline{H}$, as a function of time, for the periodic velocity $\overline{U}$ defined in Equation 5.28. The initial value of film thickness, $\overline{H}$, can be selected arbitrarily, and after a few cycles, a steady state is reached at periodic film thickness, $\overline{H}$. The periodic friction coefficient $f(\tau)$ can be determined by substituting

the film thickness, $\overline{H}$, into Equations 5.23 and 5.25. Results of the simulation are presented in the form of $(f - \overline{U})$ curves as shown in Figure 5.2.

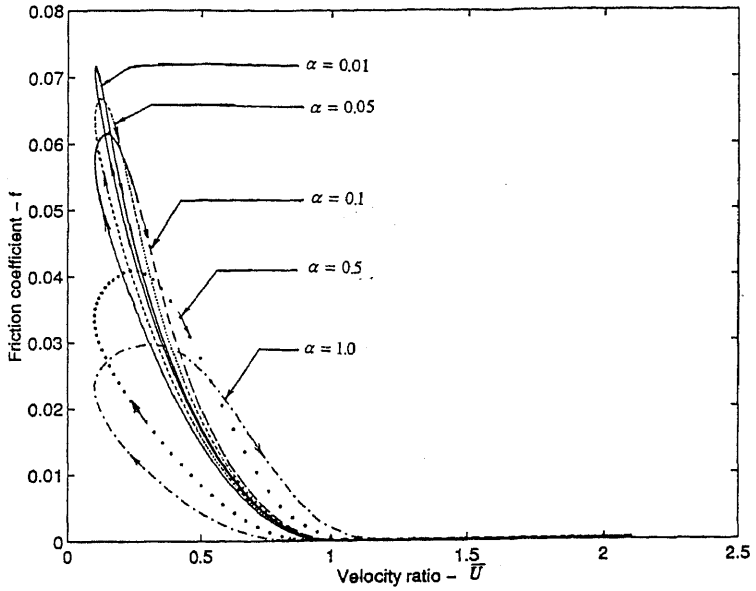

Figure 5.2 Friction coefficient, *f Vs* dimensionless velocity (velocity ratio) of the roller, $\overline{U}$ with $\overline{U} = 1.1 + \sin \alpha\tau$, and for various frequency ratio, α.

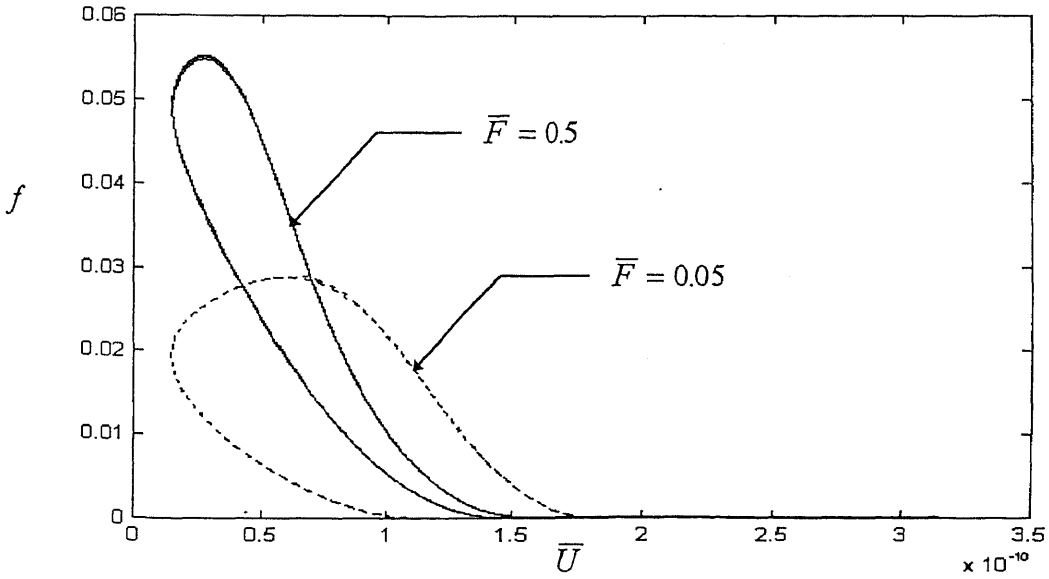

Figure 5.3 Friction coefficient, *f Vs* dimensionless velocity (velocity ratio) of the roller, $\overline{U}$ with $\overline{U} = 1.1 + \sin \alpha\tau$, and for various dimensionless load, $\overline{F}$.

The $(f - \overline{U})$ curves shown in Figure 5.2 indicate dynamic effects, such as phase lag and hysteresis. At very low frequencies of velocity oscillation $(\alpha \rightarrow 0)$, the $(f - \overline{U})$ curve reduces to the Stribeck curve. However, the hysteresis effect is more pronounced at higher frequency of velocity oscillations. It is also evident from Figure 5.2 that the maximum friction decreases with increase in frequency of oscillations. The analytical results presented in Figure 5.2 are in qualitative agreement with the experimental results of Hess and Soom (1990) which were conducted under similar conditions of line contact and unidirectional oscillating sliding velocity. The model also has been simulated for various dimensionless load, as shown in Figure 5.3.

5.3.2 Bi-directional Oscillating Sliding Velocity

A second example chosen for friction simulation is a sinusoidal velocity which passes through zero velocity. These velocity oscillations are of interest, since most of the motion in a control system involves harmonic oscillations passing between positive and negative velocity values. The velocity varies with time according to the equation:

$$\overline{U} = 2\sin(\alpha\,\tau) \qquad \text{or} \qquad \overline{U} = 2\sin(\omega t) \tag{5.29}$$

Simulation results for this velocity oscillations are presented in Figure 5.4. The friction curves exhibit a discontinuity at zero velocity as observed by Harnoy(1993, 1994). The magnitude of friction at zero velocity is less than the maximum friction. The maximum friction as well as the magnitude of the discontinuity at zero velocity decreases with increase in frequency of velocity oscillations, α.

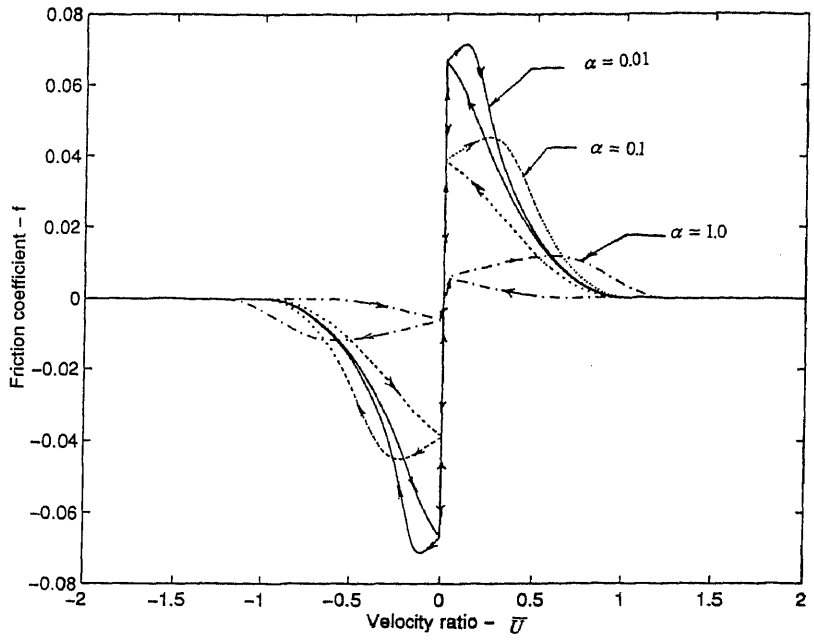

Figure 5.4 Friction coefficient, *f Vs* dimensionless velocity (velocity ratio) of the roller, $\overline{U}$ with $\overline{U} = 2\sin\alpha\tau$ for various frequency ratio, α.

Harnoy et. al. (1994) conducted experiments using a hydrodynamic journal bearing for similar sinusoidal velocity oscillations. Although the range of the sliding velocity in the experiment is limited in comparison to the wider velocity range in the simulation, results of the model indicate similar hysteresis effect and discontinuity at zero velocity as that obtained in this analytical simulation of Harnoy and Friedland (1993) and the friction measurements discussed in the Chapter 3. There is also an agreement in the trend of the decreasing magnitude of the friction step, at zero velocity. In fact, the experiments indicate that above a certain frequency of oscillations, the discontinuity is reduced and there is zero friction at zero velocity, particularly at high frequencies of velocity oscillations. This effect is predicted by the present friction model, but cannot be derived from earlier models based on friction phase lag. Bowyer also observed [see Cameron

(1979)] a similar type of hysteresis in his experiments. Polycarpou and Soom (1992) also obtained similar hysteresis in friction versus velocity curves in their friction experiments.

5.4 Comparison of Friction Curves for Steady Velocity

Although the journal and sleeve, in hydrodynamic journal bearing, form a conformal surfaces at low velocities, there is also a line contact with high contact pressure. The contact surfaces undergo deformation and the viscosity of the lubricant in the contact is affected. This deformation may play a significant role on the load capacity and fluid film thickness. In order to investigate the elastohydrodynamic effect in journal bearings, in the mixed lubrication region, friction experiments were conducted on a journal bearing at steady velocities, using the apparatus described in the Chapter 3 and Harnoy et. al. (1994), $f - \overline{U}$ (Stribeck) curve, have been plotted. The results are compared to the curves obtained from the analytical model of hydrodynamic lubrication theory developed in the Chapter 2, and Harnoy and Friedland (1994) as well as the present analytical model based elastohydrodynamic lubrication theory. The bearing data used in the experiments for the steady $f - \overline{U}$ curve is as shown in the following Table 5.3:

Table 5.3 Short journal bearing data

Radius of journal	$R = 12.7 \times 10^{-3}$ m
Length of sleeve	$L = 19 \times 10^{-3}$ m
Radial clearance in bearing	$C = 1.27 \times 10^{-5}$ m
External force	$F = 200$ N

The transition velocity, U_{tr}, was determined experimentally from the Stribeck curve as: $U_{tr} = 0.284$ m / s. The values of the equivalent viscosity, η_{eq}, and film thickness at transition, h_{tr}, were also determined from experiments as explained earlier. These coefficients were used in the simulation.

Comparison of the theoretical $f - \overline{U}$ curves derived from the hydrodynamic lubrication theory, the elastohydrodynamic theory and experimental data are shown in Figure 5.5. These curves indicate that the friction measured by the experiments in the mixed region is in better agreement with the hydrodynamic lubrication theory.

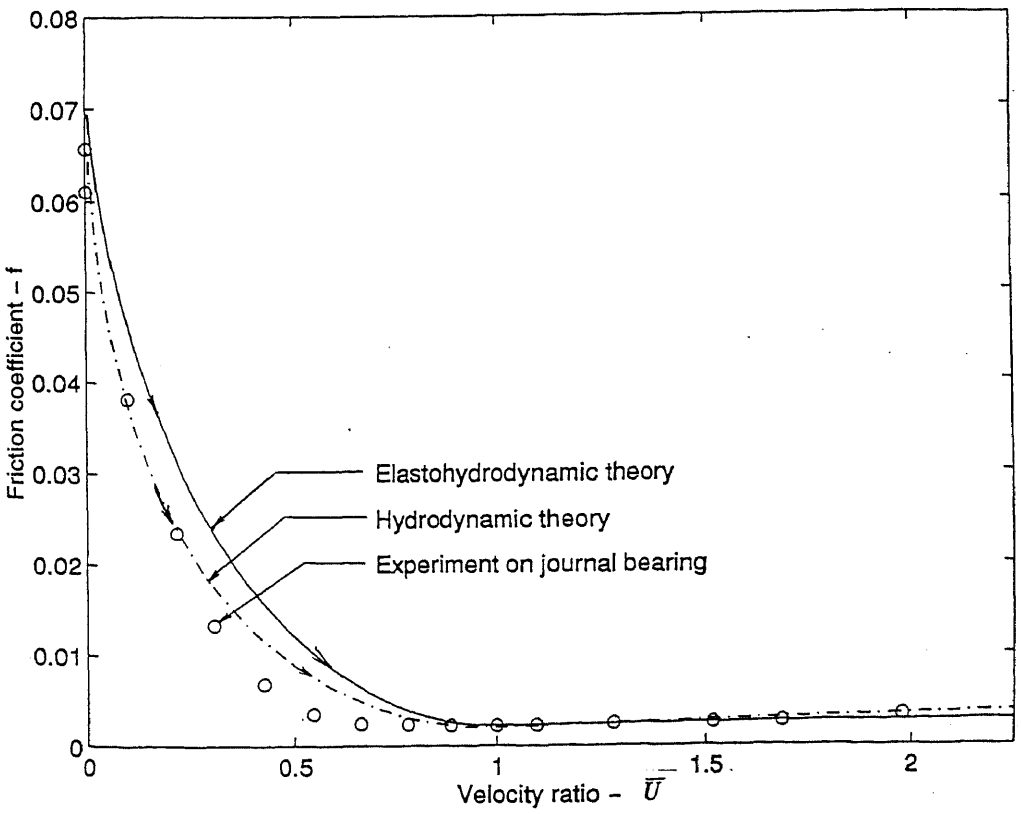

Figure 5.5 Steady Stribeck, $f - \overline{U}$ curves plotted from hydrodynamic theory, elastohydrodynamic theory and experiment on short journal bearing.

5.5 Summary

In this chapter, an analytical dynamic friction model for a non-conformal contact formed by a roller and a flat surface have been developed. The concept of the model is same as the concept used in Chapter 2, except the lubrication theory. This model is based on elastohydrodynamic lubrication theory which considers the elastic deformation of the surfaces in contact, and the viscosity variation with contact pressure. According to the results of the present model, friction is a memory function of the velocity. The $f - \overline{U}$ curves shown in results indicate that the friction is not only a function of the instantaneous velocity, but is also a function history of velocity. In the low velocity region, at any given velocity, the friction is higher for time-increasing velocity when compared to the friction for time-decreasing velocity. Moreover, the rate of change of velocity is also important, and the difference between the magnitude of friction at increasing and decreasing velocity is more pronounced as the rate increases. As a result the hysteresis effect is more pronounced at high frequencies of velocity oscillations. These trends are in qualitative agreement with the earlier experiments as well as the friction measurements on journal bearing as described in Chapter 3.

The physical explanation of the memory effect in this study, can be described as the motion of the sliding surface in the direction normal to the sliding surface. At steady velocity, the lubrication film thickness is determined by the sliding velocity. However, for time-variable velocity, there is a time-delay to squeeze the fluid film or increase it to the steady thickness level.

This model can be extended for point contacts where the deformation of the surfaces is quite different, and dynamic load is also different. The present model also can

nded to investigate the stick-slip friction phenomena in non-conformal line
s. This model can be verified by setting up a separate apparatus for friction
ements. Once the model is verified, it can be used for on-line compensation.
A model based friction compensation can offer a new effective method to enhance
cision of motion in control system. On-line estimation of equivalent viscosity, η_{eq}
rove the precision of the model. This can be achieved by on-line estimation
s, based on measured parameters such as displacement and velocity.

CHAPTER 6

CONCLUSIONS AND RECOMMENDATIONS

6.1 Conclusions

Dynamic friction behavior of lubricated contacts has been modeled for different dynamic velocity conditions including uni-directional and bi-directional oscillations. The following are the results of this investigation:

1. A friction model developed by Harnoy and Friedland (1993) for a conformal contact formed by a journal bearing operating on hydrodynamic lubrication theory shows a phase lag in the friction as manifested by hysteresis in friction versus velocity ($f - U$) curves for uni-directional and bi-directional velocity oscillations. Simulation results for bi-directional velocity oscillations show a discontinuity in friction at velocity reversals. Friction results for uni-directional velocity oscillations are in good agreement with the experimental measurements on a line contact of Hess and Soom (1990).
2. A special apparatus has been designed and built by the team using a short journal bearing to the verify the above analytical model. Experiments have been conducted to measure the dynamic friction in the bearing for uni-directional and bi-directional sinusoidal periodic velocity oscillations. Friction measurements resulted a phase lag in the friction as manifested by hysteresis in the $f - U$ curves. These results have been compared to the simulation results of the analytical model, which indicate qualitative and quantitative agreement between the analytical model and experiments. Simulation results for bi-directional velocity oscillations are in good qualitative and quantitative

agreement in mixed and hydrodynamic friction regimes. But, there is a disagreement in friction at velocity reversals. Measured friction for bi-directional velocity oscillations shows that friction at starting and stopping corresponding to zero velocity, is different when compared to the simulation results of theory, which shows that the friction at starting and stopping corresponding to zero velocity is same. The magnitude of the discontinuity in friction at velocity reversal obtained from the friction measurements is higher than the magnitude of the discontinuity in friction obtained from analytical solution which may be due to dry friction at zero velocity. The results indicate that the measured friction has dry friction at zero velocity, and the analytical model could not capture the dry friction at zero velocity. The analytical model of Harnoy and Friedland (1993) need to be modified to account this difference in friction behavior at the zero velocity by conducting experiments on dry friction.

3. The above analytical model [Harnoy and Friedland (1993)] has been extended to investigate the effect of resisting forces on the dynamic friction behavior at low speed. In this study, resisting forces such as presliding friction known as "Dahl" effect and sliding friction have been considered for modeling. Behavior of the model under uni-directional velocity oscillations are in qualitative agreement with earlier experimental and analytical work. During bi-directional velocity oscillations, the model shows an improvement in dynamic friction behavior. The improvement is that the discontinuity at the zero velocity is replaced by a slope. The simulation results indicate that the stiffness of the surface asperities plays a significant role in replacing the discontinuity to a slope.

4. The concept used in developing the analytical model for a conformal contact [Harnoy and Friedland (1993)] has been applied to develop a friction model for a non-conformal contact. In this study, a non-conformal contact formed by a roller sliding over a flat surface operating on elastohydrodynamic lubrication theory has been considered for friction modeling. Simulation results of the model for uni-directional and bi-directional velocity oscillations show a phase lag in the friction as manifested by hysteresis in $f - U$ curves as displayed by other models and experimental results.

Simulation results of the above analytical models and friction measurements indicate that there is a phase lag in the friction as manifested by hysteresis in $f - U$ curves. From this observation, it can be concluded that the instantaneous friction is not only a function of the instantaneous velocity but also is a function of the velocity history. The analytical models discussed in the above section can be improved with the aid more experimental work.

6.2 Recommendations

All the above models and the experiments have been focused on friction behavior resulted from the response of the system under given dynamic conditions. Further investigation is required to determine how this friction influences performance of the system directly or indirectly when it is subjected to dynamic conditions. In order to determine the effect of friction on the system, on-line estimation of the system parameters, such as displacement, velocity and acceleration as well as viscosity of the lubricant is recommended. Thus, the estimated parameters of the system can be used to analyze the behavior of the system.

The analysis will be very useful in friction compensation processes required for precise motion control systems.

Further, the above analytical models can be successfully used for friction compensation so that the effect of friction such as stick-slip can be eliminated. These models can be further extended for analyzing the stick-slip phenomenon. Also, these concepts can be used to develop analytical models for other non-conformal contacts such as point contacts. Techniques used in developing these models can be improved for estimating friction in dry contacts.

APPENDIX A

COMPUTER PROGRAM TO SIMULATE THE MODEL DISCUSSED IN CHAPTER 2

The analytical model of Harnoy and Friedland (1993) developed in the Chapter 2 has been simulated using numerical techniques. A computer program using FORTRAN77 has been developed for simulation. Later, the model has been simulated by using a special simulating environment as discussed in the following sections. Following is the code written using the finite difference method to solve the differential equations of the friction model represented by Equations 2.29-2.32. The details of the these equations are discussed in chapter which are given as,

$$\overline{F}\cos\varphi = \overline{\kappa}(\varepsilon)(\varepsilon - \varepsilon_{tr})\,\mathrm{sgn}(\overline{U})\Delta - 0.5J_{12}\varepsilon\overline{U} + J_{12}\varepsilon\dot{\varphi} + J_{22}\dot{\varepsilon} + \overline{m}(\ddot{\varepsilon} - \dot{\varepsilon}\dot{\varphi}^2) \qquad (2.29)$$

$$\overline{F}\sin\varphi = 0.5J_{11}\varepsilon\overline{U} - J_{11}\varepsilon\dot{\varphi} - J_{12}\dot{\varepsilon} - \overline{m}(\varepsilon\ddot{\varphi} + 2\dot{\varepsilon}\dot{\varphi}) \qquad (2.30)$$

$$\overline{F}_f = f_m\overline{\kappa}(\varepsilon)(\varepsilon - \varepsilon_{tr})\,\mathrm{sgn}(\overline{U})\Delta + \frac{CR}{L^2}\frac{2\pi}{(1-\varepsilon^2)^{0.5}}\overline{U} \qquad (2.31)$$

$$f(\tau) = \bar{f}(t) = \frac{\overline{F}_f}{\overline{F}} \qquad (2.32)$$

Following is one example of finite differences used in solving the above equations.

$$\dot{\varepsilon} = \frac{[\varepsilon(\mathrm{I}+1) - \varepsilon(\mathrm{I}+1)]}{2\Delta t} \qquad \text{and} \qquad \ddot{\varepsilon} = \frac{[\varepsilon(\mathrm{I}+1) - 2\varepsilon(\mathrm{I}) + \varepsilon(I-1)]}{(\Delta t)^2} \qquad (A1)$$

After substituting the finite differences for the variables, $\ddot{\varepsilon}, \dot{\varepsilon}, \varepsilon,$ and $\ddot{\varphi}, \dot{\varphi}, \varphi$, the following equations have been resulted.

$$A = B\varepsilon(\mathrm{I}+1) + C\varphi(\mathrm{I}+1) \qquad P = Q\varepsilon(\mathrm{I}+1) + R\varphi(\mathrm{I}+1) \qquad (A2)$$

where A, B, C, P, Q, and R are the variables derived after substituting the above mentioned finite differences and the term "I" refers to the step. The following code computes the magnitude of A, B, C, P, Q, and R for each step, and solves for the time variable ε and φ of the future step. Following are the definitions of the terms used in the code:

EC:	ε_{tr}
AC:	CR/L^2 defined in Equation 2.31.
KO:	dimensionless spring constant defined in Equation 2.35
M:	dimensionless mass defined in Equation 2.28
FM	Coulomb's friction coefficient used in Equations 2.6 and 2.31
J11, J12, J22:	are the integrals defined in Equations 2.23-2.25, J1 and J2 are at transition point used in Equation 2.33
E:	ε
FI:	φ
U:	dimensionless velocity defined in 2.36 and 2.38
FF, CF:	friction force and friction coefficient defined in Equations 2.31 and 2.32 respectively.
FX, FY:	components of load in x and y directions respectively
WE:	reaction force defined in Equation 2.3

```
      PARAMETER(N=30000)

      REAL EC,AC,K0,M,FM,J1,J2,D,EB,ALPHA,PI,DELTA
      REAL J11(N),J12(N),J22(N),E(N),FI(N),U(N),CF(N)
      REAL FF(N),FX(N),FY(N),WE(N)

      OPEN(1,FILE='indata',STATUS='UNKNOWN')
      OPEN(2,FILE='rfdata',STATUS='UNKNOWN')
      OPEN(3,FILE='rcf.dat',STATUS='UNKNOWN')

      PI=3.1415926
      EB=0.99
*     PRINT*, ' M = ? '
*     READ(*,*) M
*     PRINT*, ' ALPHA = ? '
*     READ(*,*) ALPHA
*     PRINT*,'AC=?'
*     READ(*,*)AC
*     PRINT*,'MECHANICAL FRICTION FACTOR FM=?'
*     READ(*,*)FM
*     PRINT*,'EC=?'
*     READ(*,*)EC
      READ(1,*)M,ALPHA,AC,FM,EC
      WRITE(2,10)

      PRINT*,  ' W A I T   P L E A S E  . . . . . '

* COMPUTATION OF CRITICAL FORCE FC*
      J1=PI/(2.*(1-EC**2)**1.5)
      J2=-2.*EC/(1-EC**2)**2
      FC=SQRT(((-0.5*J2*EC)**2)+((0.5*J1*EC)**2))
      K0=FC/(EB-EC)

      WRITE(2,*)'MASS=',M,'ALPHA=',ALPHA,'CONSTANT RCL2=',AC
      WRITE(2,*)'MEC.FRIC.FACTOR=',FM,'CRITICAL ECC.=',EC
      WRITE(2,*)'CRITICAL FORCE= ',FC,'SPRING CONSTANT= ',K

* DETERMINATION OF EPSILON FOR DIFFERENT VALUES OF "U"*

      WRITE(2,10)
      FI(0)=PI+(10.*PI)/180.
      E(0)=0.96
```

```
      WE(0)=0.0
      FI(1)=FI(0)
      CF(0)=0.0
      U(0)=0.0
      E(1)=E(0)
      CF(1)=CF(0)
      U(1)=U(0)
      WE(1)=WE(0)
      DT = PI/(90.*ALPHA)

      DO  100  I= 1,N
*     U(I)=2.*SIN(ALPHA*DT*I)
      U(I)=1.1+1*SIN(ALPHA*DT*I)
      J11(I)=PI/(2*(1-E(I)*E(I))**1.5)
      J12(I)=-2*E(I)/((1-E(I)*E(I))**2)
      J22(I)=(PI*(1+2*E(I)**2))/(2*(1-E(I)*E(I))**2.5).
      K=K0*(E(I)-EC)/(EB-EC)
      IF ((E(I)-EC).LT.0.0) THEN
      DELTA=0.
      ELSE
      DELTA=1.
      ENDIF
      WE(I)=DELTA*K*(E(I)-EC)
      FX(I)=1.0*FC*COS(FI(I)-PI)-WE(I)
      A1=0.5*ABS(U(I))*E(I)*J12(I)
      A2=E(I)*FI(I-1)*J12(I)/(2*DT)
      A3=E(I-1)*J22(I)/(2*DT)
      A4=2*M*E(I)/(DT*DT)
      A5=-M*E(I-1)/(DT*DT)
      A6=M*E(I)*FI(I)**2/(DT*DT)
      A7=M*E(I)*FI(I-1)**2/(DT*DT)
      A8=-2*M*E(I)*FI(I)*FI(I-1)/(DT*DT)
50    A=FX(I)+A1+A2+A3+A4+A5+A6+A7+A8
      B=J22(I)/(2*DT)+M/(DT*DT)
      C=E(I)*J12(I)/(2*DT)
      FY(I)=1.0*FC*SIN(FI(I)-PI)
      P1=-0.5*ABS(U(I))*E(I)*J11(I)
      P2=-E(I)*FI(I-1)*J11(I)/(2*DT)
      P3=-E(I-1)*J12(I)/(2*DT)
      P4=-2*M*E(I)*FI(I)/(DT*DT)
      P5=M*E(I)*FI(I-1)/(DT*DT)
      P6=M*E(I-1)*FI(I-1)/(DT*DT)
```

```
      P7=-M*E(I-1)*FI(I)/(DT*DT)
      P=FY(I)+P1+P2+P3+P4+P5+P6+P7
      Q=-J12(I)/(2*DT)-M*FI(I)/(DT*DT)+M*FI(I-1)/(DT*DT)
      R=-E(I)*J11(I)/(2*DT)-M*E(I)/(DT*DT)
      E(I+1)=(A*R-P*C)/(B*R-Q*C)
      FI(I+1)=(A*Q-P*B)/(C*Q-R*B)

* COMPUTATION OF FRICTION FORCE FF, FRICTION FACTOR CF FOR DIFFERENT U *
VALUES*

      D=1.
      IF(U(I).LT.0.0) THEN
      D=-1.
      ELSE
      D=1.
      ENDIF
      FF(I)=(D*FM*WE(I)+AC*U(I)*2*PI/((1-E(I)**2)**0.5))
      CF(I)=FF(I)/FC
      IF (I.GE.(N-300)) THEN
      WRITE(2,*)I,FI(I),E(I),U(I),FF(I),CF(I)
      WRITE(3,*)U(I),CF(I)
      ENDIF
100   CONTINUE
10    FORMAT('*_____
     &_____')
*20   FORMAT(3X,'#',4X,'EPSI',2X,'VEL',2X,'FR.FO',2X,'COF')
*30   FORMAT(2X,I8,2X,6F12.4)
      PRINT*,'        Y O U   G O T   IT'
120   STOP
      END
```

APPENDIX B

MATLAB PROGRAMS TO SIMULATE THE MODEL DISCUSSED IN CHAPTER 3 FOR COMPARING WITH EXPERIMENTAL RESULTS

The analytical model discussed in Chapter 2 also have been simulated using a different software tool to compare the experimental results as discussed in Chapter 3. Simulink tool of Matlab software have been used for the simulation purpose. The tool uses numerical integration. The differential equations to be solved by numerical integration are stored in a file as a special Matlab function, which will be accessed by the Simulink at the time of simulation. The data required for simulation also stored in a file, so that it can be supplied to the program before simulation. Following are the Matlab functions and data file. The Simulink diagram representing the model is shown in Figure A.1.

B.1. JOURN.M (Matlab function)

```
%  function defining the friction model differential equations of
%  conformal contact (Hydrodynamic short journal bearing).

function x = journal(u)

global FF EPS_CR EPS_B RCL MM FM KO

U = u(1);
eps = u(2);
epsdot = u(3);
phi = u(4);
phidot = u(5);

d = 1 - eps^2;
J11 = pi/2/d^1.5;
J12 = -2*eps/d^2;
J22 = pi*(1+2*eps^2)/2/d^2.5;


k = KO*(eps - EPS_CR)/(EPS_B - EPS_CR);
delta = 1;
if (eps<EPS_CR) delta = 0;
end

d = 0.5*eps*abs(U) - eps*phidot;

eps_dd = (FF*cos(phi) - k*(eps-EPS_CR)*delta + d*J12 - epsdot*J22)/MM +
eps*phidot^2;
```

```
phi_dd = (-FF*sin(phi) + d*J11 - epsdot*J12)/(eps*MM) -
2*epsdot*phidot/eps;

Ff = FM * k*(eps-EPS_CR)*delta*sign(U)  +  RCL*2*pi*U/(1-eps^2)^0.5;
f = Ff/FF;
x = [eps_dd  phi_dd f]';
```

B.2 JORDAT.M (Data)

```
% jordat.m   -   data file for journal bearing dynamic friction model

global FF EPS_CR EPS_B RCL MM FM KO

EPS_CR = 0.97775; % critical (or transition) eccentricity
EPS_B = 0.99;           % eccentricity at boundary to mixed transition
J11tr= (pi/(2*(1-EPS_CR^2)^1.5));
J12tr= (-2*EPS_CR/(1-EPS_CR^2)^2);
FF = sqrt((-0.5*J12tr*EPS_CR)^2+(0.5*J11tr*EPS_CR)^2) % dimensionless
                                                      % normal load
RCL = 0.01;       % dimensionless ratio of R*C/L^2
FM = 0.2;         % friction coefficient
MM = 100;         % journal mass
KO = FF/(EPS_B-EPS_CR)^1.0;   % Stifness constant fo the asperities
```

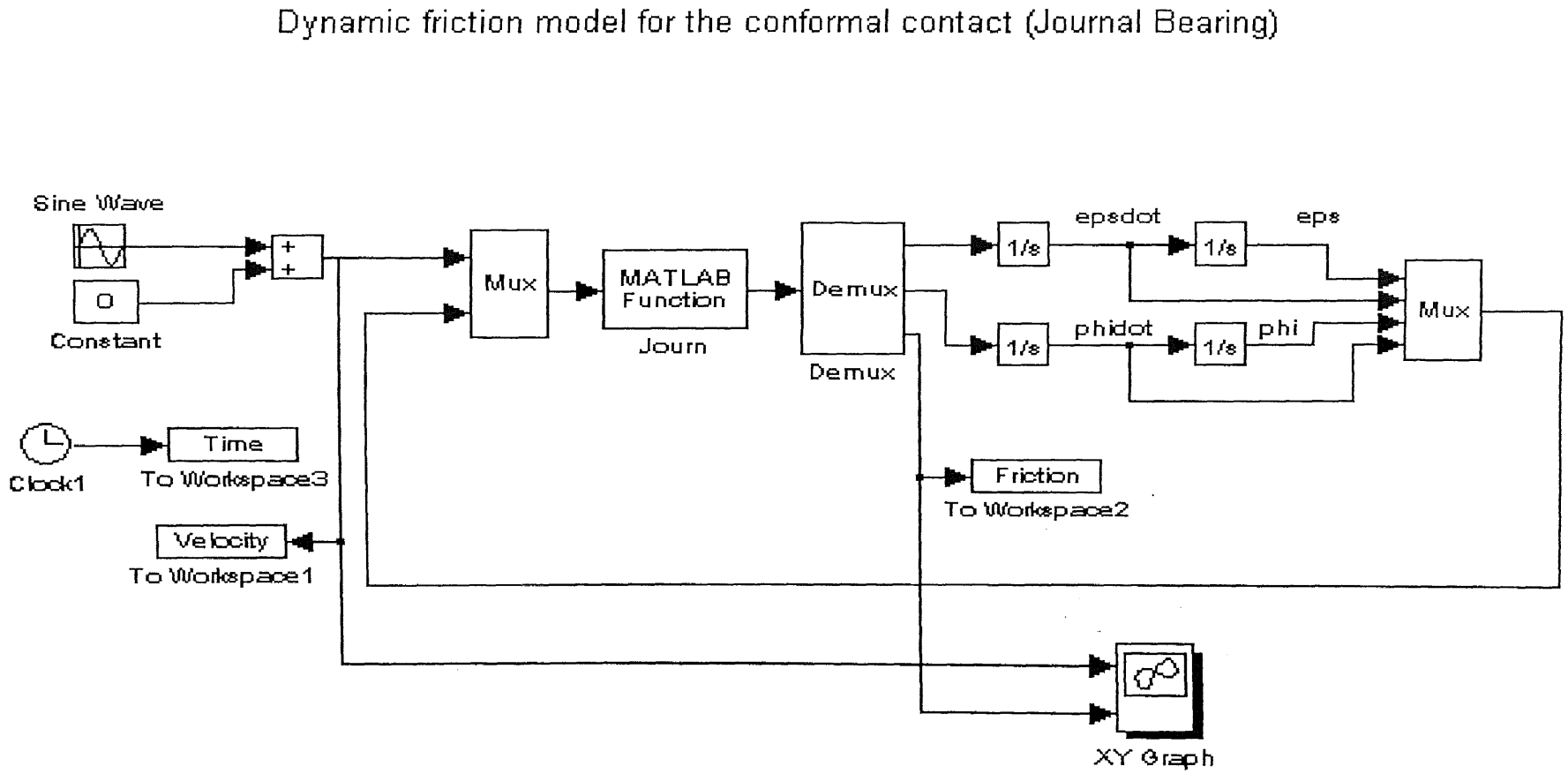

Figure B1 Visual simulation program for simulating dynamic friction in conformal contact formed by a lubricated hydrodynamic journal bearing (Chapter 3).

APPENDIX C

COMPUTER PROGRAMS

C.1 COMPUTER PROGRAMS TO SIMULATE THE MODEL DISCUSSED IN CHAPTER 4

The computer program developed for simulating the analytical model discussed in Appendix A has been modified for simulating the model discussed in Chapter 4. Following is the code to solve the differential equations of the friction model, investigating the resistance forces, including the Dahl effect. The following code is the extended version of the code discussed in the Appendix A including the equations of the model discussed in Chapter 4. The definition of the terms discussed in Appendix A are valid.

```
      PARAMETER(N=962000)

      REAL J11(N),J12(N),J22(N),E(N),U(N),FI(N),FF(N),CF(N),FX(N),FY(N)
      REAL WE(N),TJPR(N),TB(N),MWE(N),TJD(N),TBD(N),MJ(N),K(N)
      REAL MF(N)
      REAL ALPHA,DT,PI,EC,AC,DE,DF,K0,M,FM,J1,J2,D,EB,N1,N2,N3,N4
      REAL C1,C2,C3,C4,DELTA
      INTEGER NFLAG(N)

      OPEN(1,FILE='indata',STATUS='UNKNOWN')
      OPEN(2,FILE='fdata',STATUS='UNKNOWN')
      OPEN(3,FILE='cfdata',STATUS='UNKNOWN')
      OPEN(4,FILE='mfdata',STATUS='UNKNOWN')

      PI=3.1415926
      EB=0.99
      W0=2.00
      FM=0.2
      EC=0.96
      AC=0.010
      FAC=50.
*     PRINT*, ' M = ? '
*     READ(*,*) M
```

```
*       PRINT*, ' ALPHA = ? '
*       READ(*,*) ALPHA
        READ(1,*)M,ALPHA,AC,FM,EC
*       PRINT*,'ENTER TJ0,TB0'
*       READ(*,*)TJ0,TB0
        PRINT*, 'ENTER N1,N4'
        READ(*,*)N1,N4
        PRINT*,  ' W A I T    P L E A S E  . . . . . '

        N3=AC
        N2=N4+N1

* COMPUTATION OF CRITICAL FORCE FC*

        J1=PI/(2.*(1-EC**2)**1.5)
        J2=-2.*EC/(1-EC**2)**2
        FC=SQRT(((-0.5*J2*EC)**2)+((0.5*J1*EC)**2))
        K0=FC/(EB-EC)

*       WRITE(2,*)'MASS=',M,'ALPHA=',ALPHA,'CONSTANT RCL2=',AC
*       WRITE(2,*)'MEC.FRIC.FACTOR=',FM,'CRITICAL ECC.=',EC
        WRITE(2,*)'#CRITICAL FORCE= ',FC,'SPRING CONSTANT= ',K0
*       WRITE(3,*)'*MASS=',M,'ALPHA=',ALPHA,'CONSTANT RCL2=',AC
*       WRITE(3,*)'*MEC.FRIC.FACTOR=',FM,'CRITICAL ECC.=',EC
        WRITE(3,*)'*CRITICAL FORCE= ',FC,'SPRING CONSTANT= ',K0

* DETERMINATION OF EPSILON FOR DIFFERENT VALUES OF "U"*

        WRITE(4,*)'#','N1=  ',N1,'N2= ',N2,'N3= ',N3,'N4= ',N4
        WRITE(4,*)'#','MASS= ',M,'ALPHA= ',ALPHA,'EPSIINTIAL=  ',
       &EC,'A CONSTANT(AC)= ','####',AC
        WRITE(3,5)
        WRITE(4,6)
        WRITE(2,10)
        WRITE(3,10)
        WRITE(4,10)
* INITIAL CONDITONS      *
        FI(0)=0.
        E(0)=0.99
        WE(0)=0.0
        CF(0)=0.0
        U(0)=0.0
```

```
      TJPR(0)=0.
      TB(0)=0.
      TJD(0)=0.
      TBD(0)=0.
      FI(1)=FI(0)
      E(1)=E(0)
      TJPR(1)=TJPR(0)
      TB(1)=TB(0)
      CF(1)=CF(0)
      U(1)=U(0)
      WE(1)=WE(0)
      TJD(1)=TJD(0)
      TBD(1)=TBD(0)
      NFLAG(1)=0
      DT=PI/(1800.)


* COMPUTATION OF EPSILON *

      DO  100  I= 1,N
      U(I)=2.*SIN(ALPHA*DT*I)
      J11(I)=PI/(2*(1-E(I)*E(I))**1.5)
      J12(I)=-2*E(I)/((1-E(I)*E(I))**2)
      J22(I)=(PI*(1+2*E(I)**2))/(2*(1-E(I)*E(I))**2.5)

*CALCULATION OF SPRING CONSTANT k(d), DEFINING DELTA, AND ELASTIC
REACTION We*

      IF ((E(I)-EC).LT.0.0) THEN
      DELTA=0.
      ELSE
      DELTA=1.
      ENDIF
      K(I)=DELTA*K0*(E(I)-EC)/(EB-EC)
      WE(I)=DELTA*K(I)*(E(I)-EC)

*CALCULATION OF EPSILON *

      TJD(I)=U(I)
      TBD(I)=(TB(I)-TB(I-1))/DT

      FX(I)=1.0*FC*COS(FI(I))-WE(I)
```

```
      A1=0.5*E(I)*J12(I)*ABS(TJD(I)+TBD(I))
      A2=E(I)*FI(I-1)*J12(I)/(2*DT)
      A3=E(I-1)*J22(I)/(2*DT)
      A4=2*M*E(I)/(DT*DT)
      A5=-M*E(I-1)/(DT*DT)
      A6=M*E(I)*FI(I)**2/(DT*DT)
      A7=M*E(I)*FI(I-1)**2/(DT*DT)
      A8=-2*M*E(I)*FI(I)*FI(I-1)/(DT*DT)
50    A=FX(I)+A1+A2+A3+A4+A5+A6+A7+A8
      B=J22(I)/(2*DT)+M/(DT*DT)
      C=E(I)*J12(I)/(2*DT)
      FY(I)=1.0*FC*SIN(FI(I))
      P1=-0.5*E(I)*J11(I)*ABS(TJD(I)+TBD(I))
      P2=-E(I)*FI(I-1)*J11(I)/(2*DT)
      P3=-E(I-1)*J12(I)/(2*DT)
      P4=-2*M*E(I)*FI(I)/(DT*DT)
      P5=M*E(I)*FI(I-1)/(DT*DT)
      P6=M*E(I-1)*FI(I-1)/(DT*DT)
      P7=-M*E(I-1)*FI(I)/(DT*DT)
      P=FY(I)+P1+P2+P3+P4+P5+P6+P7
      Q=-J12(I)/(2*DT)-M*FI(I)/(DT*DT)+M*FI(I-1)/(DT*DT)
      R=-E(I)*J11(I)/(2*DT)-M*E(I)/(DT*DT)
      E(I+1)=(A*R-P*C)/(B*R-Q*C)
      FI(I+1)=(A*Q-P*B)/(C*Q-R*B)

* COMPUTATION OF FRICTION FORCE FF, FRICTION FACTOR CF FOR DIFFERENT U
VALUES*

      D=1.
      IF(U(I).LT.0.0) THEN
      D=-1.
      ELSE
      D=1.
      ENDIF
      FF(I)=(D*FM*WE(I)+AC*U(I)*2*PI/((1-E(I)**2)))
      CF(I)=FF(I)/FC
*     IF (I.GE.(N-300)) THEN
*     WRITE(2,*)I,ANGLE(I),FI(I),E(I),U(I),FF(I),CF(I)
*     WRITE(3,*)U(I),CF(I)
*     ENDIF
      MWE(I)=D*FM*WE(I)
```

```
* PRE-SLIDING REGION- COMPUTATION OF THETA"B",THETA"J",TORQUE MJ*

      TJPR(I)=TJPR(I-1)+DT*TJD(I)
      MF(I)=N1*(TJPR(I)-TB(I))
      IF(ABS(MF(I)).LT.ABS(MWE(I)))THEN
      NFLAG(I)=0
      ELSE
      NFLAG(I)=1
      ENDIF

      IF (NFLAG(I).EQ.0) THEN
      TJPR(I)=TJPR(I-1)+DT*TJD(I)
      MJ(I)=N1*(TJPR(I)-TB(I))
      TB(I+1)=(2.-DT**2*N2)*TB(I)-TB(I-1)+DT**2*N1*TJPR(I)
      ENDIF

* SLIDING REGION- COMPUTATION OF THETA"B",THETA"J",TORQUE MJ2*

      IF (NFLAG(I).EQ.1) THEN
      C1=(2/(DT**2))-N4
      C2=((PI*N3)/(DT*(1.-E(I)**2)**0.5))-(1/DT**2)
      C3=(2*N3*PI*TJD(I))/((1.-E(I)**2)**0.5)
      C4=(1/DT**2)+((N3*PI)/(((1.-E(I)**2)**0.5)*DT))
      TB(I+1)=(MWE(I)+C1*TB(I)+C2*TB(I-1)+C3)/C4
      TBD(I+1)=(TB(I+1)-TB(I))/(DT)
      MJ(I)=MWE(I)+2*N3*PI*(TJD(I)-TBD(I))/((1.-E(I)**2)**0.5)
      TJPR(I)=(MJ(I)/N1)+TB(I)
      ENDIF
      MJ(I)=MJ(I)/(FC)

100   CONTINUE

* PRINTING THE RESULTS *

      DO 200 I=(N-76400),N,20
*     WRITE(2,*)U(I),MJ(I),K(I),WE(I),MWE(I),E(I),NFLAG(I)
      WRITE(3,*)TJPR(I),TB(I),TJD(I),TBD(I),NFLAG(I)
      WRITE(4,*)U(I),MJ(I),NFLAG(I)*0.02

200   CONTINUE
5     FORMAT(1X,'#',4X,'TJPRIME '3X,'TB',3X,'TJD',3X,'TBD '
     &,3X,'NFLAG')
```

```
6      FORMAT('#',3X,'VELOCITY(U)',4X,'TORQUE(MJ)',3X,'NFLAG')
7      FORMAT(1X,'#',3X,'U',4X,'MJ',4X,'K',4X,'WE',4X,'MWE',4X,'EPSILON
      &',2X,'FLAG')
10     FORMAT('#_____________________________________________________
      &_____________________')
*20    FORMAT(3X,'#',4X,'EPSI',2X,'VEL',2X,'FR.FO',2X,'COF')
*30    FORMAT(2X,I8,2X,6F12.4)
       PRINT*,'         Y O U   G O T   IT'
120    STOP
       END
```

APPENDIX D

MATLAB PROGRAMS TO SIMULATE THE MODEL DISCUSSED IN CHAPTER 5

The analytical model discussed in Chapter 5 have been simulated Matlab with the help of Simulink tool. As discussed in the Appendix B, the differential equations and data required for simulation are stored in different files. These files will be accessed by the Simulink at the time of simulation. Following are the Matlab functions and data file. The Simulink diagram representing the model equations is shown in Figure A.2.

D.1 LCT.M (Matlab function)

```
%  function defining the friction model differential equation in %
% Rachoor and Harnoy model for  EHDL line contact.
%  The file name is LCT.M for the function ehdl(u).


function x = ehdl(u)

global Ftr K0 Htr Hb  Utr eta0 etaeq E Mm Fm ab etaeqb etar


UBAR = u(1);
H = u(2);
Hdot = u(3);


Kn = K0*(Htr - H)/(Htr - Hb);
delta = 1;
a = Htr - H;
if (a < 0) delta = 0;
end


Hdd = ( Kn*(Htr - H)*delta + 635.91 * UBAR^4.169 * E^2.831 * H^(-
          6.024)... - 8 * etaeqb * ab ^ 3 * H^(-3)*Hdot   - Ftr    )/Mm;


Ff = Fm * Kn*(Htr - H) * delta * sign(UBAR)  +  ...
          2 *etar * UBAR * ab /(H);
f = Ff/Ftr;
x = [Hdd   f]';
```

D.2 LCTDAT.M (Data)

```
% lctdat.m   -   data file for  EHDL dynamic friction model
```

```
% of Rachoor and Harnoy paper (2/14/95).

global Ftr K0 Htr Hb  Utr eta0 etaeq E Mm Fm ab etaeqb etar

Mm = 2.4e-2;                    % Mass
E = 4200;                % Dimensionless modulus fo elasticity
Fm = 0.1;                % Mechanical friction coefficient
Htr = 2.5775e-5;                % Film thickness at transition
Hb  = 5.e-6;                    % Film thickness at boundary
Utr = 1.5e-10;                  % Velocity at transition
Ftr = 635.91*E^2.831*Utr^4.169*Htr^(-6.024); % Load at transition
K0 = Ftr/(Htr-Hb);              % Stiffness constant
ab = (8*Ftr/pi)^0.5;            % Semiwidth of Hertizian contact
eta0=0.375;              % Viscosity at p = 0.
etaeq = 1;               % Effective viscosty
etaeqb = etaeq * Utr/eta0;
etar = etaeq/eta0 ;
```

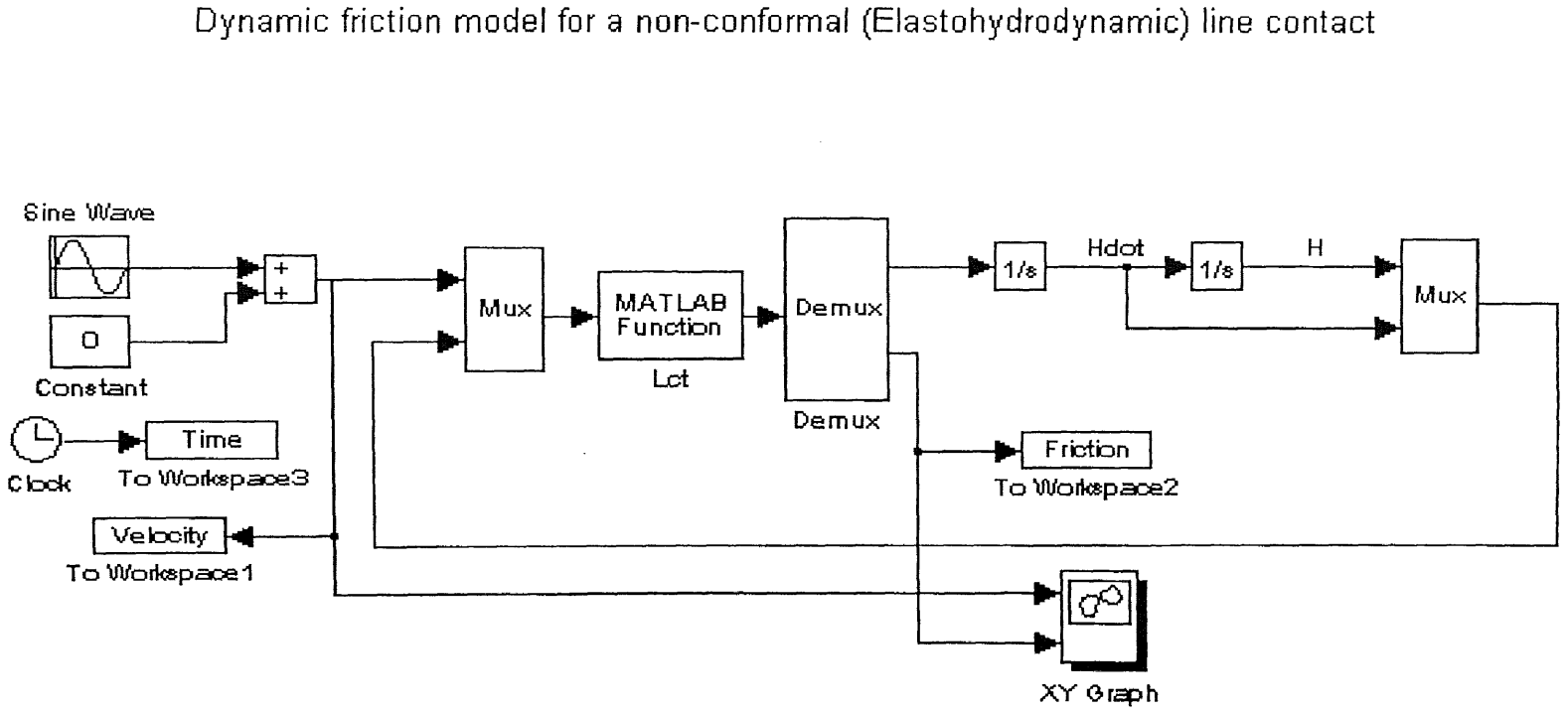

Figure D1 Visual simulation program for simulating dynamic friction in non-conformal contact (elastohydrodynamic line contact) formed by a roller and a plane surface (Chapter 5).

REFERENCES

Armstrong-Hélouvry, B. 1988. "Friction: Experimental Determination, Modeling and Compensation." *Proceedings of the 1988 International Conference on Robotics and Automation,* Philadelphia. IEEE, 3:1422-1427.

—— 1989. "Control of Machines with Non-linear Low-Velocity Friction: A Dimensional Analysis." *Proceedings of the 1st International Symposium on Experimental Robotics,* Montreal, Quebec: 180-195.

—— 1991. *Control of Machines with Friction. Kluwer Academic Publishers.*

Armstrong-Hélouvry, B., and P. Dupont. 1993. "Friction Modeling for Control." *Proceedings of the American Control Conference, San Francisco, CA.* 2: 1905-1919.

Barus, C. 1893. "Isothermals, Isopiestics, and Isometrics Relative to Viscosity." *Am. J. Sci.* 45: 87-96.

Bell, R., and Burdekin, M. 1966. "Dynamic Behavior of Plain Sideways." *Proceedings Institution of Mechanical Engineers.* Vol. 181, pt. 1, no. 8:169-183.

—— 1969. "A Study of the Stick-Slip Motion of Machine Tool Feed Drives." *Proceedings Institution of Mechanical Engineers* 184, pt. 1, no. 29: 543-560.

Bo, L.C., and Pavelescu, D. 1982. "The Friction-Speed Relation and Its Influence on the Critical Velocity of the Stick-Slip Motion." *Wear,* 82(3): 277-289.

Bowden, F.P., and Leben, L. 1939. "The Nature of Sliding and the analysis of the Friction." *Proceedings of the Royal Society, Series A,* Vol. 169: 371-91.

Cameron, A. 1979. *Basic Lubrication Theory,* New York: John Wiley and Sons: 212.

Canudas de Wit, C., H. Olsson, K. J. Åström and P. Lichinsky. 1993. "Dynamic Friction Models and Control Design." *Proceedings of the American Control Conference, San Francisco, CA.* 2: 1920-1926.

Coulomb, C.A. 1785. "Théorie des machines simples, en ayant égard au frottement de leurs, et a la roideur dews cordages." *Mém. Math Phys.,* Paris. Vol. x, 161-342.

Dahl, P.R. 1968. " A Solid Friction Model. " TOR-158(3107-18), The Aerospace Corporation, El Segundo, California.

—— 1976. " Solid Friction Damping of Mechanical Vibrations." *AIAA Journal* 14(12): 1675-1682.

—— 1977. " Measurement of Solid Friction Parameters of Ball Bearings", *Proceedings of 6th Annual Symposium on Incremental Motion, Control Systems and Devices, University of Illinois.*

Dubois, G. B., and Ocvirk, E. W. 1953. "Analytical Derivation and Experimental Evaluation of Short Bearing Approximation for Full Journal Bearings." *NASA Report*: 1157.

Dupont, P.E., and Dunlap, E.P. 1993. "Friction Modeling and Control in Boundary Lubrication." *Proceedings of the American Control Conference, San Fransisco, IEEE.*: 1910-1914.

Friedland, B., and Y. J. Park. 1992. "On Adaptive Friction Compensation." *IEEE Trans. Autom. Contr.* 37 (10): 1609-1612.

Fuller, D.D. 1984. *Theory and Practice of Lubrication for Engineers.* New York : John Wiley and Sons.

Grubin, A. N. 1949. " Fundamentals of the Hydrodynamic Theory of Lubrication of Heavily Loaded Cylindrical Surfaces." Available from Department of Scientific and Industrial Research, Great Britain, Trans. CTS-235.

Haessig, D.A., and Friedland, B. 1991. "On the Modeling and Simulation of Friction." *Journal of Dynamic Systems, Measurement, and Control,* 113 (3): 354-362.

Hamrock, B. J. 1994. *Fundamentals of Fluid Film Lubrication.* McGraw-Hill, Inc.: 435-463.

Harnoy, A. 1976. "Stress Relaxation Effect in Elastico-Viscous Lubricants in Gears and Rollers." *Journal of Fluid Mechanics,* 76: 501-517.

Harnoy, A., and H, Rachoor. 1993. "Angular Compliant Hydrodynamic Bearing Performance Under Dynamic Loads." *Transactions of American Society for Mechanical Engineers, Journal of Tribology* 115(3): 342-347.

Harnoy, A., Bernard Friedland., Richard Semenock., Hanuman Rachoor., and Atif Aly. 1994. "Apparatus for Empirical Determination of Dynamic Friction." *Proceedings of American Control Conf., Baltimore, Maryland, June,* 3(2): 546-550.

Harnoy, A., and B. Friedland. 1993. "Dynamic Friction Model of Lubricated Surfaces for Precise Motion Control." STLE *Tribology Transactions.* 37, 3: 608-614. Presented at *STLE/ASME Tribology Conference,* New Orleans, LA.: 24-27.

Harnoy, A., B. Friedland, and H. Rachoor. 1994. "Modeling and Simulation of Elastic and Friction Forces in Lubricated Bearings for Precise Motion Control." *Wear,* 72: 155-165.

Harnoy, A. 1995. " Model-Based Investigation of Friction During Start-Up of Hydrodynamic Journal Bearings." *Transactions of American Society for Mechanical Engineers, Journal of Tribology*, 117(4): 667-673.

Hess, D.P., and Soom, A. 1990. " Friction at a Lubricated Line Contact Operating at Oscillating Sliding Velocities." *Journal of Tribology*, 112,1: 147-152.

Karnopp, D. 1985. "Computer Simulation of Stick-Slip Friction in Mechanical Dynamic Systems." *ASME Journal of Dynamic Systems, Measurement and Control*, Vol. 107: 100-103.

Morin, A.J. 1833. "New Friction Experiments Carried Out at Metz in 1831-1833." *Proceedings of the French Royal Academy of Sciences*, Vol. 4: 1-128.

Pan, P., and B. J. Hamrock. 1989. "Simple Formulae for Performance of Parameters used in Elstohydrodynamically Lubricated Line Contacts." *Journal of Tribology*, 111(2): 246-251.

Pinkus, O., and Sternlicht B. 1961. *Theory of Hydrodynamic Lubrication.* New York, McGraw-Hill Co: 12, 48.

Polycarpou, A., and Soom, A. 1992. "Transition Between Sticking and Slipping." *Proceedings of ASME Winter Annual meeting*, Anahem, DE. 49: 139-148.

Rabinowicz, E. 1951. "The Nature of the Static and Kinetic Coefficients of Friction." *Journal of Applied Physics*, 22,11: 1373-1379.

—— 1956. "Autocorrelation Analysis of the Sliding Process." Journal of Applied Physics, 27(2):131-135.

—— 1956*a* (May). "Stick and Slip." Scientific American, 194(5): 109-118.

—— 1958. "The Intrinsic Variables Affecting the Stick-Slip Process." *Proceedings of the Physical Society of London*, 71(4): 668-675.

—— 1965. *Friction and Wear of Materials.* New York, John Weily and Sons.

Rachoor, H., and A. Harnoy. 1995. "Modeling of Dynamic Friction in Lubricated Line Contact for Precise Motion Control." *STLE Tribology Transaction* 39(2):(to appear in 1996). Presented at *50th STLE Annual meeting* at Chicago, IL., May 1995.

Rice, and Ruina. 1983. "Stability of Steady Frictional Slipping." *Journal of Applied Mechanics*, 50(2): 343-349.

Sampson, T.B., Morgan, F., Reed, D.W., and Muskat, M. 1943. "Frictional Behavior During the Slip Portion of the Stick-Slip Process." *Journal of Applied Physics*, 14, 12: 689-700.

Stribeck, R. 1902. "Die wesentlichen Eigenschaften der Gleit- und Rollenlager - (The Important Qualities of Sliding and Roller Bearings)" *Zeitschrift des Vereines Seutscher Ingenieure*, 46,39: 1432-1437.

Szeri, A. Z. 1980 *Tribology: Friction, Lubrication and Wear, Hemisphere CO*: 64.

Thomas, S. 1930. "Vibrations Damped by Solid Friction." *Philosophical Magazine*. 7(9): 329.

Ting., L.L. 1993. "Development of a Reciprocating Test-rig for Tribological Studies of Piston Engine Moving Components - Part I: Rig Design and Piston Ring Friction Coefficients Measuring Methods; Part II: Measurements of Piston Ring Coefficients and Rig Test Confirmation." *Tribology of Engines and Engine Oils (SP-959), SAE International Congress*.

Walrath, C.D. 1984. "Adaptive Bearing Friction Compensation Based on Recent Knowledge of Dynamic Friction." *Automatica*, 20(6): 717-727.